PHYSICAL MODELS OF SEISMIC ATTENUATION MEASUREMENTS IN THE LAB

A Thesis Submitted to the

College of Graduate Studies and Research

in Partial Fulfillment of the Requirements

for the degree of Master of Science

in the Department of Geological Sciences

University of Saskatchewan

Saskatoon

By

Trevor Coulman

PERMISSION TO USE

In presenting this thesis in partial fulfilment of the requirements for a Postgraduate degree from the University of Saskatchewan, I agree that the Libraries of this University may make it freely available for inspection. I further agree that permission for copying of this thesis in any manner, in whole or in part, for scholarly purposes may be granted by the professor or professors who supervised my thesis work or, in their absence, by the Head of the Department or the Dean of the College in which my thesis work was done. It is understood that any copying or publication or use of this thesis or parts thereof for financial gain shall not be allowed without my written permission. It is also understood that due recognition shall be given to me and to the University of Saskatchewan in any scholarly use which may be made of any material in my thesis.

Requests for permission to copy or to make other use of material in this thesis in whole or part should be addressed to:

Head of the Department of Geological Sciences

University of Saskatchewan

Saskatoon, Saskatchewan S7N 5E2

ABSTRACT

Classical continuum mechanics with dissipation allows the description of observed creep and phase-lag attenuation effects in solids. The frequency-dependent Q or time-dependent moduli, compliances, or creep functions which are often used to describe such observations may be empirical characteristics reflecting not only the properties of the materials but also the dimensions and shapes of the samples.

The theoretical paradigm employed in this study is strongly different from the conventional, Q-based (often called "viscoelastic") model. Instead of a single, but arbitrarily frequency-dependent Q attributed to a solid, a number of specific physical parameters of energy-dissipation mechanisms (such as viscosity or thermoelasticity) are considered. The model is based on first physical principles and focuses on inverting for the intrinsic (time- and frequency-independent) properties of the material.

The observed frequency-dependent Q's or time-dependent creep ("memory") functions are generally explained by the non-linearity of solid viscosity, which can be described by selecting the Lagrangian dissipation function. This fundamental conclusion was suggested as long ago as by Knopoff (1964) but appeared to be little developed since. I only consider a specific, power-law form of this function, and show that it is consistent with the strain-rate dependence of effective viscosity used in geodynamics. Power-law nonlinearity of solid viscosity combined with thermoelastic effects allows quantitatively predicting all key observations, such as creep, stress-strain phase lags in torsional and longitudinal oscillations, and broadening of spectral amplitude peaks near resonance. Analytical and numerical modeling of longitudinal-oscillation phase-lag measurements in Plexiglas cylinders suggest the value of rheological exponent ~ 0.56. This is interpreted as a "near-dry" internal friction in solids. The physical models of internal friction also suggest methods for inverting for the *in situ* dissipation properties of materials. Finally, the new models suggest several ways for enhancing the theoretical knowledge about the physical properties of Earth materials.

ACKNOWLEDGEMENTS

This dissertation would not have been possible without the guidance and the help of several individuals who in one way or another contributed and extended their valuable assistance in the preparation and completion of this study.

First and foremost, my utmost gratitude to my graduate supervisor, Dr. Igor Morozov, whose sincerity and encouragement I will never forget. Dr. Morozov has been my inspiration as I hurdled all the obstacles in the completion of this research.

Dr. Jim Merriam, Head of the Department of Geological Sciences, for his encouragement to pursue a graduate degree in geophysics;

Dr. Sam Butler, who expanded my knowledge of geophysical techniques and provided me opportunity and guidance;

The Department of Geological Sciences administration, who kept me on task with registration and program milestones;

My colleagues Amin Baharvand Ahmadi and Gao Le, who made coming to work each day a pleasure;

My wonderful girlfriend Maya, who stood by me and supported me during my studies;

My parents Lorraine and Bruce, who provided support and care.

CONTENTS

LIST OF TABLES

LIST OF FIGURES

CHAPTER 1

INTRODUCTION

Measurement of seismic-wave attenuation is one of the most important geophysical techniques for characterization of the composition and physical state of the rock. Granularity, fluids, fractures, temperature variations, and a number of other internal factors cause anelastic behaviour of Earth materials (e.g. Nowick and Berry, 1972; Mavko and Nur, 1975; Lakes, 2009). However, the relation of the observed wave attenuation to the *in situ* anelasticity is not simple and straightforward. Careful understanding of the mechanism of rock anelasticity and analysis of the experimental environments are required for elucidating this relation in each specific case.

Solid anelasticity is present at a broad range of scale lengths and oscillation periods, such as free oscillations of the Earth, tides, seismic-wave attenuation and lab measurements with rock samples several centimetres in length. Current explanations of anelasticity include empirical models, microstructural interpretations, chemical-kinetic models, and also formal mathematical theories using complex-valued parameters of the media in the frequency domain and material memory in time. The internal friction within materials is characterized by the inverse "quality factor", denoted Q^{-1}, and often also called the "specific dissipation function" (Anderson and Archambeau, 1964) and attributed to the material. This property is typically determined empirically and often is frequency-dependent.

Physical models of anelasticity are also well developed in theoretical physics but rarely used in materials science and seismology. In this description, there is no Q, and mechanical-energy dissipation is described by using the laws of mechanics and thermodynamics. The general goal of the present research is thus to try reconciling these two pictures and providing a physical, rigorous, and quantitative picture of seismic attenuation. This study should also clarify the physical meaning of Q measured in typical lab experiments and determine its properties.

The specific goal of this research is to accurately describe the physical processes required to
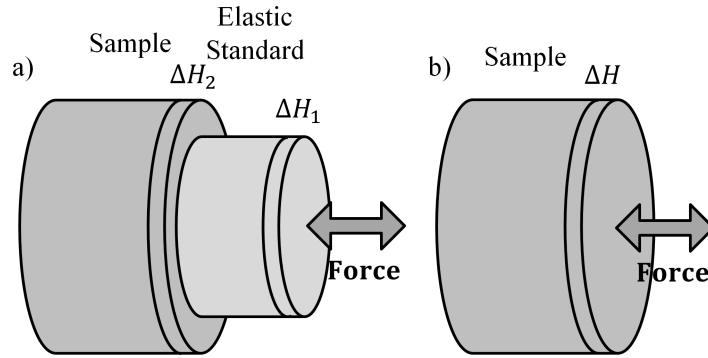
Figure 1.1: Basic experimental setup for a) phase lag experiments and b) resonance or creep experiments.

explain observed phase-lag and creep results in experimental seismic attenuation experiments. The basic idea is to analytically and numerically simulate several typical attenuation measurements in the lab.

1.1   Subject of this Research

The types of experiments considered here often include one or two cylinders placed in series, one being an anelastic rock sample and the other being a known elastic standard. A sinusoidal force is applied to the standard and through it, to the rock sample. Two types of observations can be conducted with such an arrangement (Nowick and Berry, 1972; Bourbié et al., 1987). First, the central frequency and the width of the resonant peak provide information about the elastic modulus and internal friction within the specimen. Such measurements are usually conducted with a single cylinder or bar and conducted at relatively high frequencies (Figure 1.1b).

The second key type of observation of seismic attenuation is the phase-lag measurements, which currently provide the most important information at low frequencies and conditions similar to those encountered by seismic waves traveling within the deep crust and mantle (Jackson and Paterson, 1993). In this case, the objective is to measure the phase lag of the deformation (strain) relative to the applied force.

Due to the anelasticity of the rock sample, its response will lag the elastic standard. Since the standard is elastic, it will be in phase with the applied force and the net result is a measurement of the phase lag between the driving force and rock sample. This phase lag will give us insight into the
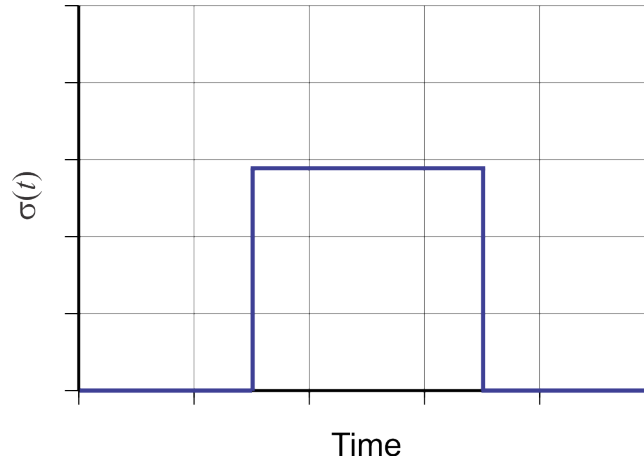
Figure 1.2: Boxcar stress function. Typical stress value are around 10-100 MPa and time scales are minutes to hours.

nature of the anelasticity of the rock sample. The tangent of this phase lag ($\tan\phi$) is often used as a primary characteristic of wave attenuation within materials (Lakes, 2009). It is generally believed to equal the above Q^{-1} and to serve as its extension to low (sub-resonant) frequencies. The same quantity is the primary measure of tidal energy dissipation in planetary dynamics.

1.2 Existing Models of Mechanical Dissipation in Materials

Properties of mechanical behaviour under stress have been routinely tested in numerous materials. Lakes (2009) gives probably the largest collection of results for various types of materials, including such unusual ones as brain tissue. There exists a broad variety of methods of such testing, ranging from measuring amplitudes of waves generated by earthquakes to static and vibrational experiments in the lab. Some of the key observations of these kinds will be described in section 1.4. However, despite this broad variability, the behaviour of materials under stress follows a common pattern, which is best observed in a constant-stress loading/relaxation experiment in the lab. In an idealized loading/relaxation experiment, a specimen is subjected to a sharp increase of stress, which is maintained constant afterwards and instantly removed after a long time. Below, I refer to this stress schedule as the "boxcar" function (Figure 1.2). If we limit ourselves to the behavior known as "anelastic" (with more discussion of this term given in section 1.2.1), there are three key observations that all types of models must reproduce in such an experiment:

3

1. Instantaneous (elastic) (sometimes called "static") response appearing and disappearing practically synchronously with stress;

2. Gradual, progressively decelerated movement ("creep") towards the equilibrium levels, both after loading and unloading;

3. Complete recovery of the initial state (no residual deformation).

There exist several types of models explaining the above observations. These models can be differentiated by the degree of the use of mechanical theory compared to empirical laws derived directly from such observations. In the following, I will differentiate between empirical, mechanical-analogue, and physical (theoretical) models.

1.2.1 Mechanical models

Mechanical-analog models attempt to explain observed creep phenomena using properties attributed to the material. Such models can be understood as "empirical" in the sense of their trying to reproduce the observed behaviours rather than discovering the true mechanisms of physical interactions within materials. At the same time, these models contain physically-meaningful properties, such as elasticities and viscosities of the materials. Thus, mechanical models are valuable as providing both simple and intuitive explanations for the observations and also connections to the rigorous physical models discussed below.

Several types of mechanical models are built from two fundamental elements: the spring and the dashpot (Figure 1.3). The spring represents elastic properties, while the dashpot represents dissipative properties. Work performed on the spring is entirely recovered, as the energy is stored within the spring whereas work performed on the dashpot is entirely dissipated. The stress on the spring, σ_{spring} is assumed to be Hookean and depend linearly on strain. The stress on the dashpot, σ_{dashpot} is assumed to be Newtonian and depend linearly on strain rate:

$$\sigma_{\text{spring}} = M\varepsilon, \quad \sigma_{\text{dashpot}} = \eta\dot{\varepsilon}, \tag{1.1}$$

where ε is the strain, M and η are elastic modulus and viscosity, respectively and an overhead dot denotes the time derivative. The goal is to build a model based on these two elements correctly
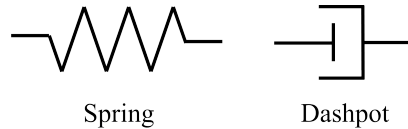
Spring   Dashpot

Figure 1.3: Basic mechanical elements constituting analog models used to represent viscoelastic materials.

a)

b)

Equilibrium level

$\varepsilon(t)$

creep

creep

Stress on   Stress off

σ   σ

ε
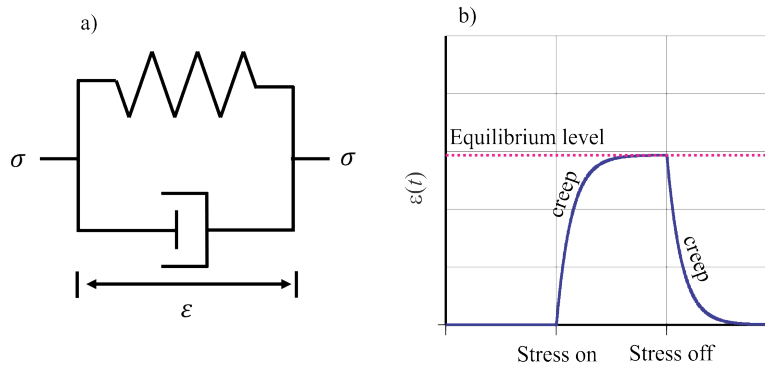
Figure 1.4: a) Kelvin-Voigt model with a spring and dashpot in parallel. Stress (σ) and strain (ε) are indicated. b) Strain response to boxcar stress for Kelvin-Voigt model.

reflecting observations of creep in solids.

The simplest two-parameter models place the spring and dashpot in parallel or in series. A model containing a spring and dashpot in parallel is called the Kelvin-Voigt model (Figure 1.4a). In this model, the deformations of both the spring and dashpot are equal and the forces of their responses are combined. The dashpot will strongly resist the initial applied force, as the strain rate will become high as soon as the stress is applied. This causes a non-instantaneous deformation. As the spring approaches its equilibrium point ($\varepsilon = M/\sigma_0$), the strain rate will decrease, lessening the effect of the dashpot until eventually the stress is carried entirely by the spring. The lack of instantaneous elastic response is clear from Figure 1.4b. However, the process does display recoverability and creep - two of the observations required for an anelastic material.

The Maxwell model is the other simplest two-parameter model (Figure 1.5a). This time, the spring and dashpot are placed in series. In the Maxwell model, the deformations of the spring and dashpot are added together, whereas the force is common to the two elements. Importantly, such combinations of strain and stress become possible due to the presence of an internal degree of freedom in this system (Figure 1.5a). Under a constant external force, the spring will develop a finite extension resulting in "instantaneous" elastic deformation, and the dashpot will move at a
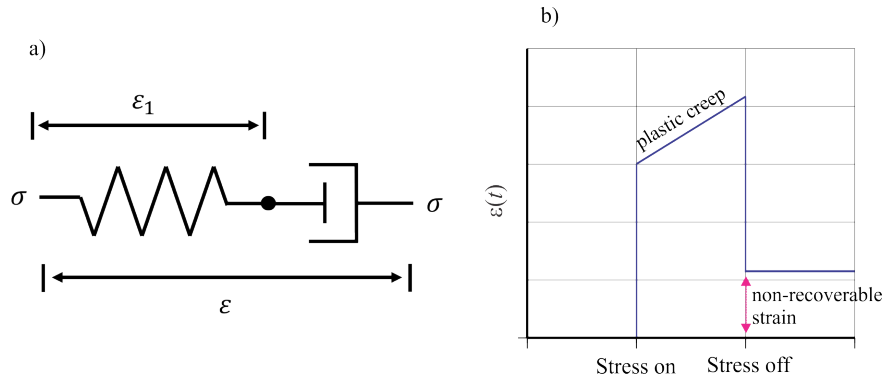
Figure 1.5: a) Maxwell model with a spring and dashpot in series. Stress (σ) and strain (ε) are indicated, the black dot shows the internal degree of freedom (ε_1). b) Strain response to boxcar stress for Maxwell model.

constant rate, until the force is removed. Upon removal of the force, there will once again be an instantaneous response from the spring, but the absence of external force will mean the dashpot will not be engaged and will not exhibit recovery. The end result is plastic deformation (Figure 1.5b).

Figure 1.5b shows that the Maxwell model only satisfies one of the observations of anelastic behaviour - instantaneous elastic response. It is neither recoverable nor does it creep towards an equilibrium value. The creep exhibited from the Maxwell model is plastic flow and is the source of the non-recoverability seen when the stress is turned off.

Neither the Kelvin-Voigt nor Maxwell models explain all three of the observed features of anelasticity of materials. For that reason, higher-level models, containing three or more mechanical elements were devised in an effort to satisfy all the observations of anelasticity. One such model is the Standard Anelastic Solid (SAS) (Nowick and Berry, 1972), also often referred to as the Zener model or the Standard Linear Solid. The SAS consists of a Kelvin-Voigt unit in series with a spring (Figure 1.6a).

Similarly to the Maxwell's body (Figure 1.5a), the SAS model has an internal variable corresponding to the extension of spring A (variable ε_1 in Figure 1.6a). This variable is responsible for the instantaneous elastic response. Upon application of constant stress, spring A will yield instantaneously while the Kelvin-Voigt unit remains undeformed, as the dashpot prevents quick motion. Over time, the system will creep due to the dashpot allowing motion at a finite rate. Eventually, the system will reach an equilibrium strain at which the stress is carried entirely by springs A and B.

6
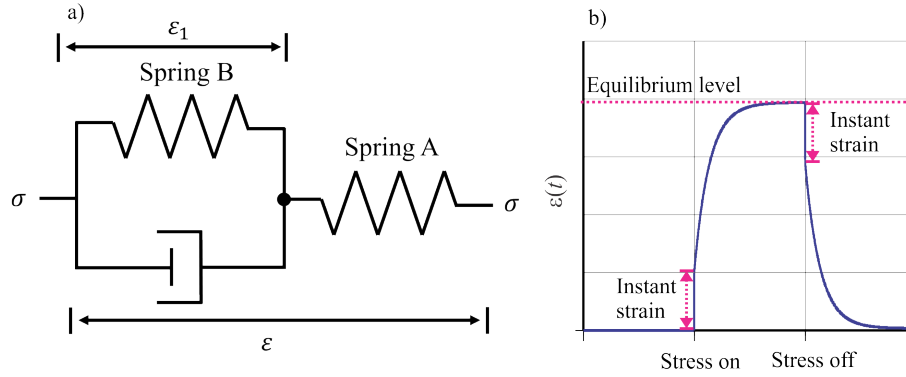
Figure 1.6: a) Standard Anelastic Solid model with Kelvin-Voigt unit in series with a spring. Stress (σ) and strain (ε) are indicated, the black dot shows the internal degree of freedom (ε_1). b) Strain response to boxcar stress for SAS model.

This model will similarly display an instantaneous elastic deformation and creep upon removal of the stress. The result of applying a "boxcar" stress to the SAS model is shown in Figure 1.6b.

Another widely used model is the Burgers model (Figure 1.7a). This model satisfies all three criteria for anelasticity as well as explains plastic deformations, and it is generally considered a realistic model for most rocks (Karato, 2008; Lakes, 2009). The Burgers model attempts to not only explain the behaviour of an anelastic material, but also the plastic deformation. The Burgers model is a four-parameter model consisting of a Kelvin-Voigt unit connected in series with a Maxwell unit (Figure 1.7a). It can also be viewed as an SAS with a second dashpot. Again, note that the Burgers model contains two internal variables (denoted ε_2 and ε_3 in Figure 1.7a). The first of these variables accounts for the quick elastic response, and the second - for steady-state plastic creep. The Burgers model combines both the properties of the Kelvin-Voigt model (creep and creep relaxation) and Maxwell model (instantaneous and plastic deformation) to describe all observed processes, both anelastic and plastic.

The strain response for the Burgers model is a combination of Kelvin-Voigt and Maxwell responses. It essentially represents Figure 1.4b and Figure 1.5b combined. This model exhibits instantaneous deformation, creep, plastic deformation and creep relaxation. In this thesis, I only focus on strictly anelastic behaviour of materials, and thus the additional plastic deformation is not of interest. For this reason, the Burgers model will no longer be considered, and we will perform all subsequent comparisons to the SAS model. The SAS and Maxwell models are also commonly used for implementing anelasticity in the algorithms for computing seismic wave synthetics (Carcione,
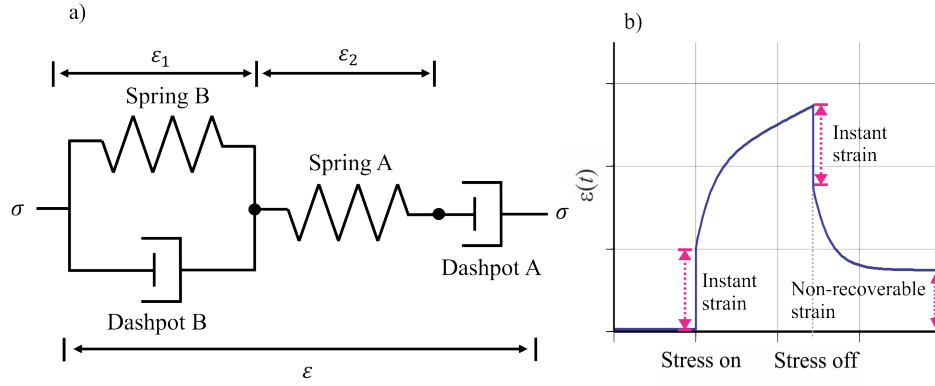
Figure 1.7: a) Burgers model consisting of a Kelvin-Voigt unit and Maxwell unit in series. Stress (σ) and strain (ε) are indicated, black dots show the internal degrees of freedom (ε_1 and ε_2). b) Strain response to boxcar stress for Burgers model.

Table 1.1: Summary of mechanical models and their features.

		Model			
	Observation	**Kelvin-Voigt**	**Maxwell**	**SAS**	**Burgers**
Recoverable	Instantaneous deformation	No	Yes	Yes	Yes
	Creep	Yes	No	Yes	Yes
Non-recoverable	Plastic deformation	No	Yes	No	Yes

2007; Petersson and Sjögreen, 2010).

Table 1.1 summarises the properties of the four mechanical models above. As will be shown below, all of these models can be expressed by using Lagrangian mechanics. Among these models, only the Kelvin-Voigt model uses no "hidden" internal variables, and as shown in section 2.1, this model arises as a natural, first-order approximation to the macroscopic mechanics of anelastic solid. The drawback of this model is the lack of instantaneous response to stress (Table 1.1). However, as also shown in section 3.2.3, lifting the assumption of linearity on the dashpot to include non-linearity will add an (approximately) instantaneous deformation to the list of features above. Thus, one of the principal observations of this thesis will be that with a non-linear "dashpot", the Kelvin-Voigt model becomes consistent with the actual observations of anelastic solids and may represent a simple and relatively accurate physical picture of elasticity and anelasticity in solids.
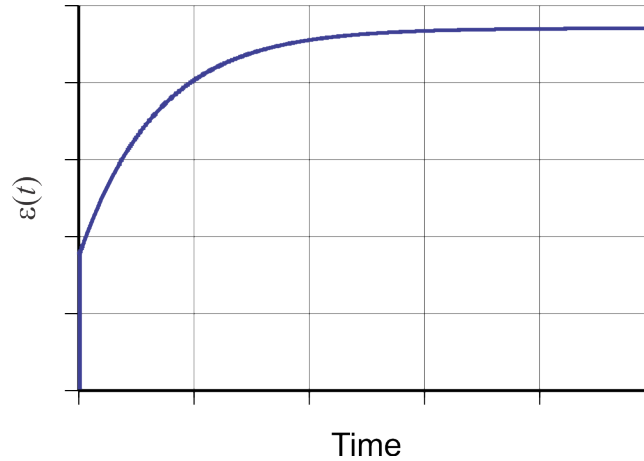
Figure 1.8: Schematic anelastic creep response for stressed material.

1.2.2 Empirical models

Several types of purely empirical models are broadly used to explain observed creep curves. Specifically, such models attempt to reproduce the general character of the anelastic creep, including an elastic response followed by an increase of deformation with time. The rate of this increase is also roughly proportional to the distance from equilibrium but decreases with time.

This general character of the observed anelastic creep has been approximated by using exponential, power and logarithmic functions. Generally, the goal of selecting the optimal empirical law consists in finding an acceptable data fit by using the smallest parameterization.

One of the currently most broadly used empirical model for anelastic creep is the Andrade law (Andrade, 1910). The Andrade law proposes that transient creep can be reproduced by a power-law dependence on time:

$$\varepsilon(t) = \varepsilon_{el} + At^n, \tag{1.2}$$

where the power n is determined empirically and typically is around 1/3. One problem with this model is that strain is divergent at $t \to \infty$, and no equilibrium level is reached. However, this problem does not appear to be significant for empirical models, because they are formulated specifically to explain experimental observations, which are limited in time.

Another empirical model characterizes the anelastic creep by using a logarithmic function of time (Phillips, 1905):

$$\varepsilon(t) = \varepsilon_{el} + b \log t. \tag{1.3}$$

This function is only valid for larger values of t, because $\log t$ is divergent for $t \to 0$. This function also diverges for large t but at a much slower rate than any power-law function in equation (1.2). An alternate formulation of Phillips law (1.3) avoiding the divergent nature of the log function for small values of t was proposed by Lomnitz (1957):

$$\varepsilon(t) = \varepsilon_{\text{el}} + b \log(1 + at). \tag{1.4}$$

The additional term in the log function shifts the curve to the left, allowing the log function to be well-behaved near $t = 0$ as long as $at \gg 1$.

Another natural option for empirically describing anelastic creep is the exponential function:

$$\varepsilon(t) = A(1 - e^{-t/\tau}). \tag{1.5}$$

The exponential model in (1.5) is characterized by a relaxation time, τ, over which the system approaches the state of equilibrium. The advantage of this function is that it is finite for both small and large values of t. Also, the exponential model is precisely the transient part of the of the linear Kelvin-Voigt, SAS, or Burgers models described in section 1.2.1. Thus, the exponential function in equation (1.5) implies some sort of mechanism behind it (Figure 1.4, Figure 1.6 and Figure 1.7), whereas the Andrade, Phillips', and Lomnitz's laws (formulas (1.2), (1.3) and (1.4)) represent purely empirical curves constructed by data fitting.

In many cases, neither of the laws (formulas (1.2), (1.3) and (1.4)) are accurate enough to describe the observed time evolutions of strain, and combinations of such empirical laws are used. For example, Gribb and Cooper (1998) discuss fitting their data for polycrystalline olivine specimens by using either combinations of Burgers bodies or Andrade curves. Such superpositions of elementary responses are another empirical approach to constructing realistic stress-strain relations.

The superposition approach is mostly used with exponential laws (1.5), typically by using Burgers or SAS bodies (Liu et al., 1976). Paired with the linearity of stress with respect to strain rate, the principle of superposition (called the Boltzmann's principle; Nowick and Berry, 1972) states that:

$$\varepsilon(t) = A \int_0^\infty (1 - e^{-t/\tau}) D(\tau) d\tau, \tag{1.6}$$

where A is the total strength of the stress-strain response, and $D(\tau)$ is the function characterizing the relative "strengths" of the "relaxation mechanisms" with relaxation times τ. With arbitrary $D(\tau)$, this formula gives a very powerful empirical data-fitting tool. Essentially any observed transient creep curve of the general shape shown in Figure 1.8 can be fit with an appropriate distribution of relaxation times.

The superposition expression (1.6) is attributed great significance in seismology. One of the most important and spectacular theories of the anelasticity of the Earth's mantle called the Absorption Band Model (Anderson et al., 1977), describes the mantle as containing an infinite spectrum of SAS-type relaxation mechanisms (Liu et al., 1976). This model reproduces the observed seismic Q, which is weakly variable with frequency. In Earth materials science, combinations of such mechanisms are also used to explain the "high-temperature background", which consists of Q values increasing with frequency (Cooper, 2002).

The Andrade and logarithmic empirical formulas in (1.2) and (1.3) can be reproduced by using (1.6) with suitable distributions of relaxation times. Similarly, multiple Andrade laws (within a finite interval of times, t) can also be used to reproduce the logarithmic or exponential time dependences. Once a distribution of "relaxation mechanisms" is considered, the choices of empirical laws become non-unique. This is because the above criterion of minimal parameterization becomes relaxed. However, if the minimal number of parameters as important, the differences between the functional forms of laws (1.2), (1.3), (1.4) and (1.6) become significant. Gribb and Cooper (1998) argued for an advantage of the Andrade model in certain cases, in which it allowed fitting a single power-law function instead of two or three exponential functions (1.6). However, in many other cases, Burgers models are successfully used (Green et al., 1990; Chopra, 1997).

1.2.3 Classical continuum mechanics

In contrast to the mechanical analogs and empirical models above, in this thesis, I try approaching the description of anelasticity from the opposite direction, namely from considering the internal mechanisms of elasticity and internal friction. The general mechanical approach to mechanics of media with dissipation was formulated by Landau and Lifshitz (1976a), as part of their classical 10-volume Course of Theoretical Physics. Below, I follow the logic of their approach.

The macroscopic mechanics of anelastic medium, as well as the mechanics of any system,

is described in three steps: 1) establishing the equations of equilibrium, 2) equations of motion, and 3) dissipation of mechanical energy. All three of these problems are solved by applying the appropriate variational principles. To obtain the equations of equilibrium, we need to minimize the free energy of the system. For small deformations of an elastic body, the free energy, F, can be expanded in second powers of the strain tensor, ε_{ij}:

$$\varepsilon_{ij} = \frac{1}{2}\left(\frac{\partial u_i}{\partial x_j} + \frac{\partial u_j}{\partial x_i}\right).$$

(1.7)

$$F = F_0 + \frac{1}{2}\lambda(\varepsilon_{kk})^2 + \mu\varepsilon_{ij}\varepsilon_{ij},$$

(1.8)

where u_i is the displacement, λ and μ are Lamé parameters and F_0 is the free energy in the absence of deformation (for example, the internal energy due to heat).

Since the free energy is a scalar quantity, all of the terms in the expansion of ε_{ij} should also be scalar. The simple form of (1.8) with only two constants describing the medium arises from the requirement of isotropy (rotational symmetry) of the medium. Because of this symmetry, the free energy is expressed through the only two second-order rotational invariants of the strain tensor: the trace (ε_{kk}); and the sum of the squares of all components ($\varepsilon_{ij}\varepsilon_{ij}$). There also exists a third invariant, the determinant of the strain tensor, $\det(\varepsilon)$; however it is not used because it is third order and adding it to the free energy removes linearity.

The free energy (1.8) can also be written by separating the purely dilatational (volumetric) and purely deviatoric (non-volumetric, shear) strains. Dilatational strain equals the trace of the strain tensor ($\Delta = \varepsilon_{kk}$), whereas deviatoric strain has zero trace:

$$\tilde{\varepsilon}_{ij} = \varepsilon_{ij} - \frac{1}{3}\delta_{ij}\varepsilon_{kk}.$$

(1.9)

Using this strain tensor in (1.8) leads to another expression for free energy:

$$F = F_0 + \frac{1}{2}K(\varepsilon_{kk})^2 + \mu\tilde{\varepsilon}_{ij}\tilde{\varepsilon}_{ij},$$

(1.10)

where $K = \lambda + \frac{2}{3}\mu$ is the bulk modulus. The benefit of writing the free energy in this way is that the volumetric and shear deformations are explicitly separated.

The relation between the free energy of a system and the stress comes from thermodynamics and states that stress is the derivative of the free energy with respect to strain, holding temperature constant,

$$\sigma_{ij} = \left(\frac{\partial F}{\partial \varepsilon_{ij}} \right)_T = K\varepsilon_{kk}\delta_{ij} + 2\mu\tilde{\varepsilon}_{ij}. \tag{1.11}$$

This yields the well-known Hooke's law or basic constitutive equation of elasticity. Note that the quantity K here is therefore the *isothermal* bulk modulus. If temperature variations occur during deformations (e.g., during adiabatic deformation, typical in seismic waves), K would contain contributions from thermal expansion and the modulus would be different (Landau and Lifshitz, 1976a).

Switching to non-equilibrium but conservative problems, equations of motion for an isotropic, homogenous body undergoing deformation can be determined by using a Lagrangian formulation of mechanics and the Hamiltonian action principle. The free energy above is the energy of strain, which will be called the potential energy and denoted V below. The kinetic energy of a system undergoing deformation is a function of the velocity of a point at a given time, $\dot{u}_i$. The Lagrangian for an isotropic, homogenous body can be written as,

$$L = T - V = \int_V \left(\frac{1}{2}\rho\dot{u}_i\dot{u}_i - \frac{1}{2}K(\varepsilon_{kk})^2 - \mu\tilde{\varepsilon}_{ij}\tilde{\varepsilon}_{ij} \right) dV, \tag{1.12}$$

where ρ is the density of the body.

In expression (1.12), displacements u_i can be viewed as special cases of the more general "generalized coordinates", α. Once the Lagrangian is expressed in terms of generalized coordinates and their time derivatives, the equations of motion become completely general and obtained via the Euler-Lagrange equations:

$$\frac{d}{dt}\frac{\partial L}{\partial \dot{\alpha}_i} - \frac{\partial L}{\partial \alpha_i} = A_i, \tag{1.13}$$

where A_i are the non-conservative forces (such as a driving force or force of friction). Coordinates α can also be the valuess of u_i at a certain point or some other parameters measuring the amplitude of oscillation. In section 2.1, I will use such coordinates in the form of relative deformations of the bodies involved in lab testing of rock samples.

So far, the case of purely elastic deformation was considered. Elastic deformation results in

13

oscillations and P- and S-waves traveling within the medium at velocities

$$V_P = \sqrt{\frac{K + \frac{4}{3}\mu}{\rho}} \quad \text{and} \quad V_S = \sqrt{\frac{\mu}{\rho}}, \tag{1.14}$$

respectively.

If stress is applied to a purely elastic system, that system will often oscillate near its equilibrium state, at frequencies determined by its size and other factors (boundary conditions) reflected in the construction of the Lagrangian. If the stress is subsequently removed from the system, the system will continue to oscillate but about its previous un-stressed state. In reality, in the systems in which we are interested in this thesis, such oscillations will quickly attenuate. Mechanical energy will be dissipated into heat due to the "friction" occurring within the system.

To describe the internal friction caused by the motion of the system itself, the concept of the dissipation function ("pseudo-potential") is used. The dissipation function is formulated much in the same way as the potential energy of the system. However, unlike the potential energy, the dissipation function principally depends on the strain rate as opposed to the strain. Just as with the free energy, the dissipation function of an isotropic material should be invariant under rotation and translations. The dissipation function should therefore be built out of invariants of the strain-rate tensor, $\dot{\varepsilon}_{ij}$. To produce linear equations of motion (i.e., Navier-Stokes equations for fluids), the dissipation function should also be quadratic in $\dot{\varepsilon}_{ij}$. Using the same procedure as outlined for free energy (1.8), we arrive at the following two-parameter expression for the dissipation function of anisotropic medium:

$$D = \frac{1}{2}\eta_K(\dot{\varepsilon}_{kk})^2 + \eta_\mu \dot{\tilde{\varepsilon}}_{ij}\dot{\tilde{\varepsilon}}_{ij}. \tag{1.15}$$

The parameters η_K and η_μ can be considered the "bulk viscosity" and "shear viscosity", respectively. These parameters are well known for fluids (Landau and Lifshitz, 1976a), for which η_μ is the dynamic viscosity and η_K is called second viscosity (although rarely used in practice). These viscous parameters control the amounts of energy dissipation caused by the two respective types of deformation.

The force resultant from the dissipation function (σ'_{ij}) is derived in the same way as the elastic

stress in (1.11) but taking a derivative with respect to the strain rate:

$$\sigma'_{ij} = \frac{\partial D}{\partial \dot{\varepsilon}_{ij}} = \eta_K \dot{\varepsilon}_{kk} \delta_{ij} + 2\eta_\mu \dot{\tilde{\varepsilon}}_{ij}. \tag{1.16}$$

The dissipation function (1.15) gives rise to a non-conservative force, that is, mechanical energy is lost from the system via viscous friction. The dissipated power per unit volume can be written in terms of stress σ'_{ij} using (1.16):

$$D = \frac{1}{2}\sigma'_{ij}\dot{\varepsilon}_{ij}. \tag{1.17}$$

Hooke's law including dissipation can now be rewritten as the sum of elastic and viscous stresses,

$$\sigma_{ij} + \sigma'_{ij} = \delta_{ij}\left(K + \eta_K \frac{d}{dt}\right)\varepsilon_{kk} + 2\left(\mu + \eta_\mu \frac{d}{dt}\right)\tilde{\varepsilon}_{ij}, \tag{1.18}$$

or in is most general form, removing the assumption of an isotropic homogenous system,

$$\sigma_{ij} + \sigma'_{ij} = \left(C_{ijkl} + \eta_{ijkl}\frac{d}{dt}\right)\varepsilon_{kl}. \tag{1.19}$$

In terms of the Euler-Lagrange equations, the dissipation function adds a non-conservative generalized force,

$$\frac{d}{dt}\frac{\partial L}{\partial \dot{\alpha}_i} + \frac{\partial D}{\partial \dot{\alpha}_i} - \frac{\partial L}{\partial \alpha_i} = F_i, \tag{1.20}$$

where F_i is the external force applied to the system.

Equation (1.20) produces the fundamental equations of motion of an anelastic system subject to an external force, that is to say, a system which contains both elastic and dissipative properties. This Lagrangian approach, or "energy approach" is based on simple mechanical principles describing the energy of a continuum. The kinetic and potential energies, as well as the dissipation function, are all that is needed to describe both motion and deformation of any system. Hooke's law is derived from the scalar fields of elastic and free energies, making this approach universal and physically robust. The definition of anelastic properties is also tightly controlled by the principles of symmetry and conservation of energy, and the resulting parameters (η_K and η_μ) are unequivocally associated with the medium as opposed to the effective elasticities and viscosities used to explain specific deformation histories of the specimens. The great challenge, however, is to relate these basic

quantities to the observed parameters of attenuation, such as the amplitudes and relaxation times for transient creep in various experiments.

1.2.4 Linear viscoelastic theory

The mathematical model known as linear viscoelasticity generalizes the strain-stress strain relations of mechanical models in section 1.2.1 by generalizing the concept of elastic moduli. Nowick and Berry (1972) formulated this approach, which is now considered standard. It begins from Hooke's law relating stress (σ) and strain (ε) for an elastic material:

$$\sigma = M\varepsilon \quad \text{and} \quad \varepsilon = J\sigma, \tag{1.21}$$

where M is the elastic modulus, and $J = 1/M$ is the compliance. For dynamic experiments, a sinusoidal stress at frequency ω is applied to the material, which can be written as the real part of the complex-valued stress:

$$\sigma = \sigma_0 e^{i\omega t}. \tag{1.22}$$

If the material is purely elastic, the strain is in phase with stress, and modulus M and compliance J are real-valued. However, because of internal friction, materials deform non-instantaneously, and their responses generally lag the applied stress in time. This phenomenon is referred to as anelasticity. Strain resulting from the harmonic stressing of anelastic materials at frequency ω will thus be out of phase with the stress by some phase angle ϕ:

$$\varepsilon = \varepsilon_0 e^{i(\omega t - \phi)}. \tag{1.23}$$

This leads to the notion of a *complex modulus* $M^\star$:

$$M^\star = \frac{\sigma}{\varepsilon} = \frac{\sigma_0}{\varepsilon_0} e^{i\phi} \equiv |M(\omega)| e^{i\phi(\omega)}, \tag{1.24}$$

which is generally thought of as a function of ω. The complex modulus can also be written in terms of its real and imaginary parts:

$$M^\star(\omega) = M_{\text{re}}(\omega) + iM_{\text{im}}(\omega). \tag{1.25}$$

16

Likewise, the compliance can be written as:

$$J^\star(\omega) = J_{re}(\omega) - iJ_{im}(\omega). \tag{1.26}$$

In both cases, the phase lag ϕ is the ratio of imaginary to real parts of the modulus:

$$\tan\phi(\omega) = \frac{M_{im}(\omega)}{M_{re}(\omega)} = \frac{J_{im}(\omega)}{J_{re}(\omega)}. \tag{1.27}$$

This quantity $\tan\phi$ is considered the principal characteristic of internal friction in materials (Lakes, 2009) and is often associated with the "quality factor": $Q = (\tan\phi)^{-1}$.

In summary, the main principle behind the linear viscoelastic approach is the generalization of the elastic modulus to:

1. Include an imaginary part and;
2. Become frequency-dependent.

Creep is also explained similarly to the above phase-lag experiment, that is, through the generalization of the elastic modulus. This can be done by using the Laplace or Fourier transforms of $M(\omega)$ and $J(\omega)$ in equations 1.25 and 1.26, or equivalently, from the following argument. Consider a constant stress of σ_0 turned on at time $t = 0$:

$$\sigma = \begin{cases} 0 & \text{if } t < 0, \\ \sigma_0 & \text{if } t \geq 0. \end{cases} \tag{1.28}$$

The strain response of an anelastic material to such stress will consist of an instantaneous elastic response followed by an anelastic "creep" over time towards a stationary state (Figure 1.8). Recalling Hooke's law (1.21), the observed time-dependent creep function from applied stress (1.28) is generalized as:

$$J(t) \equiv \frac{\varepsilon(t)}{\sigma_0} \quad \text{for } t \geq 0. \tag{1.29}$$
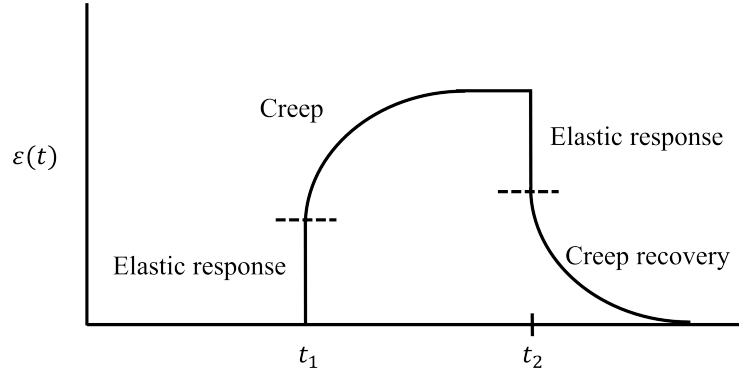
Figure 1.9: Strain response to boxcar stress of an anelastic material.

Now consider a boxcar stress function as follows,

$$\sigma = \begin{cases} 0 & \text{if } t < 0, \\ \sigma_0 & \text{if } t_1 \leq t \leq t_2, \\ 0 & \text{if } t > t_2. \end{cases} \tag{1.30}$$

The strain response of an anelastic material with stress turned on at time t_1 will consist of an instantaneous elastic response followed by an anelastic "creep" over time towards a stationary state (just as described in eq. (1.28)). When the stress is turned off at time t_2, the material will once again undergo instantaneous elastic relaxation followed by creep recovery towards the initial, pre-stressed state (Figure 1.9). The observed time-dependent creep recovery function from applied stress 1.29 is generalized as follows:

$$N(t, \Delta t) \equiv \frac{\varepsilon(t)}{\sigma_0} \quad \text{for } t > t_2, \tag{1.31}$$

where $N(t, \Delta t)$ is the creep recovery function and $\Delta t = t_2 - t_1$ is the amount of time the stress was on. The creep recovery function depends on the amount of time the stress was on *prior* to turning it off as the material may have not relaxed completely.

The viscoelastic approach thus generalizes the elastic moduli to be time-dependent (known as "fading memory") in the time domain and complex-valued (with negative complex arguments) in the frequency domain. This stands in contrast with the mechanical approach, which maintains that the elastic moduli are real-valued and constant with time and frequency[1]. The fundamental

---

[1]In fact, the moduli can be time- and frequency-dependent in the mechanical approach. This may result, for exam-

difference of the viscoelastic model from Lagrangian mechanics described in section 1.2.3 is that in mechanics, the evolution of the system is completely determined by its current state, whereas in viscoelasticity, it comes from an extended "memory" of the material. The relation of these models is that of a phenomenological description to the basic physical theory. The introduction of a basic anelastic parameter such as solid viscosity η (1.15) and solving the Euler-Lagrange equations of motion (1.20) for the conditions of the experiment in question should yield the time-dependent moduli and compliances observed in this experiment.

In terms of fitting experimental data, the viscoelastic model is generally much more permissive than the mechanical model. Inferring a compliance function $J(t)$ from creep observations is relatively straightforward, which allows using empirical laws for it (for example, section 1.2.2; Gribb and Cooper, 1998; Cooper, 2002; Faul et al., 2004). By contrast, deriving the correct form of the dissipation function and inverting for its parameters is much more complicated, and this would almost surely provide a poorer fit to the data. However, this first-principle approach appears to be far more valuable in terms of revealing the true physical properties of the material. This approach is therefore undertaken in this study.

1.2.5   Semi-empirical models

An important alternative to the compliance-function based model is given by explicit modeling of the hysteresis occurring during cyclic loading of rocks. The Preisach model (Guyer et al., 1995) is an example of such an approach, inspired by models of hysteresis in diamagnetic materials. As opposed to the linear viscoelastic theory, which uses a time-retarded stress-strain relation (see section 1.2.4), the Preisach model uses an *instantaneous* stress-strain relation:

$$\varepsilon = \sigma J(\sigma), \tag{1.32}$$

where $J(\sigma) = M^{-1}(\sigma)$ is the stress-dependent compliance and $M(\sigma)$ is the stress-dependent modulus. These are the same quantities as in section 1.2.4 (equations (1.25) and (1.26), except they are

---

ple, from temperature variations or chemical alterations occurring during deformations. With non-linear elasticity, the moduli may also effectively depend on the amplitudes of deformation. However, these dependences are not essential parts of the mechanical model, whereas for linear viscoelasticity, the entire model relies on the time-retarded character of the moduli.
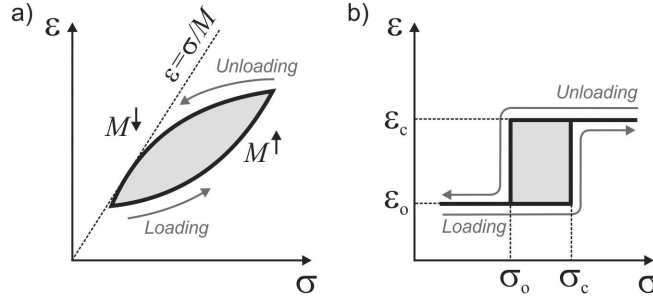
Figure 1.10: a) General hysteresis loop with stress-strain dependent loading and unloading moduli ($M^\uparrow$ and $M^\downarrow$). b) Elementary "hysteretic mesoscopic unit" or hysteron switching between the "open" and "closed" states (subscripts *o* and *c*, respectively) under increasing or decreasing stress (arrows).

not time dependent). Not only is the modulus dependent on stress, it also differs for loading ($\dot{\varepsilon} > 0$) and unloading ($\dot{\varepsilon} < 0$), with $M^\uparrow \geq M^\downarrow$ (Figure 1.10a). For loading conducted in equal stress increments, $\sigma_j = \sigma_0 + j\Delta\sigma$ (with $j = 1...N$), the respective compliances are defined as a combination of the responses of multiple elementary "hysteretic mesoscopic units" or, "hysterons", denoted p_i^j:

$$J^\uparrow(\sigma_i) = \alpha \sum_{j=1}^{i} p_i^j \quad \text{and} \quad J^\downarrow(\sigma^j) = \alpha \sum_{i=j}^{N} p_i^j, \tag{1.33}$$

where α is some scaling factor. This can be seen as summing rows of matrix p_i^j during loading and summing its columns during unloading. A graphical picture of this process is shown in Figure 1.11. In Figure 1.11a, as strain is applied, stress will increase discontinuously in steps. Once a particular strain is achieved, the stress will jump and then stay constant until the next characteristic strain level is reached, whereupon stress will jump again. Figure 1.11b shows the unloading process which occurs in the same discrete manner, but columns are removed during unloading as opposed to rows which are added during loading.

In practice, the distribution of $N(N+1)/2$ values of p_i^j is constructed by fitting the $2N$ values of J measured along the experimental loading and unloading curves (Guyer et al., 1995). This gives an under-determined system of equations, which is regularized and solved by using simulated annealing. The resulting matrix p_i^j allows reproducing the observed strain-stress curves and also to predict the behaviour of the system for loading/unloading schedules not tested in the experiments. In this way, this empirical model steps beyond simply reproducing the experimental data. At the same time, the Preisach model still has no mechanical background. Its strain-rate independence
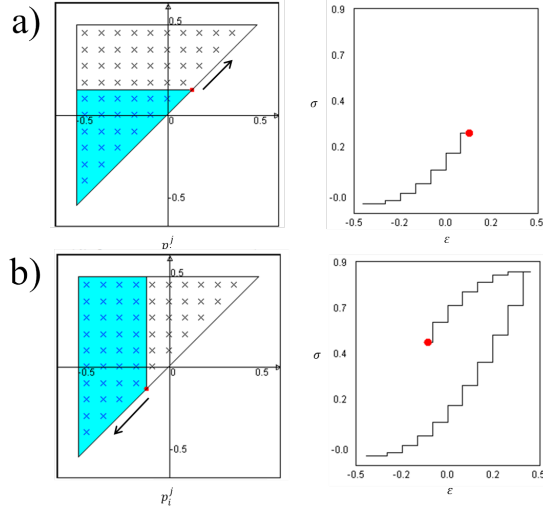
Figure 1.11: a) Discrete Preisach model during loading with $N = 10$ hysterons. Each $\times$ indicates a hysteron. The loading process is mathematically seen as summation along rows. b) Discrete Preisach model during unloading with $N = 10$ hysterons. Each $\times$ indicates a hysteron. The unloading process is mathematically seen as summation along columns.

(eq. (1.32)) also represents a significant limitation, as experiments show that materials' responses to stress may depend on strain rates (Claytor et al., 2009).

1.3 Quality Factor

Both seismic attenuation and anelasticity are conventionally described by the quality factor, usually denoted Q. This factor was introduced from an analogy with a mechanical (acoustical) or electric resonator (Knopoff, 1964). However, there exist several ways to carry out this analogy, and also several ways to measure the Q. In the theory of forced oscillations, the quality factor of an oscillator is defined so that its inverse, Q^{-1} , gives the relative amount of damping in it. Among the several approaches to characterizing this quantity, the one commonly used in seismology defines Q as a ratio of peak elastic energy in the system E to energy lost after one cycle of oscillation, ΔE (Aki and Richards, 2002):

$$Q = 2\pi \frac{E}{\Delta E}. \tag{1.34}$$

This quantity is commonly thought to be a basic property of the material, responsible for its dissipation of weak elastic oscillations. The choice of the elastic energy as the numerator in (1.34) is

21

dictated by the notion of the dissipation being caused by the "imperfect" elastic modulus experiencing internal friction (Anderson et al., 1965). At the microscopic level, this friction is explained by a number of mechanisms discussed in section 2.2.

Despite the simplicity of eq (1.34), neither E nor ΔE in it are directly observable and the fact that Q is a property of the material is not obvious. There exist several methods of arriving at Q as combinations of observational parameters. The following three methods summarize the most common principles of seismic Q measurements in the lab. Most importantly for understanding the various definitions of the quality factor, we need to differentiate between forced and resonant oscillations, and also between time- and frequency-domain measurements.

First, for a resonant system, which is usually considered with low damping, the Q can be measured by relating the width of the peak in the power spectrum ($\Delta\omega$) to the resonant frequency, ω_0 by the following expression:

$$Q_{\text{spec}} = \frac{\omega_0}{\Delta\omega}. \tag{1.35}$$

This is the spectral Q, which is most convenient when stationary, forced oscillations at a range of frequencies near the resonance are studied.

In contrast to the spectral Q, the logarithmic-decrement Q is measured from the time decay of free oscillations, taken in the time domain and near the single resonant frequency. This Q is the measure of the average rate at which the system damps over n cycles:

$$Q_{\text{decay}} = \sqrt{\frac{\pi^2}{\chi^2} + \frac{1}{4}} \approx \frac{\pi}{\chi}, \quad \text{where} \quad \chi = \frac{1}{n}\log\left|\frac{y_1}{y_{n+1}}\right|. \tag{1.36}$$

and y_n are the oscillation amplitudes at cycles $n = 1...N$. Because they are measured on basically the same system (linear oscillator near resonance), Q_{decay} and Q_{spec} are consistent with each other.

The third broadly used method of measuring the phase-lag Q uses forced oscillations conducted far from resonance, typically at $\omega \ll \omega_0$. In this method, Q is determined from the phase lag, ϕ, between the driving force and the resulting strain response (e.g., Jackson and Paterson, 1993):

$$Q_{\text{phase}} = \frac{1}{\tan\phi}. \tag{1.37}$$

Note that the phenomenological definition of Q (1.34) and its empirical measures (1.35), (1.36)
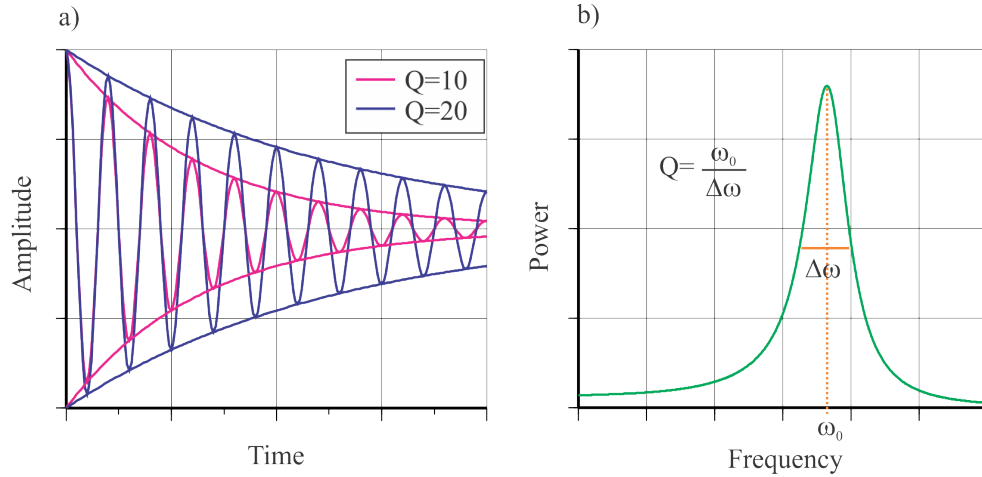
Figure 1.12: a) Example decay curves for $Q = 10$ and $Q = 20$. Waves will damp out faster for lower Q values. b) Example resonance peak with $Q = 20$. Q_{spec} can be measured from the peak.

and (1.37) are defined only for a "damped linear oscillator" in mechanics, and they are equivalent only for measurements (1.35) and (1.36) conducted near the natural frequency ω_0. Considering the energy-based Q (1.34) for a linear oscillator, Morozov (2011e) showed that it is equivalent to Q_{phase} (1.37) for $\omega \ll \omega_0$, but subject to uncertainties in the definition of "stored" energy E in (1.34).

For complex systems, such as seismic waves or the free oscillations of the Earth, the above values of Q may deviate from each other further. In particular, it is clear that all four of the above Q's relate to some kind of a "linear oscillator" which is not necessarily a simple spring-mass arrangement. For complex mechanical or electric systems, the elementary oscillators are represented by certain ("normal") oscillation modes and do not correspond to any specific part of the system. Therefore, each of the above Q's also becomes multi-valued and associated with the specific oscillation modes. When extended to forced oscillations, the Q defined in (1.34) is frequency-dependent for seismic waves and even the simplest mechanical systems (Morozov, 2011e). For the phase-lag Q (1.37), this is also shown in section 3.1.1. Finally, for very complex systems, observational seismology also uses the concept of "scattering Q", which empirically describes the results of attenuation measurements using scattered waves. This type of Q was also inferred from an analogy with plane body waves and eq. (1.34) (Aki and Chouet, 1975). Recently, Morozov (2009, 2010a) pointed out that this Q is a highly controversial and ambiguous quantity. I do not address the complex issue of scattering Q in this Thesis.

Thus, in interpreting the results of attenuation measurements, it is important to clearly see the specific nature of the observed parameters without relying on intuituve analogies. The best approach is likely to abandon the use of Q as rock property (1.34) altogether and adhere to first physical principles in describing the processes of energy dissipation. By modeling the various observable factors of types (1.35)-(1.37) from first principles, we become able to explain the observations and rigorously constrain the intrinsic dissipative properties of the material.

1.4   Experimental Observations

Many experimental techniques for attenuation measurements involve stressing a cylindrical sample in some way. Stress is typically applied through torsion (twisting) or axial deformation (stretching/compressing) (Figure 1.13). In addition, stress may be quasi-static, oscillatory, or impulsive. When using harmonic oscillations, another major distinction between the different types of measurements is in using frequencies that are either comparable or much lower than the resonant frequencies of the apparatus. The two major variables are thus the stress amplitude and frequency.

In the following, I give brief outlines of the principles of lab experiments which are the closest to the type of the dissipation process analyzed in this thesis. Such experiments generally use time intervals (or periods) comparable or longer than the periods of free oscillations of the bodies. Free oscillation of the Earth or "slow" deformation of a rock specimen in the lab represent examples of such experiments. However, I do not consider a vast range of techniques which use seismic pulses traveling through the body of interest. Such experiments include most measurements with body- and surface waves done in seismology, as well as ultrasonic measurements in boreholes and in the lab.

As shown below, for near-resonant or sub-resonant experiments, a common type of quantity is measured, which is typically related to the viscoelastic quality factor of the material, Q. As shown in section 1.3, this parameter can be obtained from two complementary types of approaches: time-domain and frequency-domain. For time-domain measurements, the Q is obtained from the variations of deformation with time, and for frequency-domain - from the shapes of amplitude spectra (near resonances) and phase shifts (below the resonances).
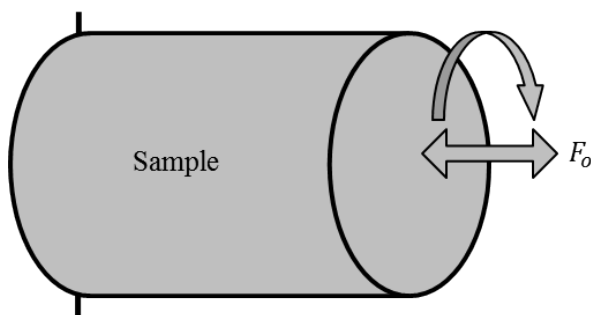
Figure 1.13: Schematic creep experiment. Constant tensile or torsional force is applied to one end of the sample while the other end is fixed.
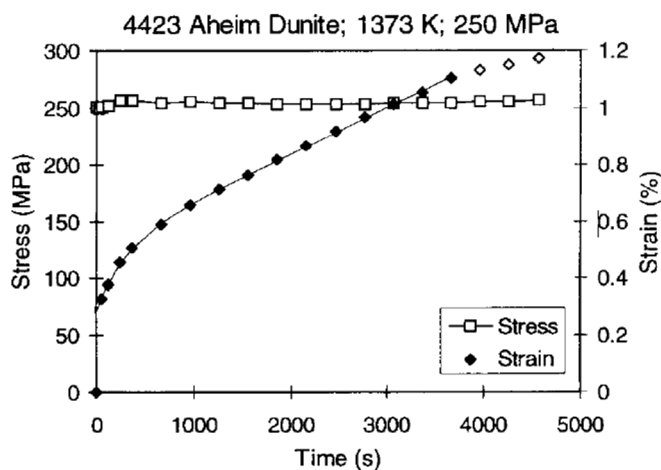
Figure 1.14: Example creep curve for olivine from Chopra (1997). Dark squares indicate strain and light squares indicate stress. Instantaneous elastic deformation followed by anelastic creep and then plastic deformation is seen.

1.4.1 Creep

In creep experiments, a constant stress is applied to the sample for an extended period of time (on the order of hours), and the resultant deformation is measured as a function of time. Anelastic (as well as more generally, inelastic) properties of the material manifest themselves as non-instantaneous deformations. Typical strain amplitudes in creep experiments are large, greater than 10^{-5} (Chopra, 1997; Jackson et al., 2004). As explained in section 1.2.2, experimental creep curves are usually subdivided into an instantaneous elastic deformation followed by anelastic creep and then plastic deformation (Figure 1.7b).

Creep curves are often fit with Burgers models (Figure 1.7) or other empirical laws, such as Andrade (1.2), Lomnitz (1.4) or exponential (1.5). In certain cases, combinations of multiple empirical
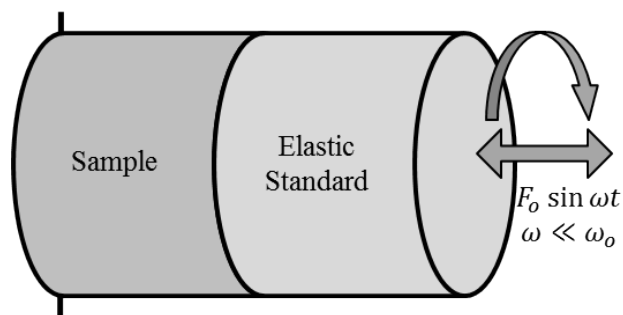
Figure 1.15: Schematic apparatus for phase-lag attenuation measurements. A torsional or tensile oscillatory force is applied to the elastic standard and through it, to the sample. The response of the sample will lag the standard and as such, the driving force. The phase lag is an indication of anelasticity in the sample. The elastic standard should be in phase with the driving force.

curves are needed to achieve an accurate fit to the data.

The advantage of quasi-static creep experiments is in emphasizing the steady-state, plastic deformation. Such deformation is achieved at very high strains of about 10^{-4} to 10^{-2} (Figure 1.14). However, in this thesis, I am only interested in the recoverable (anelastic+elastic) deformations at low strains comparable to those in seismic waves. Such recoverable deformations are best studied by frequency-domain methods described below.

1.4.2 Phase lag methods

Phase-lag experimental setups are similar to creep tests except they use weak forces oscillating near-harmonically at a specific frequency, as opposed to constant forces in creep experiments. Phase-lag experiments rely on measuring the phase lag between the applied force and the resulting strain. The force-strain lag is difficult to measure directly, and in order to obtain this lag, an additional elastic standard is usually attached in series with the rock sample (Figure 1.15). Also, the oscillation frequency is varied and the phase lag between the deformations of the sample and elastic standard is measured. The tangent of this phase lag, $\tan \phi$, is viewed as the key characteristic of attenuation within the material (Lakes, 2009), and often treated as the inverse quality factor: $Q^{-1} = \tan \phi$ (section 1.3; Faul et al., 2004; Jackson et al., 2004; Tisato et al., 2010).

Phase-lag experiments are typically carried out at seismic frequencies, from 10^{-3} to 1 Hz for Jackson and Paterson (1993) and at 1 to 50 Hz for Tisato et al. (2010). These frequencies are significantly lower than the resonant frequency of typical $10 - 20$ cm samples, which often have
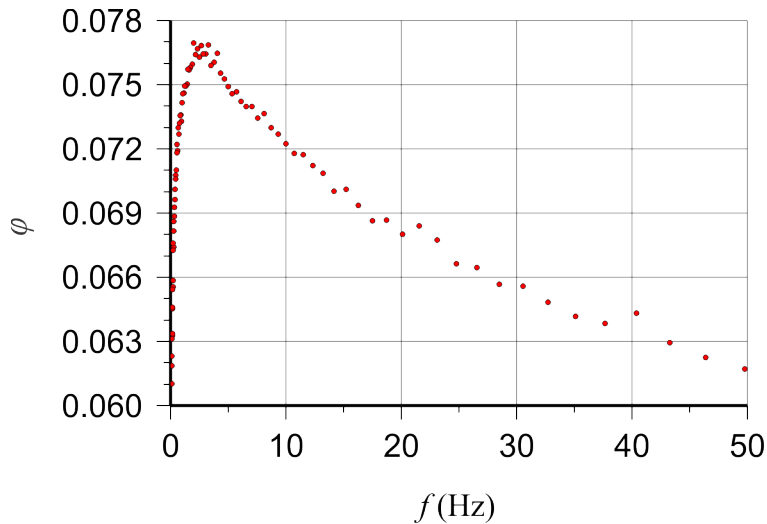
Figure 1.16: Example longitudinal phase-lag data for Plexiglas (Tisato et al., 2010). Notice the existence of a spectral peak around 3 Hz followed by a decrease with frequency.

resonant frequencies in the kHz range.

Phase-lag results often show the phase lags decreasing with frequency (Figure 1.16, Jackson et al., 2004; Tisato et al., 2010). In materials science, this decrease of Q^{-1} with frequency is called the "high-temperature background" (Cooper, 2002), and in seismology, a similar decrease is attributed to the "absorption band" of the mantle (Anderson et al., 1977). If dissipation in materials behaves linearly, phase lag should increase linearly with frequency (see section 3.1.1). This can be thought of as follows: as the specimen is cycled in strain, the amount of energy dissipated increases slower than the frequency. Explaining the phenomena of phase lag decreasing with frequency is the focus of considerable research. Phase lags, as well as the seismic Q^{-1} in general, also increase with temperature (Ito and Sato, 1991; Cooper, 2002).

Phase-lag experiments allow substantial sophistication in achieving the conditions close to those experienced by the rocks within deep crust and mantle. For example, the torsional apparatus by Jackson and Paterson (1993) contains a pressure vessel and a furnace (Figure 1.17) which allows conducting measurements at pressures up to 300 MPa and temperatures to 1500 K. Because of these capabilites, such experiments are presently viewed as the most reliable source of information about the *in situ* attenuation properties of the Earth's mantle. At the same time, potentially, this more complicated design also creates additional sources of friction, such as caused by the viscosity of the argon atmosphere and by significant thermal gradients within the assembly. These issues
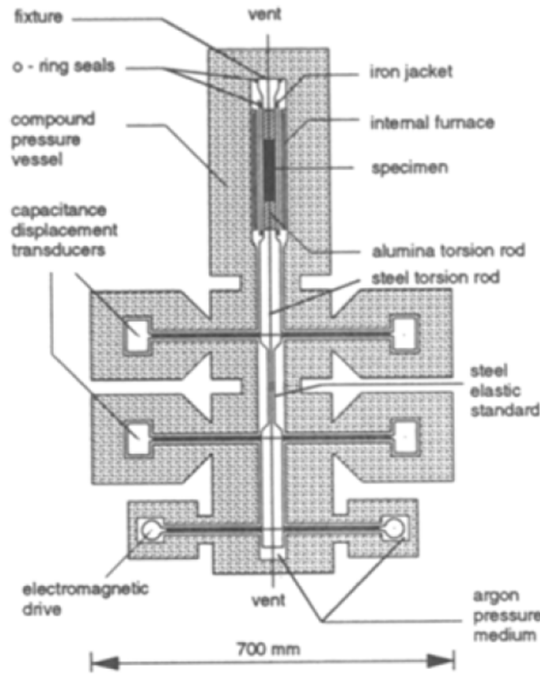
Figure 1.17: Torsional attenuation measurement apparatus including internal furnace and pressure vessel (Jackson and Paterson, 1993).

are dealt with by using a number of empirical corrections (Jackson and Paterson, 1993). In the present study, I do not attempt to consider the full complexity of this problem but only focus on the physical model of dissipation attributed to the specimen and standard (Figure 1.15).

1.4.3 Resonance methods

Performing essentially the same forced oscillation experiment but at much higher frequencies, produces a plot of the resonant peak of the sample as opposed to phase lag. Only the sample is required in this case, and the standard is not necessary since phase lag will not be measured. This experiment is also often done with a bar instead of a cylinder and using flexural forces as opposed to tensile or torsional (Johnson et al., 2004). For a purely elastic body, the resonant peak would occur at the natural frequency of free oscillation and have a width of zero. Anelasticity causes the width of the resonant peak to increase (eq. (1.35) and Figure 1.19). The relative width of the peak is closely related to the phase lag in a sub-resonant, low-frequency experiment (section 1.3). Several resonant peaks for PVC specimens (polyvinyl chloride) are shown in Figure 1.19. For deformations up to about 10^{-5}, PVC behaves linearly, and varying the driving amplitude does not affect the location or width of the peak. The quality factor can be extracted from resonance peaks by taking the ratio

28
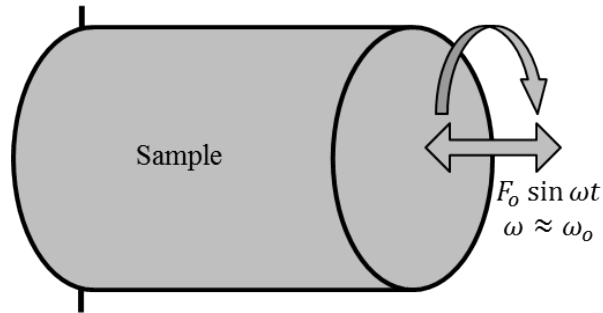
Figure 1.18: Schematic resonance experiment. The sample is also often a bar and the force can also be flexural. A frequency sweep near resonance is performed, and the width of the resonant peak measured.
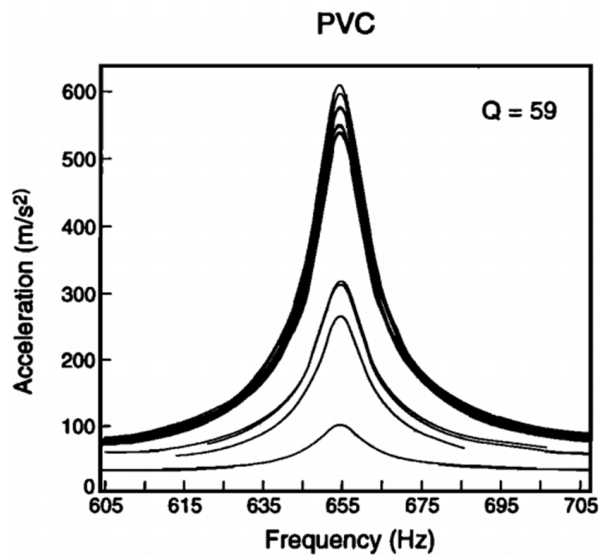
Figure 1.19: Response for PVC to various strains displays a linear response. The upward and downward sweeps coincide (Johnson et al., 1996).

of spectral width to spectral peak. For most rocks, this process is highly non-linear and the spectral Q is a function of strain (Figure 1.20).

1.4.4 Slow Dynamics

A relatively new class of mechanical-energy dissipation effects reported for several geomaterials since mid-1990's is called "slow dynamics" (TenCate, 2011). Slow-dynamics experiments are carried out in much the same way as resonance experiments, but the strains used to measure the resonant peaks are very low. These strains are about 10^{-8}, compared with typical $10^{-5} - 10^{-2}$ strain amplitudes used in the traditional creep experiments (Jackson and Paterson, 1993; Chopra,
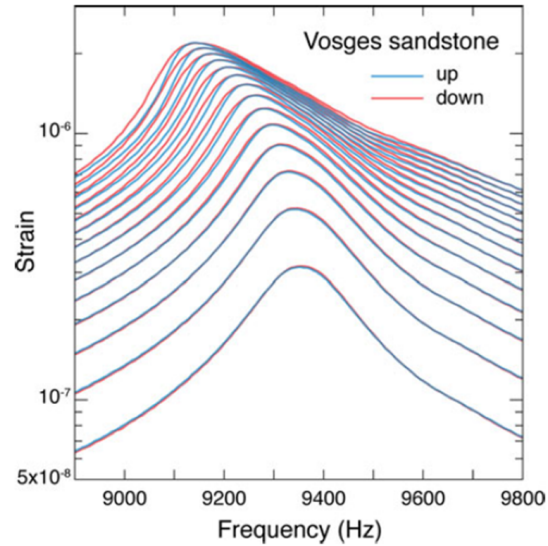
Figure 1.20: Response of a typical rock (Vosages sandstone) to various strains displaying non-linear behaviour. The peak is asymmetric and frequency of the peak changes with strain amplitude. The lower the strain, the closer to a symmetric "linear" peak. Note the up/down sweep asymmetry that becomes more apparent for higher strains (TenCate, 2011).

1997; TenCate, 2011). Another peculiarity of slow-dynamics experiments is that resonant strains are measured on top of much stronger "conditioning" strains. Slow dynamics investigates how the resonant peak moves and becomes asymmetric with respect to frequency sweep direction as it is conditioned with different amplitudes of strain (Figure 1.20). The non-linear effects on spectral-peak shapes are also called "peak bending".

In a slow-dynamics experiment, there are two strains applied, one is the larger conditioning strain that runs at the resonant frequency of the sample and the other is the weaker strain sweep frequency that determines the resonant frequency. Most rocks show linear resonant peaks up until around 10^{-6} strain amplitude. At higher strains, peak bending begins to occur, and the peaks obtained by up-sweep and down-sweeps in frequency begin to differ (Figure 1.20). The up/down asymmetry is dependent on the sweep rate and is referred to as the "rate effect". If the sample is given ample time to equilibrate at a particular frequency before the measurement is made, rate effects are eliminated (TenCate, 2011). If the times between frequency steps are small, rate effects are observable and the material is thought to possess a "memory" of being at a particular strain level (TenCate, 2011, Figure 1.20).

When the conditioning strain is switched on and off for periods of about 15 minutes, the elastic
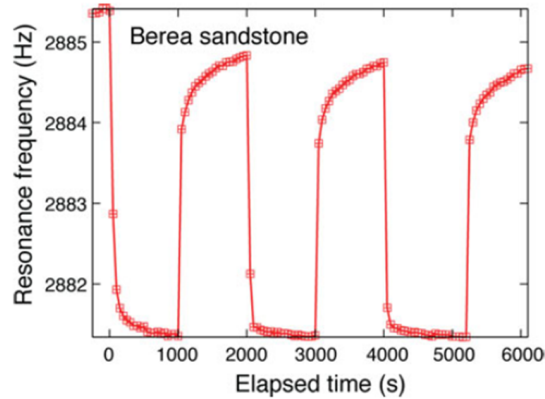
Figure 1.21: Resonant frequency as a function of time for Berea sandstone. A conditioning strain of 10^{-6} is applied at 0 seconds and kept on for 1000s. The resonant frequency is measured every 50 seconds using a very low strain and exhibits a creep response. The conditioning strain is cycled every 1000s. (TenCate, 2011).

modulus changes, leading to weak ($\sim 0.1\%$) variations in the resonant frequency (Figure 1.21). Shapes of these variations are very similar to those obtained in quasi-static creep (section 1.2.1), with "instantaneous" responses followed by gradual relaxation as about $\log(t)$. Similarly to creep, these phenomena are observed upon both turning the conditioning strain on and switching it off (Figure 1.21).

Current explanations of slow dynamics in rocks are similar to those of recoverable (anelastic) creep (TenCate, 2011). An intriguing question is how the strain energy ("memory") of such low magnitude gets stored within the microscopic structure of the rock, which is subjected to much stronger conditioning. It is believed that microcracks, "sticky fractures", and thermoelastic effects at crack tips are important factors for this type of dissipation. TenCate (2011) also performed investigations of the effects of pore water and found that slow dynamics is present even in extremely dry rock specimens in ultra-high vacuum.

However, overall, it appears that the understanding of slow dynamics is still insufficient. With regard to our model (chapter 2), slow dynamics is important as a clear indicator of non-linear effects taking place during oscillations and energy dissipation. Similarly to interpretations of the creep and phase-lag experiments, this understanding could be improved by utilizing the physical concepts developed in the present study.

CHAPTER 2

APPROACH

The mathematical foundation of the analytical and numerical models of this thesis follows the Landau and Lifshitz's (1976) approach to continuum mechanics in section 1.2.3. The basic principle of this method is to determine the kinetic and potential energies of the system as functions of some generalized coordinates and velocities and, using the Hamiltonian variational principle and Euler-Lagrange equations (1.20), derive the equations of motion for these generalized coordinates.

The models of this study consist of simple arrangements of one or two cylinders (section 1.4), which reproduce the key features of several devices currently used for seismic attenuation measurements in the lab (Jackson and Paterson, 1993; Gribb and Cooper, 1998; Tisato et al., 2010). Two types of experimental apparatuses to measure the phase-lags between driving forces and system responses have been built by using cylindrical rock samples. These same apparatuses are also capable of performing creep experiments. Generally, one type of such systems uses compression along the length of the cylinder (Tisato et al., 2010), while the other applies torsion to one end of the cylinder (Figure 2.1) (Jackson and Paterson, 1993). The advantage of the first of these designs is in assessing the longitudinal deformations, whereas the second specifically focuses on shear deformation. Ideally, it would be best to carry out both of such experiments with the same specimen.

The traditional interpretations and even the designs of such experiments are influenced by the viscoelastic model of solids. For example, in the design of the longitudinal phase-lag apparatus, it is assumed that the *in situ* strain of the specimen is phase-delayed with respect to stress, and that the deformation of the elastic standard gives the phase of the stress (Jackson and Paterson, 1993), However, the *in situ* stress is very difficult to measure, and it consists, for example, of elastic, viscous, and thermoelastic parts which may be difficult to separate. These stresses may also depend on the shapes of the specimen and other parts of the device, which may be far from the simplified cylinders (Figure 1.15 on page 30). Therefore, one needs to be careful about making assumptions

about a universal "phase-lag" property of the material and resort strictly to the "observables", such as the measured deformations of the cylinders, and to physical laws. Below, I describe such a rigorous approach using the Lagrangian mechanical model and thermoelastic effects to numerically simulate the behaviours of experimental apparatuses. This is still a strictly macroscopic description, in which the mechanics of the medium is described by very few parameters averaged over large numbers of elementary units, such as atoms, grains, defects in the crystalline lattices, or dislocations. At the end of this chapter, I will discuss the dislocation and kinetic effects as potential microscopic mechanisms of anelasticity.

2.1 Model

In this model, I consider a system of two cylinders attached along the z-axis, held at the base, and subject to a periodic driving force applied at the opposite end (Figure 2.1). Two types of deformation are considered, one with the force applied in the z-direction (longitudinal) and another with a torque applied in the θ-direction (torsional). The cylinder attached to the base is called the standard and is assumed to have no internal dissipation, as in the apparatus by Jackson and Paterson (1993). The cylinder attached on top of the standard is the specimen in which the internal dissipation is being measured. Because of internal friction, its deformation will lag the standard by a phase-lag angle, which is being measured (Figure 2.1). Thus, in this model, the measured phase lag reflects the difference in the observable strains in two parts of the experimental device, and no assumptions about the internal stress are being made. This is the key difference of the present approach from the traditional viscoelastic model. In the viscoelastic interpretation, the phase lag is a property of the material (Lakes, 2009) and directly related to the material Q of the specimen by eq. (1.37) (Jackson and Paterson, 1993; Cooper, 2002; Tisato et al., 2010). However, note that the phase of the stress is only an inferred quantity, which is different, for example, when the elastic or total stress is considered. The unambiguous and actually measured quantity is the phase lag between the deformations of the two cylinders. In the following, I predict this phase lag theoretically and numerically for both the torsional and compressional scenarios, and show that it depends on frequencies and in certain cases - on the shape of the specimen. Thus, the simple formula (1.37) becomes generally insufficient.
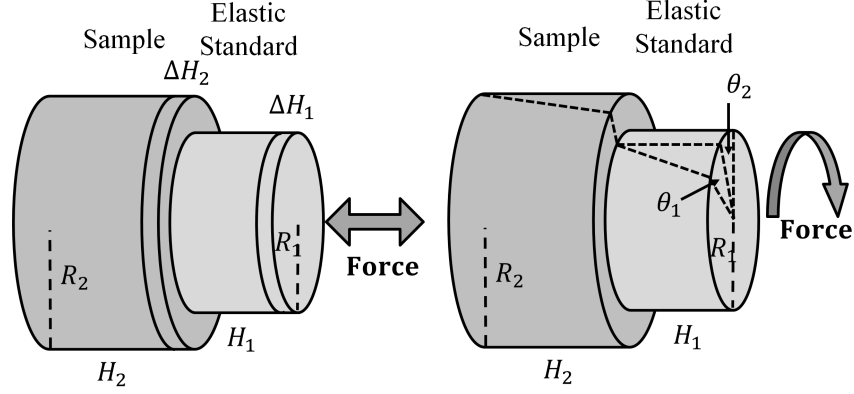
Figure 2.1: Schematic for measuring phase lags for a) compression or tension and b) torsion.

The Lagrangian for the system can be written as follows:

$$L = T - V = \int_V \left(\frac{\rho}{2} \dot{u}_i \dot{u}_i - \frac{1}{2} K (\varepsilon_{kk})^2 - \mu \tilde{\varepsilon}_{ij} \tilde{\varepsilon}_{ij} \right) dV, \qquad (2.1)$$

where ρ is the density of the cylinder, K is the bulk modulus, μ is the shear modulus, $\dot{u}_i$ is the velocity of a point, ε is the strain tensor and $\tilde{\varepsilon}$ is the deviatoric strain tensor (1.9), and V is the total volume of the system. Denoting any of the three quantities in the right-hand side of eq. (2.1) by f, the integrals over the total volume break integrals over the sample and the other over the standard:

$$\int_V f dV = \int_{V_1} f dV_1 + \int_{V_2} f dV_2 = \int_0^{2\pi} \int_0^{R_1} \int_0^{H_1} f r dr dz d\theta + \int_0^{2\pi} \int_0^{R_2} \int_0^{H_2} f r dr dz d\theta. \qquad (2.2)$$

By utilizing the simple geometry of these experiments, the relative deformation of each of the two cylinders can be considered as near-uniform and described by a single parameter, $\alpha_i = \Delta H_i / H_i$ for compression and $\alpha_i = \theta_i$ for torsion, where $i = 1$ for the standard and $i = 2$ for the specimen. For the resonance and creep experiments, the subscript i is dropped, as there is only the sample. With these definitions of "generalized coordinates" α, solutions for $\vec{u}$ are given in Appendix A. The Lagrangian and dissipation functions can then be written in matrix form as follows:

$$L = T - V = \dot{\alpha}_i T_{ij} \dot{\alpha}_j - \alpha_i V_{ij} \alpha_j \quad \text{and} \quad D = \dot{\alpha}_i D_{ij} \dot{\alpha}_j, \qquad (2.3)$$

where $\dot{\alpha}$ is the rate of deformation. In this expression, matrices T_{ij} and V_{ij} for both longitudinal and
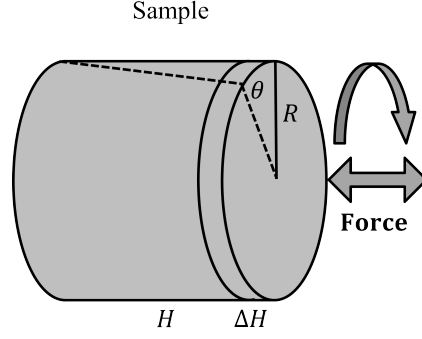
Figure 2.2: Schematic for resonance or creep experiment. Both tensional (ΔH) and torsional (θ) deformations are shown.

torsional deformations can be found in Appendix A.

Another type of experiment simulated with a similar arrangement of cylinders involves measurement of the width of the spectral peak near resonance. In this case, the standard is not used (Figure 2.2). The specimen is driven by either harmonic compression or torsion applied to its end, and the displacement amplitude(s) measured. From these amplitudes, Q is derived by using eq. (1.35). From the expressions for the Lagrangian (eq. 2.1), the complete Euler-Lagrange equations of motion are:

$$\frac{d}{dt}\frac{\partial L}{\partial \dot{\alpha}_j} - \frac{\partial L}{\partial \alpha_j} = F_i(t).$$
(2.4)

These equations describe the mechanical behaviour of the conservative system of the modelled one- or two-cylinder system in the absence of energy dissipation. Similarly to the above decomposition of the Lagrangian, the quadratic dissipation function (1.15) can also be expressed as a quadratic form in terms of $\dot{\alpha}$:

$$\dot{\alpha}_i D_{ij} \dot{\alpha}_j = \int_V \left(\frac{1}{2}\eta_\Delta \dot{\Delta}^2 + \eta_\mu \dot{\tilde{\varepsilon}}_{ij} \dot{\tilde{\varepsilon}}_{ij} \right) dV,$$
(2.5)

with matrix elements D_{ij} given for longitudinal and torsional cases given in Appendix A. With this dissipation, the equations of motion modify to:

$$\frac{d}{dt}\frac{\partial L}{\partial \dot{\alpha}_n} + \frac{D}{\partial \dot{\alpha}_n} - \frac{\partial L}{\partial \alpha_n} = F_n(t).$$
(2.6)

35

2.1.1 Linear rheology

Linear rheology (with forces of friction proportional to the strain rates) corresponds to a quadratic dissipation function eq. (1.15). Using the Euler-Lagrange equations of motion (2.6) the equation of motion becomes:

$$T_{nm}\ddot{\alpha}_m + D_{nm}\dot{\alpha}_m + V_{nm}\alpha_m = F_n. \tag{2.7}$$

In the case of the resonance and phase-lag experiments, the driving force is harmonic ($F_n(t) = F_n e^{i\omega t}$), and so the response will also be harmonic ($\alpha_m(t) = \alpha_m e^{i\omega t}$). Substituting these quantities into equation (2.7), we obtain a system of one or two equations (for one- and two-cylinder cases, respectively) for a damped, driven linear harmonic oscillator:

$$\mathbf{K}\vec{\alpha} = \vec{F} \quad \text{where} \quad \mathbf{K} = -\omega^2\mathbf{T} + i\omega\mathbf{D} + \mathbf{V}, \tag{2.8}$$

where matrices $\mathbf{T}$, $\mathbf{V}$, and $\mathbf{D}$ describing the kinetic and potential energies, and energy dissipation rates and are given in Appendix A. The stationary response of the system is given by the inverse matrix:

$$\begin{pmatrix} \alpha_1 \\ \alpha_2 \end{pmatrix} = \mathbf{K}^{-1} \begin{pmatrix} F_1 \\ F_2 \end{pmatrix}. \tag{2.9}$$

For any given external force vector $\vec{F}$, the resulting α_1 represents the response of the standard and α_2 represents the response of the sample. Both of these values are complex quantities and functions of ω, which allows evaluating both the amplitudes and phases of responses to the force. From these responses, all types of observable Q values in eqs (1.35), (1.36) and (1.37) can be obtained.

The low-frequency limit, useful for sub-resonant phase lag experiments, can be simplified by removing the kinetic term $\mathbf{T}$. The inverse matrix $\mathbf{K}^{-1}$ can be approximated for low frequencies using a geometric series as follows:

$$\mathbf{K}^{-1} \approx (\mathbf{V} + i\omega\mathbf{D})^{-1} = \mathbf{V}^{-1}(\mathbf{1} + i\omega\mathbf{D}\mathbf{V}^{-1})^{-1} \approx \mathbf{V}^{-1}(\mathbf{1} - i\omega\mathbf{D}\mathbf{V}^{-1}). \tag{2.10}$$

In creep experiments, a single cylinder is subject to a constant force. Equation (2.7) becomes one

dimensional and the equation of motion becomes:

$$T\ddot{\alpha} + D\dot{\alpha} + V\alpha = F, \tag{2.11}$$

where T, D and V are kinetic energy, dissipation and potential energy, respectively. Expressions for these quantities for a single cylinder are given in Appendix A.

2.1.2 Non-linear rheology

As suggested by early models of anelasticity by Knopoff (1964), more recent studies of mantle rheology (Karato and Spetzler, 1990), by recent viscosity modeling of the free oscillation of the Earth (Morozov, 2010c), and also by the results in this thesis, dissipation in solids is likely non-linear. Linear rheology is characterised by a quadratic dissipation function (1.15) and as a result, quadratic dependence of the energy-dissipation rate on frequency for harmonic oscillations:

$$P \sim \dot{\hat{\varepsilon}}^2 = \omega^2 \hat{\varepsilon}^2, \tag{2.12}$$

where $\hat{\varepsilon}$ is the strain amplitude of oscillations. Because the dissipated power is proportional to ω^2, Q^{-1} linearly increases with frequency. Such an increase is rarely observed for seismic waves, for which Q^{-1} tends to be closer to a constant or decreases with frequency. A constant Q can result from "dry" (Coulomb) friction (Knopoff and MacDonald, 1958). In terms of the Lagrangian formalism, such models imply non-quadratic dissipation functions.

In fluid dynamics, non-Newtonian fluids, for which the viscous stress tensor non-linearly depends on strain rates, are well known (Tropea et al., 2007). Examples of such fluids include machine oils, paints, ketchup, blood, and shampoo. The dependence of stress on strain rate and other factors (temperature, pressure, chemical composition of the surfaces, as well as oscillatory or static character of shear) in such fluids can be complex. In geodynamics, the "rheological" flow of mantle rock is also treated as non-Newtonian fluid flow. The strain-rate stress relation for the mantle is non-linear and written in the form of power-law relations between the applied stress, σ, and the resultant deformation rate, $\dot{\varepsilon}$ (Karato, 2008):

$$\dot{\varepsilon} \propto \sigma^n, \tag{2.13}$$

37

where the rheological parameter n depends on the interpreted microscopic dissipation mechanism and equals ~ 1 for diffusion creep and 3.5 for dislocation creep in olivine within the upper mantle (Karato and Wu, 1993).

Equation (2.13) is usually interpreted as giving the rate of steady-state flow responding to certain stress. However, to transform it into a mechanical law, it is important to express the viscous stress as a function of strain rate:

$$\sigma \propto \dot{\varepsilon}^{\nu}, \tag{2.14}$$

where $\nu = 1/n$ becomes the new rheologic parameter. Similar to eq. (1.16), such viscous stress can be obtained from a dissipation function D with a power-law dependence on $\dot{\varepsilon}$. Similarly to the case of elasticity (section1.2.3), for an isotropic medium, such dissipation function can be written in terms of the first two invariants of the strain-rate matrix, $\dot{\varepsilon}$:

$$I_K = \tau_K^2 \frac{\dot{\Delta}^2}{2}, \quad I_\mu = \tau_\mu^2 \frac{\dot{\tilde{\varepsilon}}_{ij} \dot{\tilde{\varepsilon}}_{ij}}{2}. \tag{2.15}$$

Using these invariants (the deviatoric strain, $\tilde{\varepsilon}$ and dilatational strain, Δ), let us construct a dissipation function:

$$D = \frac{\eta_K}{\tau_K^2} D_K(I_K) + \frac{2\eta_\mu}{\tau_\mu^2} D_\mu(I_\mu), \tag{2.16}$$

where η are dissipation parameters (solid viscosities) corresponding to dilatational and deviatoric deformation, respectively. Parameters τ in the denominators are necessary to keep the values of η measured in viscosity units ([Pa·s]). These parameters are determined by the units selected for η and can be set equal 1 sec for convenience.

Further, we will use power-law forms for the dissipation functions corresponding to the dilatational and deviatoric strains, and assume that these strains do not interact:

$$D_K = I_K^{\nu_K} \text{ and } D_\mu = I_\mu^{\nu_\mu}. \tag{2.17}$$

Therefore, the power-law non-linear dissipation function, D^{nl} becomes:

$$D^{\mathrm{nl}} = \int_V \left[\frac{\eta_K}{\tau_K^2} \left(\tau_K^2 \frac{\dot{\Delta}^2}{2} \right)^{\nu_K} + \frac{2\eta_\mu}{\tau_\mu^2} \left(\tau_\mu^2 \frac{\dot{\tilde{\varepsilon}}_{ij} \dot{\tilde{\varepsilon}}_{ij}}{2} \right)^{\nu_\mu} \right] dV. \tag{2.18}$$

38

This dissipation function evaluated for our two- or one-cylinder systems for both tensional and torsional deformations is shown in Appendix A. When $\nu_K = \nu_\mu = 1$, this dissipation function reduces to the quadratic case in eq. (1.15) and leads to linear equations of motion. This case corresponds to fluid viscosity. A power of $\nu = 0.5$ corresponds to dry friction, with the resulting frictional stress being independent of strain rates. Results from free oscillations of the Earth suggest a power between 0.5-0.6 for Earth materials (Morozov, 2010c). Results closer to dry friction appear intuitive as solids can be expected to be "drier" than liquids.

We can similarly extend the equations of motion (1.16) to non-linear rheology. Consider the dissipation function per unit volume for a torsional system with $\tau_\mu = 1$:

$$D^{\mathrm{nl}} = \eta_\mu \left(\frac{\dot{\bar{\varepsilon}}_{ij}\dot{\bar{\varepsilon}}_{ij}}{2} \right)^\nu .$$ (2.19)

The viscous stress arising from this dissipation function is:

$$\sigma'_{ij} = \frac{\partial D^{\mathrm{nl}}}{\partial \dot{\bar{\varepsilon}}_{ij}} = \nu\eta_\mu \left(\frac{\dot{\bar{\varepsilon}}_{ij}\dot{\bar{\varepsilon}}_{ij}}{2} \right)^{\nu-1} \dot{\bar{\varepsilon}}_{ij} = \eta_{\mathrm{eff}}\dot{\bar{\varepsilon}}_{ij} \ , \text{ where } \ \eta_{\mathrm{eff}} = \nu\eta_\mu \left(\frac{\dot{\bar{\varepsilon}}_{ij}\dot{\bar{\varepsilon}}_{ij}}{2} \right)^{\nu-1} .$$ (2.20)

The ratio of viscous stress to strain rate gives the "effective viscosity", η_{eff}. This effective viscosity is constant for linear rheology ($\nu = 1$) but depends on the strain rate for non-linear rheology ($\nu \neq 1$). Expressions for η_{eff} for both torsional and tensional experiments are given in Appendix A.

The parameters reflective of anelasticity are now the non-linear viscosities, η and the rheologic exponents, ν. The exponents are responsible for the fundamental nature of the microscopic mechanism of anelasticity, whereas η's represent the amount of contribution from this mechanism.

Along with non-linearity, equation 2.18 emphasize another important aspect of the rheological model used in this Thesis: the non-Newtonian solid is compressible, and consequently possesses both shear and bulk dissipation. Usually, in fluid-flow models, bulk viscosity is disregarded because of the predominance of shear deformations. However, in small anelastic deformations of solids (such as in a seismic P wave), bulk deformations are significant, and in general, the associated viscosity cannot be ignored.

In phase-lag observations, the phase lags are usually small (below ~ 0.1 rad), which suggests that the stresses caused by dissipation are much weaker than elastic stresses. I will therefore still

consider the elasticity as linear (quadratic in terms of energy), and only assume a non-quadratic, power-law dissipation function. To approximately account for weak non-linear dissipation, I will try replacing it with an "equivalent" linear dissipation. Consider the equation of motion for forced harmonic oscillations:

$$\left(-\omega^2 T_{ij} + V_{ij}\right) q_j + \frac{\partial D}{\partial \dot{q}_i} = F_i, \tag{2.21}$$

where T_{ij} and V_{ij} are the coefficients of quadratic forms for the kinetic and potential energies, respectively, and D is the non-quadratic dissipation function. Let us assume we have a solution for the dissipation-free case determined for the same external force:

$$\vec{q}^0 = \left(-\omega^2 \mathbf{T} + \mathbf{V}\right)^{-1} \vec{F}. \tag{2.22}$$

In order to solve eq (2.21) approximately, let us replace the dissipation function D with a quadratic one:

$$D_2 = \frac{1}{2} \tilde{D}_{ij} \dot{q}_i \dot{q}_j, \quad \text{where} \quad \tilde{D}_{ij} \equiv \tilde{D}_{ji}, \tag{2.23}$$

which approximates the average energy dissipation in each of the generalized variables q_i:

$$\left\langle \dot{q}_i \frac{\partial D_2}{\partial \dot{q}_i} \right\rangle = \tilde{D}_{ij} \langle \dot{q}_i \dot{q}_j \rangle = \left\langle \dot{q}_i \frac{\partial D}{\partial \dot{q}_i} \right\rangle, \tag{2.24}$$

where all averages are evaluated for the solution $\vec{q}^0$. With our selection of variables non-interfering in terms of dissipation ($q_i = \alpha_i$), a diagonal matrix can be taken for $\tilde{D}_{ij}$, with ith diagonal element:

$$\tilde{D}_{ii} = \left. \frac{\left\langle \dot{\alpha}_i \frac{\partial D}{\partial \dot{\alpha}_i} \right\rangle}{\dot{\alpha}_i^2} \right|_{\vec{\alpha} = \vec{\alpha}^0} \tag{2.25}$$

With this new dissipation function, the solution becomes:

$$\vec{\alpha} = \left(-\omega^2 \mathbf{T} + i\omega^{2\nu - 1} \tilde{\mathbf{D}} + \mathbf{V}\right)^{-1} \vec{F}, \tag{2.26}$$

where expressions for $\mathbf{T}$, $\tilde{\mathbf{D}}$ and $\mathbf{V}$ are given in Appendix A. For any frequency ω, this solution should be close to $\vec{\alpha}^0$ and dissipate the correct average amount of energy through each degree of freedom of the system.

Using the non-linear power-law dissipation function in (2.18) but setting the powers $\nu_K = \nu_\mu = \nu$ and $\tau_K = \tau_\mu = 1$, we obtain:

$$D = \int_V \left[\eta_K \left(\frac{\dot{\Delta}^2}{2} \right)^\nu + 2\eta_\mu \left(\frac{\dot{\varepsilon}_{ij}\dot{\varepsilon}_{ij}}{2} \right)^\nu \right] dV. \qquad (2.27)$$

Because the concepts of bulk and shear viscosities in Earth solids are still not well established, the relative magnitudes of these viscosities are unclear. For simplicity, I always use identical values of the power-law exponents ν for these viscosities. With regard to the relative levels of η for them, several approaches can be taken. First, from seismic observations, bulk attenuation appears to be much lower than the shear one ($Q_K^{-1} \approx 0$; Knopoff, 1964), and consequently we may try $\eta_K \approx 0$ (note that in the same paper, Knopoff (1964) also showed cases requiring non-zero Q_K^{-1}). On the other hand, the approach to dissipation draws from analogies with elasticity, in which the elastic moduli for rocks are comparable: $\lambda \approx \mu$ and $K \approx 5\mu/3$, it appears reasonable to also suggest that maybe the viscosities ar also comparable: $\eta_\lambda \approx \eta_\mu$ and $\eta_K \approx 5\eta_\mu/3$. Another interesting choice is the case of zero Poisson's ratio: $\lambda \approx 0$, and the elastic solid deforming without additional transverse deformation. For friction, this could be the simplest *a priori* assumption. Taking this case for an analogy, we would have $\eta_\lambda \approx 0$ and $\eta_K \approx 2\eta_\mu/3$. However, because of this variability of ideas and general complexity of the problem, in the examples below, I only approximate the above models by taking either $\eta_K \approx 0$ or $\eta_K \approx \eta_\mu$ as characteristic examples.

2.2 Dislocations and Kinetic Effects

Viscosity expressions (2.18) give only a macroscopic picture of mechanical-energy dissipation, and only for purely mechanical friction. At the microscopic level, these mechanisms should be described by relative movements of various parts of the material, such as grain boundary sliding, sliding on dislocations in the crystalline lattice, and similar processes. Apparently, such mechanical processes can be considered "instantaneous" and causing the greatest energy dissipation during the fastest deformation. Thus, the characteristic property of viscosity is its direct relation to the strain rate, $\dot{\varepsilon}$.

Another important cause of mechanical energy being dissipated, and consequently $\tan\phi$ de-

creasing with frequency (Figure 1.16), could be in non-mechanical effects, such as electric and magnetic interactions, diffusion of point defects, movements of dislocations (Nowick and Berry, 1972), and other internal changes occurring within material under stress. The characteristic feature of such effects is in their progressive development with time, as a response to variation in the stress within the material. The operation of kinetic relaxation in a constant-stress creep experiment (section 1.2.1) can be described as follows: 1) when the stress is quickly applied, the deformation is fast, but no dissipation occurs, 2) while remaining under constant stress, the elastic modulus slowly "relaxes" due to internal changes occurring within the material. During this modulus relaxation, the elastic energy continues to increase, and yet the dissipation of energy also occurs. This picture is opposite to viscosity, for which the fast phase 1) would account for most of the dissipated energy. The magnitude of kinetic effects for seismic waves within the mantle is also debatable, because for seismic strain levels (10^{-10} to 10^{-8}), the corresponding pressure variations are 10^{-9} to 10^{-7} of the ambient pressure, and thermoelastic temperature variations have similar magnitudes. Nevertheless, this kinetic picture is almost exclusively used for explaining anelasticity in Earth materials (Nowick and Berry, 1972; Karato and Wu, 1993; Karato, 2008; Lakes, 2009).

Kinetic processes are characterized by their "strengths" and relaxation times. In the existing models (Karato, 2008), these relaxation times are recognised from the positions of the absorption peaks in the Q^{-1} or phase-lag spectra (apparently close to 0.2-0.3 s in the Plexiglas study by Tisato et al., 2010; Figure 1.16 in section 1.4.2). The dissipation is most effective at oscillation periods close to these times. This increase in dissipation effectively makes the viscosity parameters frequency-dependent for harmonic processes.

To describe the kinetic processes mathematically, viscoelastic treatments (e.g., Liu et al., 1976; Cooper, 2002) usually invoke the frequency-dependence of the *in situ* material properties, or equivalently, material memory (see section 1.2.4). Such time-delayed or frequency-dependent effects are inconsistent, or at least very awkward to reconcile with our Lagrangian model, which is based on the traditional instantaneous mechanical interactions. However, such time-delayed interactions are also not needed, and the Lagrangian model can adequately describe relaxation processes. Note that generally, kinetic processes (diffusion, thermal fluxes) take place in space and cannot be reduced to local material memory (Morozov, 2011e,f).

Beyond relying on the empirical relaxation times, kinetic processes are also difficult to describe

42

mechanically. Models for dependences of relaxation strengths on pressure and temperature were created based on the Arrhenius equation known in chemistry (e.g., Karato and Wu, 1993); however, the stress fields produced by kinetic processes have been poorly studied. In the existing theory of anelasticity, kinetic processes comprise numerous microscopic processes within the material (Nowick and Berry, 1972). One, and perhaps the most important process of such kind is thermoelasticity, which is related to variations of temperature and consequently heat dissipation as a result of thermal expansion of the material. Thermoelastic effects are "kinetic" in the above sense, i.e., this energy dissipation gradually increases with time. However, rigorously, these processes have no definite "relaxation times", which can vary from zero to infinity, depending on how the heat exchange is maintained within the system (Morozov, 2011f). Morozov (2011f) estimated that thermoelastic dissipation can in principle be responsible for the entire seismic attenuation within the upper mantle ($Q \geq 80$) and in the deep crust ($Q \approx 1000$); see also Table B.4 in Appendix A). In the experiment considered here, thermoelastic effects likely explain the approximately 20% absorption peak in the present device (Figure 2.1a). Consequently, this type of kinetic processes deserves special attention. Also, fortunately, the physics of thermoelastic effects is well known (Landau and Lifshitz, 1976a), and they can be readily described at the macroscopic level used in this thesis.

2.3   Thermoelasticity

Thermoelastic effects represent an important cause of energy dissipation in solids (Hayden et al., 1965). Such mechanisms should be most pronounced for grainy, polycrystalline materials, and they lead to Q^{-1} decreasing with frequency (Landau and Lifshitz, 1976a). In our case, compression of the cylinder (Figure 2.1) will cause a reduction of its volume and an increase of temperature. Conversely, quick relaxation will cause an increase in volume and a decrease in temperature. If one of these states is maintained for a certain time interval, the heat will be redistributed, irreversibly annealing the temperature and adding to the mechanical dissipation described above. The temperature variation in a solid due to adiabatic deformation is (Landau and Lifshitz, 1976a):

$$T - T_0 = -\frac{T_0 K_{ad} \alpha}{\rho C_p} \varepsilon_{kk}, \tag{2.28}$$

where T_0 is the equilibrium temperature, ε_{kk}[1] is the dilatational strain (relative volume change), K_{ad} is the adiabatic bulk modulus, C_p is the specific heat at constant pressure per unit mass, α is the thermal expansion coefficient at constant pressure, and ρ is the density. Consequently, thermoelastic energy dissipation is a function of volumetric change, ε_{kk} whereas the solid viscosity-related dissipation is due to the rate of change of the strain tensor, $\dot{\varepsilon}_{ij}$. Even for a perfectly uniform Plexiglas sample of this study, the associated heat should release into the environment during low-frequency cycling of deformation.

According to Landau and Lifshitz (1976, pp. 157-159), there exist three end-member regimes of thermal relaxation in polycrystalline (grainy) bodies:

i For very low frequencies $\omega \ll \vartheta/a^2$ (where a is the size of the grain and ϑ is the thermometric conductivity, defined as the ratio of the thermal conductivity κ to some specific heat per unit volume C), the grains equilibrate within each period of oscillation, and the oscillation occurs nearly isothermally. In this case, $\tan\phi \propto \omega$, similarly to the case of regular linear viscosity (shown in section 3.1.1).

ii For frequencies $\vartheta/a^2 \ll \omega \ll c/a$ (where c is the speed of sound in the medium), equilibration takes place by means of "temperature waves" across the boundaries of grains. This process is similar to the skin effect in electromagnetism, and the corresponding $\tan\phi \propto 1/\sqrt{\omega}$.

iii At frequencies $\omega \gg c/a$, wave processes take place within the grains and $\tan\phi \propto \omega$ again.

The above case of extremely high frequencies (iii) is irrelevant for the present problem and so regimes (i) and (ii) will be considered below. As we will see, the transition from ω to $1/\sqrt{\omega}$ may represent the low- and high-frequency slopes of the observed absorption peaks. It appears that along with elastic scattering (Morozov, 2011), thermoelasticity is the only mechanism that can provide phase lags decreasing with frequency.

---

[1]Einstein summation convention is used, i.e., ε_{kk} is the trace of the strain tensor (dilatational strain).

CHAPTER 3

RESULTS

In this chapter, I summarize the results from anaytical and numerical simulations of several types of phase-lag, resonance and creep experiments. Most of these simulations were conducted for parameters approximating the measurements of mechanical dissipation in an experiment with a Plexiglas cylinder by Tisato et al. (2010). Glassy Plexiglas is a broadly available, inexpensive, relatively uniform and transparent material, which makes a natural choice for testing ideas and devices for measuring anelastic properties of solids. Its physical properties are well known and reproducible, although somewhat variable by manufacturer. Polymers such as Plexiglas possess significant internal friction which can be reliably measured. Interestingly, the relatively large values of phase lags corresponding to Q of $\sim 15 - 50$ reported in recent lab tests on mantle olivine aggregates (Jackson et al., 2004; Faul et al., 2004) are similar to those measured in polymers (Figure 3.1; Lakes, 2009), although their elastic moduli are of course much larger[1]. Plexiglas also shows strong thermal expansion (Table 3.1) and spectral peaks in dissipation (Figure 3.2). In terms of the models presented in this Thesis, this suggests that thermoelastic effects may be significant when measuring mechanical dissipation in Plexiglas.

Tisato et al. (2010) recently reported a new apparatus for axial phase-lag measurements in comparatively large rock samples with variable fluid saturations. These authors kindly provided their phase-lag data obtained during initial testing of this apparatus using Plexiglas cylinders (Figure 3.2).

For comparison, Figure 3.2 also shows earlier Plexiglas phase-lag and elastic-moduli data from Lakes (2009), and (Figure 3.3) shows creep data for Plexiglas by McLoughlin and Tobolsky (1952). So far, these data have been interpreted purely empirically, as time and frequency variations of the

---

[1]Note that it therefore appears that energy dissipation in olivine is much stronger than even in polymers.
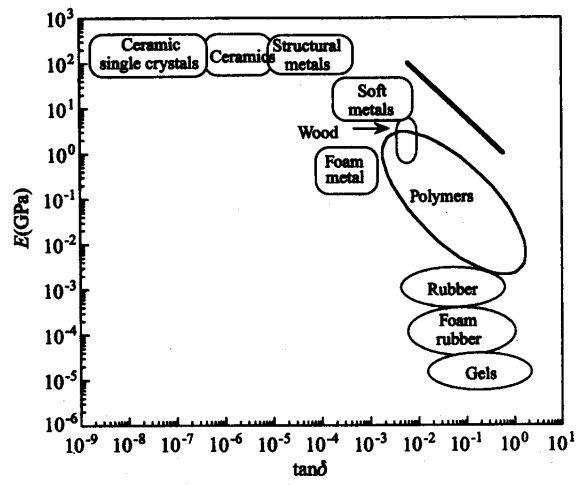
Figure 3.1: Phase lags and empirical moduli for various materials (Lakes, 2009). Notice that polymers (including Plexiglas) have phase lags similar to those of of olivine aggregates (Jackson and Paterson, 1993; Faul et al., 2004).
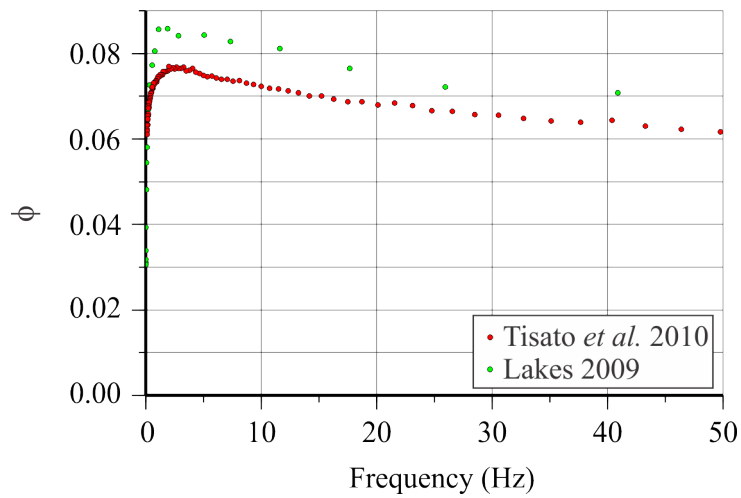
Figure 3.2: Experimental phase lag data for Plexiglas cylinders (Tisato et al., 2010; Lakes, 2009).
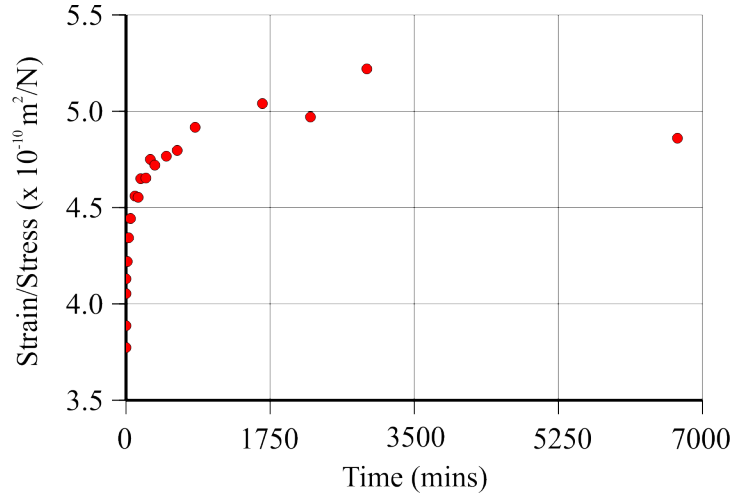
Figure 3.3: Experimental creep data for Plexiglas with linear plastic flow removed (McLoughlin and Tobolsky, 1952).

viscoelastic moduli. In my modeling, I attempt explaining these data from the physical viewpoints presented in section 1.2.3. Phase lag and creep are simulated for both linear and non-linear rheologies. In addition, resonance-type Q is also investigated.

Simulation parameters for the models in Figure 2.1 and 2.2 are shown in Table 3.1. Sample dimensions are chosen to match the Plexiglas phase lag experiment by Tisato et al. (2010). Moduli and the Poisson ratios for Plexiglas are taken from a Plexiglas manufacturing company, ALTU-GLAS (1987). Viscosity parameters in Table 3.1 correspond to only one characteristic case of linear rheology (section 3.1.1). As discussed below, for non-linear rheologies and different levels of strains and strain rates, these parameters may be strongly different. Generally, as the modeling below shows, non-linear dissipation effects exhibit great variety in behaviours and values of parameters and may sometimes look unusual. Nevertheless, as this study suggests, non-linear effects in dissipation are significant.

3.1 Modelling Using Linear Rheology

3.1.1 Sub-resonant forced oscillations

A simulation for both torsional- and longitudinal-deformation cases was carried out using the parameter values in Table 3.1. In Tisato et al. (2010) and similar experiments (Jackson and Paterson, 1993), the measured quantity is the phase lag between the deformations of the sample (α_2 in my

Table 3.1: Input parameters for simulation (ALTUGLAS, 1987) in Figure 2.1 and 2.2. Parameters for anelasticity, η are given for linear rheology.

Standard (Aluminum)		Sample (Plexiglas)	
Parameter	Value	Parameter	Value
H_1	0.080m	H_2	0.250m
R_1	0.033m	R_2	0.076m
ρ_1	2700kg/m^3	ρ_2	1180kg/m^3
ν_1	0.334	ν_2	0.35
μ_1	26.0GPa	μ_2	1.15GPa
E_1	70.0GPa	E_2	3.10GPa
$\eta_{E,1}$	0Pa$\cdot$s	$\eta_{E,2}$	2.02MPa$\cdot$s
$\eta_{\mu,1}$	0Pa$\cdot$s	$\eta_{\mu,2}$	0.82MPa$\cdot$s
$\eta_{K,1}$	0Pa$\cdot$s	$\eta_{K,2}$	0.54MPa$\cdot$s

notation) and standard (α_1). This phase lag is conventionally expressed through its tangent (Lakes, 2009). In our numerical experiment, the key observed quantity therefore is:

$$\tan\phi = \text{Arg}\left(\frac{\alpha_2}{\alpha_1}\right). \tag{3.1}$$

Figure 3.4 shows the response of the phase lag between the sample and standard for a broad range of driving frequencies from 1 Hz to 6 kHz. As I show below, for realistic levels of dissipation within the specimen, the oscillations are over-damped, as it is likely typical in similar measurements. Under such conditions, the phase lag increases close to linearly below the fundamental-mode frequency of the system, after which it starts decreasing (Figure 3.4).

The low-frequency limit is most important in practical measurements, as seismic frequencies are far below the natural frequency. For example, in our 15-cm long Plexiglas example, the natural frequency is about 750 Hz for torsion, and in experiments with smaller rock samples they are much higher. Given our general inverse problem (2.9), and the expression for $\mathbf{K}^{-1}$ (2.11), the phase lag results for torsion and tension are:

$$\tan\phi_{\text{comp}} = \frac{\eta_E}{E}\omega \quad \text{and} \quad \tan\phi_{\text{tors}} = \frac{\eta_\mu}{\mu}\omega, \tag{3.2}$$

where E is the Young's modulus, $\eta_E = \eta_K(1-2\sigma)^2 + 4/3\eta_\mu(1+\sigma)^2$ and σ is Poisson's ratio. The
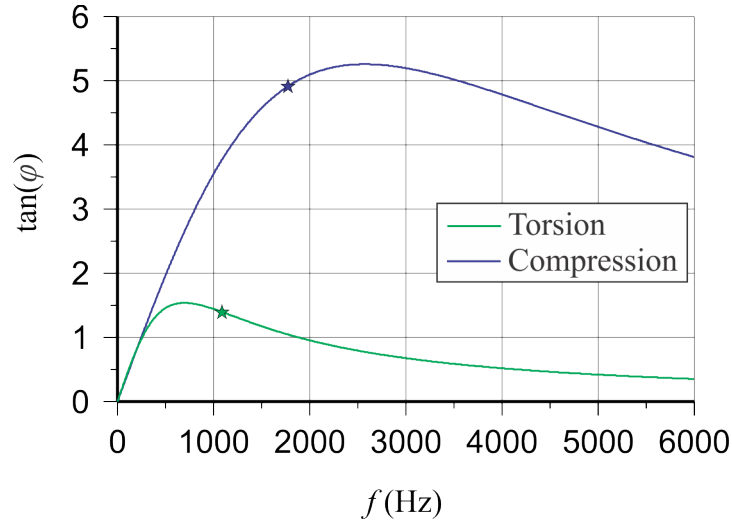
Figure 3.4: Tangents of phase lags for torsional and longitudinal deformations as functions of driving frequency, f. Asterisks ($*$) indicate the resonant frequencies.

low-frequency linear trends shown by numerical simulations in Figure 3.4 are clearly shown in Figure 3.5. Notably, these phase lags for longitudinal deformations (eq. 3.2) are independent of the dimensions of the standard and rock specimen. This makes these lags relatively reliable estimators of the intrinsic energy-dissipation parameters of the rock. However, these phase lags also depend on the frequency of the external force driving the oscillations. Thus, medium viscosity corresponds to the magnitude of phase lags, whereas their frequency dependence is explained by the rheologic exponent ν. In the present case of $\nu = 1$, this frequency dependence is linear.

3.1.2 Forced oscillations near resonance

Another method of assessing the anelastic properties of a rock specimen is by measuring the width of the resonance peak of the squared amplitude of deformation under forced oscillation ($\Delta\omega$ in eq. (1.35) on page 25). A standard is not required to measure resonant peaks, and for one cylinder, the equations simplify considerably. In the following, I will be specifically interested in the dependences of various quantities on the solid viscosity and the length of the cylinder, H.

Kinetic energy, potential energy and dissipation functions for a single cylinder undergoing tensional or torsional stress are given in Appendix A. For weak damping, the value of ω_0 can be
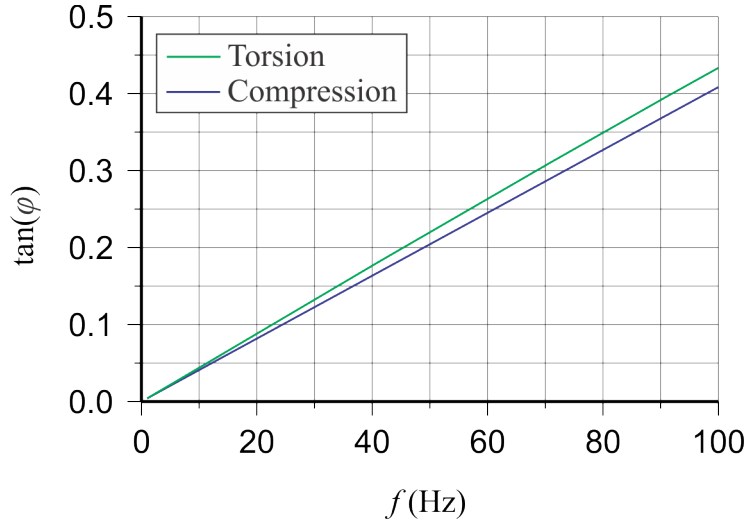
Figure 3.5: The linearity of the low-frequency limit. The input parameters are given in Table 3.1.

derived from the equipartioning of energy, which requires $T = V$:

$$\omega_0 = \sqrt{\frac{E}{I}}. \tag{3.3}$$

where E is the Young's modulus and I is a mass parameter which can be found in Appendix A. An expression for $\Delta\omega$ can be determined by solving for ω at half-maximum of the power spectrum:

$$\Delta\omega = \frac{\eta_E}{I}. \tag{3.4}$$

Combining eqs. (3.3) and (3.4) gives an expression for the spectral quality factor:

$$Q_{\text{spec}} = \frac{\sqrt{IE}}{\eta_E}. \tag{3.5}$$

Expressions for Q_{spec} for both torsional and compressional modes are explicitly written in terms of system parameters below:

$$Q_{\text{spec,t}} = \frac{\sqrt{\frac{1}{3}\rho\mu}}{\eta_\mu}H \quad \text{and} \quad Q_{\text{spec,c}} = \frac{\sqrt{\frac{1}{3}\rho\left(1 + \frac{3R^2}{2H^2}\sigma^2\right)E}}{\eta_E}H. \tag{3.6}$$

Figure 3.6 illustrates the effect of varying the length of the sample on Q_{spec}. Unlike for the phase-

50
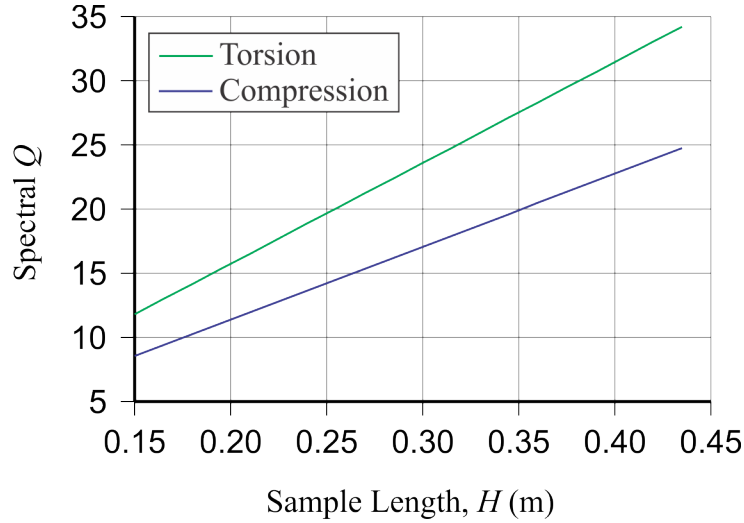
Figure 3.6: Spectral Q simulations for various sample lengths show a linear relationship between spectral Q and sample length. The compressional mode includes a very small non-linear term by virtue of the geometry. $\eta_E = 0.163\text{MPa}\cdot\text{s}$, $\eta_\mu = 0.072\text{MPa}\cdot\text{s}$.

lag Q at low frequencies, the length and radius of the cylindrical specimen affects Q_{spec}. For all experiments, spectral Q is: 1) nearly proportional to the length of the body, 2) proportional to the square root of the respective (Young's or shear) elastic modulus and density, and 3) inversely proportional to the appropriate solid viscosity. Additionally, for compressional experiments, an additional dependences on the radius, sample length, Young's modulus, and the Poisson's ratio are present (eq. (3.5)).

3.1.3 Static creep

In creep experiments, a constant force is applied to the sample, and the resulting deformation is measured as a function of time. The Lagrangian formulation above is equally applicable to this case, with the difference from the above phase-lag calculation being in using a constant external force switching on at time $t = 0$. Also, creep experiments do not require an elastic standard in series with the sample, and therefore the problem can be considered with only one cylinder.

As shown in eqn. (2.11) using the matrix expressions for energies and dissipation functions (Appendix A) for axial compression and extension of the cylinder, the equation of motion is:

$$I\ddot{\alpha} + \eta_E\dot{\alpha} + E\alpha = \tilde{F}, \tag{3.7}$$

51
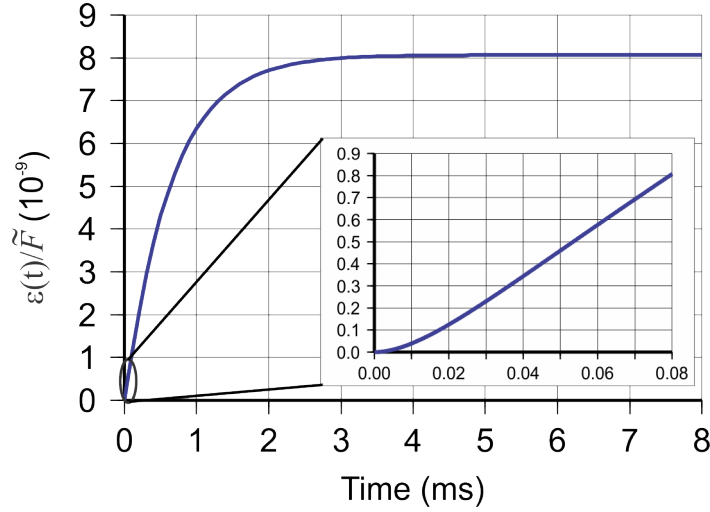
Figure 3.7: Linear creep response (eq. (3.8)). What appears to be high velocity at $t = 0$ is in fact rapid acceleration shown on inset. In the linear regime, the applied force only changes the magnitude of deformation, and not the "relaxation time" of the curve.

where $\tilde{F}$ is the generalized force equal the Newtonian force applied to the end of the cylinder divided by its volume: $\tilde{F} = F/(\pi R^2 H)$. Equation (3.7) is again the equation of a linear, damped harmonic oscillator. For a constant force, the solution can be written as:

$$\alpha(t) = \frac{\tilde{F}}{\omega_0^2}\left[1 - e^{-\beta\omega t}\left(\cosh\omega t + \frac{1}{\sqrt{1 - \frac{1}{\beta^2}}}\sinh\omega t\right)\right], \tag{3.8}$$

where $\omega_0 = \sqrt{E/I}$, $\beta = \frac{\eta_E}{2\sqrt{EI}}$, $\omega = \omega_0\sqrt{\beta^2 - 1}$ and $\beta > 1$. This solution is appropriate for the case of high viscosity, which leads to an over damped (non-oscillatory) behaviour. In the under-damped case, $\beta < 1$, and the hyperbolic functions in (3.8) become ordinary trigonometric functions. The deformation history predicted by eq. (3.8) is illustrated in Figure 3.7. Starting from the initial state of rest, the deformation quickly accelerates within time $\tau_1 \approx \omega^{-1}$ (Figure 3.7, inset), and then slowly decelerates over "relaxation time" $\tau_2 \approx (b\omega)^{-1} \gg \tau_1$. The exponential relaxation part of this dependence corresponds to the behaviour of the Kelvin-Voigt body (section 1.2.1). The initial stage of fast acceleration is caused by the finite mass of the specimen (i.e., by its natural oscillation) and has no analogues in the equivalent mechanical models of materials. Note that as mentioned in section 1.2.1, mechanical models assume massless internal variables, and consequently their initial responses are instantaneous. However, creep observations in the lab focus on relatively slow,

52

quasi-static processes, and the mass should not be a significant factor for their explanation.

3.2 Modelling Using Non-Linear Rheology

Experimental results (such as Tisato et al., 2010) indicate that the simple Newtonian (quadratic) viscosity is insufficient for explaining the observations. This was also noted in constructing early mechanical models of seismic attenuation by Knopoff (1964). In phase-lag measurements, near-constant dependences of $\tan\phi$ on ω are usually found, often decreasing with ω (Faul et al., 2004) and sometimes showing spectral peaks (Figure 3.2). In creep observations, a segment of fast, "instantaneous" deformation (often referred to as "static" or "elastic") is usually seen. This segment is only weakly expressed in the deformation of a Newtonian (Kelvin-Voigt) body (Figure 3.7). In the following, I try achieving these effects by considering two new mechanisms of dissipation: 1) non-Newtonian viscous friction, and 2) thermoelastic effects. This requires a non-linear treatment of dissipation and incorporation of thermodynamics.

3.2.1 Sub-resonant forced oscillations

The resultant phase lags from solving eqn. (2.26) with dissipation function (2.25) are given by:

$$\tan\phi = \frac{\eta_{\text{eff}}^{\phi}}{M}\omega^{2\nu-1}, \tag{3.9}$$

where η_{eff}^{ϕ} is the phase-lag effective viscosity (see Appendix A for expressions for both tensional and torsional cases) and M is the elastic modulus (Young's for tension and shear for torsion). The effective viscosity is an important quantity determined from the approximate dissipation function in eq. (2.25) and is generally dependent on strain α. The expression for phase-lag effective viscosity for a longitudinal system is as follows:

$$\eta_{\text{eff}}^{\phi} = 2\nu\alpha^{2\nu-2}\left\langle\cos^{2\nu}y\right\rangle\eta_{nl},$$
$$\text{where} \quad \eta_{nl} = \frac{1}{2^{\nu-1}}\left[\eta_K(1-2\sigma)^{2\nu} + \frac{2^{\nu+1}}{3^{\nu}}(1+\sigma)^{2\nu}\right]. \tag{3.10}$$

In experiments with lab samples, the empirical frequency-dependent modulus G is defined as the ratio of the magnitude of the stress to strain, $G = |\sigma/\varepsilon|$ (for example, Figure 3.1 from Lakes,
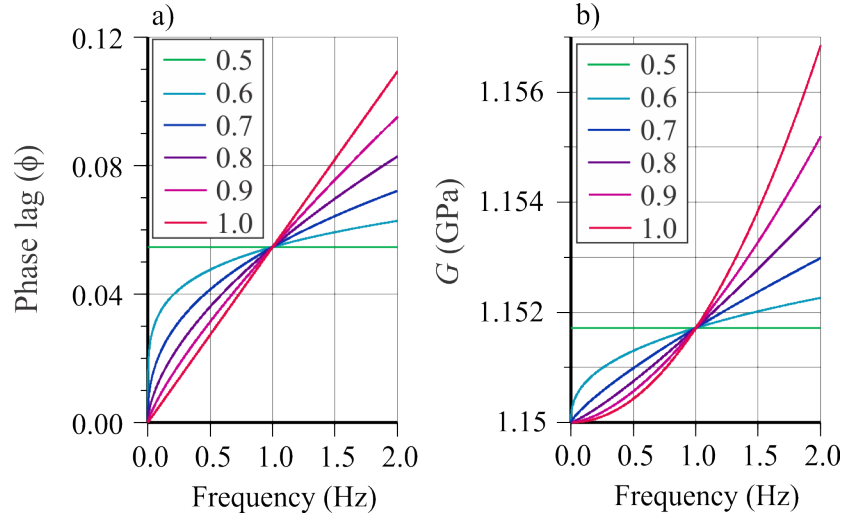
Figure 3.8: a) Phase-lag results for varying powers. Insets show the values of power-law exponents ν. A power of 1.0 corresponds to linear "Newtonian" dissipation and $\tan\phi$ is proportional to frequency. A power of $\nu = 0.5$ corresponds to "dry friction" and $\tan\phi$ for this ν is frequency-independent. b) Frequency-dependent modulus G for varying ν.

2009). This quantity can also be measured from $\tan\phi$ as follows:

$$G = M\sqrt{1 + \tan^2\phi} = M\sqrt{1 + \left(\frac{\eta_{\text{eff}}^{\phi}}{M}\omega^{2\nu-1}\right)^2}. \tag{3.11}$$

For purely elastic materials with $\eta_{\text{eff}}^{\phi} = 0$, $G = M$, and the measured stress to strain ratio equals the frequency-indepenent elastic modulus. However, for anelastic materials, the strain to stress ratio will generally be frequency dependent. Curves for $\tan\phi$ and G for my non-linear model with $0.5 \leq \nu \leq 1.0$ are given in Figure 3.8. To facilitate their comparison, viscosities η in this Figure were selected so that the "effective viscosity" (Appendix A) is the same at 1 Hz for all ν values. As Figure 3.8b shows, the dependence of $\tan\phi$ and G on frequency reduces for smaller ν. For "dry" friction ($\nu = 0.5$), the resulting phase lag and empirical modulus are constant with frequency.

3.2.2 Forced oscillations near resonance

Similar to linear mechanical systems, systems with weak non-linear dissipation produce resonant peaks from which Q values can be measured. For a single-cylinder system, the scalar equation of

motion for the deformation of the cylinder, α, is similar to (2.26):

$$\alpha = \left(-\omega^2 T + i\omega\tilde{D} + V\right)^{-1} F,$$ (3.12)

where expressions for $T, \tilde{D}$ and V are given in Appendix A. It is important to note that the dissipation parameter, $\tilde{D}$, is determined by using the approximation in (2.25). The quality factor of the resonance, Q, is determined as the ratio of resonance frequency to peak width (1.35). The resonance frequency is the same as (2.10) ($\omega_0 = \sqrt{E/I}$), whereas the peak width, $\Delta\omega$, is given by:

$$\Delta\omega = \frac{\eta_{\text{eff}}^{res}(\omega_0)}{I} = \frac{\eta_{\text{eff}}^{\phi}\omega_0^{2\nu-2}}{I}.$$ (3.13)

Note that generally, η_{eff}^{res} is a function of ω. If we evaluate η_{eff}^{res} at ω_0, the expression for resonant Q becomes:

$$Q = \frac{\omega_0}{\Delta\omega} = \frac{I\omega_0}{\eta_{\text{eff}}^{\phi}\omega_0^{2\nu-2}} = \frac{E}{\eta_{\text{eff}}^{\phi}}\left(\frac{E}{I}\right)^{\frac{1-2\nu}{2}} \propto \alpha^{2-2\nu}$$ (3.14)

The non-linear rheology thus predicts a dependence of Q on strain amplitude, which is absent for linear rheology (3.5).

However, the nature of the non-linear rheology amplitude spectrum is such that if a suitable viscosity is selected, even for the same strain, the linear rheology amplitude spectrum can be reproduced at least near the peak (Figure 3.9a). As shown in Figure 3.9b, the shape of the spectrum does indeed differ for non-linear rheology.

The effective non-linear viscosity η_{eff} (eq. 3.10) possesses a dependence on strain amplitude, α, and therefore a series of experiments carried out at different deformation amplitudes could give an insight into the behaviour of materials with such properties. Figure 3.10 shows an example of the spectral Q in a dissipatively non-linear material changing as a function of deformation amplitude. As the cylinder is driven by progressively stronger forces, the spectral quality factor increases due to a decrease in the "effective" viscosity (η_{eff}^{ϕ} eq. 3.10). This increase in Q occurs despite the material viscosities η_{μ} and η_K remaining constant.

At present, it is unclear how strongly the non-linear effects modeled above are represented in real materials. Some experiments, for example resonance curves in PVC (Figure 1.19 section 1.4.4), show linearity in dissipation - as the driving force is increased, the spectral Q remains
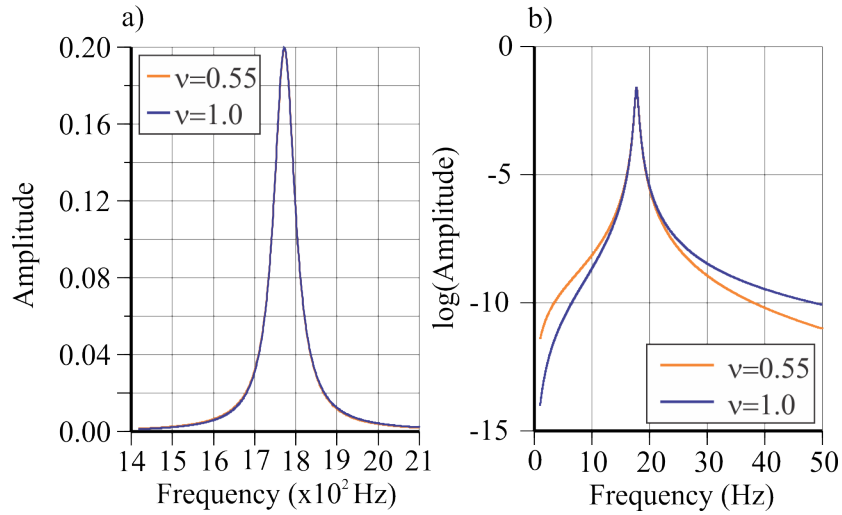
Figure 3.9: a) Non-linear and linear rheologies producing similar amplitude spectra near resonance. The non-linear rheology ($\nu = 0.55$) has $\eta_\mu = 98$ Pa·s while the linear rheology has $\eta_\mu = 4100$Pa·s. b) A log plot of spectra over a larger frequency band to show the divergence away from the peak.
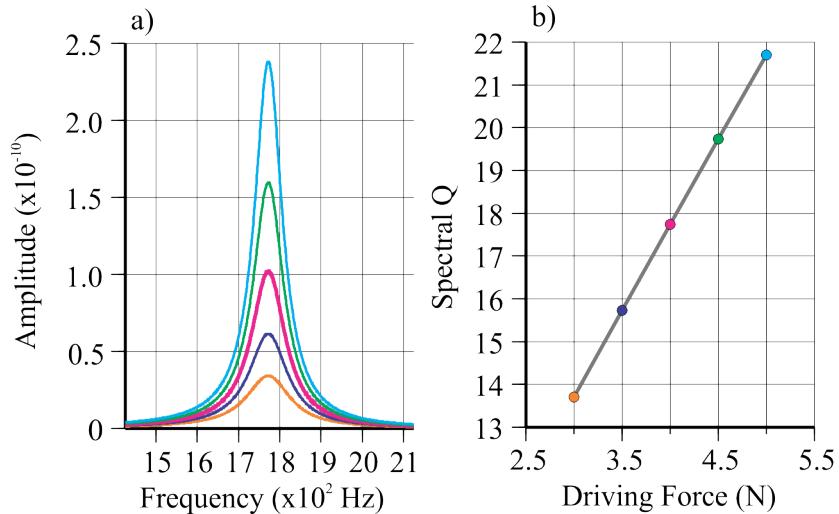
Figure 3.10: Variation of attenuation with amplitude for non-linear solid viscosity with $\nu = 0.55$, $\eta_\mu = 200$: a) Resonance peaks at different amplitudes of driving forces (colours); b) Measured spectral Q's as functions of driving force. As ν approaches 1, the spectral Q becomes near-constant.

constant. Interestingly, non-linearity of my model with respect to strain amplitude can be easily removed from the above model while keeping the non-linear dependence on strain rates. This modification is briefly described in the Discussion. At he same time, experiments in sandstones (Figure 1.20) suggest a non-linearity at deformations $\sim 10^{-6}$. Finally, it appears that the observed weak frequency-independence of Q for body seismic waves can only be explained by non-linear dissipation (Knopoff, 1964).

3.2.3 Static creep

For power-law rheology (3.7), the equation of motion is:

$$I\ddot{\alpha} + \eta_{\text{eff}}^c \dot{\alpha}^{2\nu-1} + E\alpha = I\tilde{F}, \tag{3.15}$$

where η_{eff}^c is the effective viscosity for creep (eq. 2.20; table B.1). When $\nu = 1$, this is simply the equation of a damped, driven linear harmonic oscillator (3.7) in which $\eta_{\text{eff}}^c = \eta_E$.

For a constant external force, the general equation of motion for a one-cylinder system with power-law D (3.15) can be solved differently in two end-member cases. Similarly to the case of linear creep (Figure 3.7), the system will quickly accelerate from the state of rest, after which it will slowly deform quasi-statically. For the second of these regimes, we can approximate the acceleration as negligibly small. Setting $\ddot{\alpha} = 0$, equation (3.15) becomes a separable first-order equation:

$$\frac{d\alpha}{dt} = \left[\frac{I}{\eta_{\text{eff}}^c} \left(\frac{\tilde{F}}{I} - \omega_0^2 \alpha \right) \right]^\kappa, \tag{3.16}$$

where $\kappa = 1/(2\nu - 1)$, $\omega_0^2 = E/I$ and $\tilde{F} = F/(\pi R^2 HI)$. This expression means that the rate of residual deformation $\alpha_R = \tilde{F}/\omega_0^2 - \alpha$, is a power of the deformation itself:

$$\dot{\alpha}_R = -\left(\frac{E}{\eta_{\text{eff}}^c} \right)^\kappa \alpha_R^\kappa. \tag{3.17}$$

In lab measurements, the characteristic "relaxation time" is often measured by relating the residual deformation to its rate of decrease: $\tau_R = -\alpha_R/\dot{\alpha}_R$ (Chopra, 1997). In our case, this ratio gives:

$$\tau_R = \left(\frac{\eta_{\text{eff}}^c}{E} \right)^\kappa \alpha_R^{1-\kappa}. \tag{3.18}$$
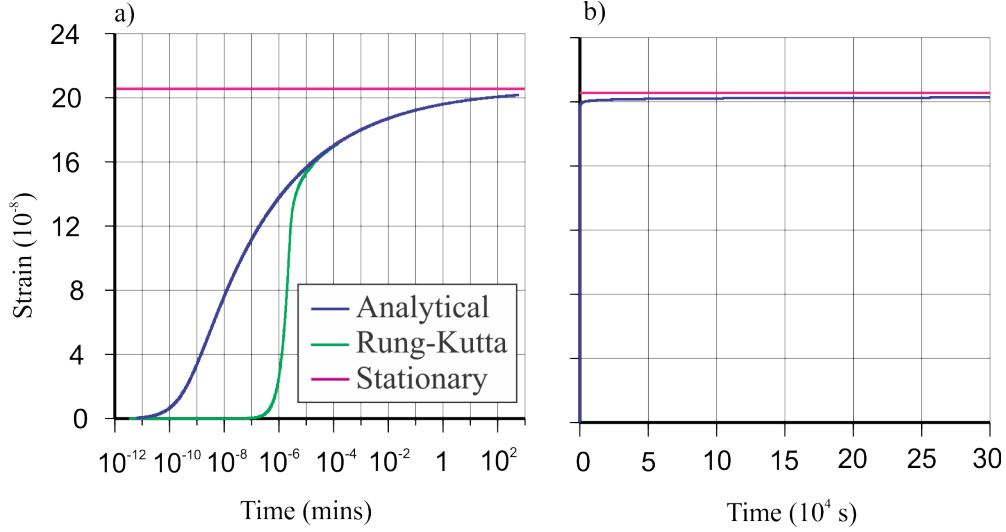
Figure 3.11: Model of creep with power-law dissipation with $\nu = 0.56$ (Table 3.1): a) Comparison of the approximate analytical and Runge-Kutta solutions on a log time scale. The effect of the mass occurs at very short time scales (less than 10^{-5} minutes; green), after which the solution approaches the analytical approximation (blue curve). b) On a linear time-scale plot, the deformation appears to be a large "instantaneous" response followed by a very slow creep towards stationary level.

Thus, the characteristic relaxation time measured on a body with power-law solid viscosity increases with increasing viscosity and also with strains approaching the equilibrium level. For a fixed α_R, (i.e., measuring the times of approaching a certain level of deformation), the relaxation time is proportional to $\tau_R \propto \left(\eta_{\text{eff}}^c/E\right)^\kappa$. Therefore, if we want to maintain τ_R matching the observed relaxation times while varying ν, we need to adjust the effective viscosity accordingly.

With an appropriate substitution, the full solution to (3.16) is:

$$\alpha(t) = \frac{\tilde{F}}{\omega_0^2} - \left[\left(\frac{\tilde{F}}{\omega_0^2}\right)^{1-\kappa} + \left(\frac{E}{\eta_{\text{eff}}^c}\right)^\kappa (\kappa-1)t\right]^{\frac{1}{1-\kappa}}. \tag{3.19}$$

This expression gives the asymptotic solution for long deformation times. For short times, a solution of (3.15) can be obtained numerically. I used the 4$^{\text{th}}$ order Runge-Kutta scheme (Butcher and Wiley, 2003) to provide the initial parts of the creep curves and to measure the significance of the mass term $I\ddot{\alpha}$ (Figure 3.11).

Figure 3.11b shows that non-linear dissipation is capable of producing what appears to be a near-instantaneous deformation followed by slow creep. For smaller ν values, this separation into
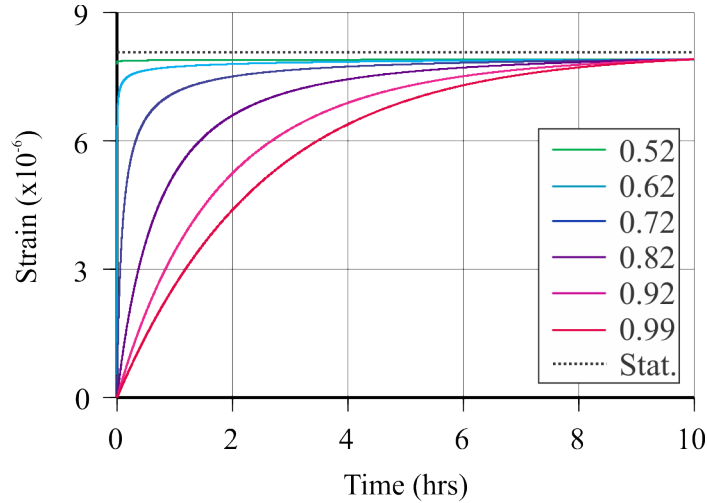
Figure 3.12: Creep curves for non-linear rheology. Inset shows the values of ν. For each ν, η^c_{eff} is selected so that 98% of the stationary deformation is reached in 10 hours (see table 3.2). Note that for $\nu = 0.52$, the strain appears to be almost constant after a large "instantaneous" jump.

Table 3.2: Non-linear rheology effective viscosities that lead to a 10-hr relaxation time (Figure 3.12).

ν	$\eta^{\mathbf{c}}_{\text{eff}}(\mathbf{Pa \cdot s})$
0.52	1.61×10^3
0.62	3.49×10^5
0.72	5.49×10^7
0.82	6.84×10^9
0.92	7.27×10^{11}
0.99	2.73×10^{13}

"fast" and "slow" deformations is much stronger than for linear rheology (Figure 3.7). While the "fast" response is rigorously non-instantaneous, it appears as such within typical observation time scales, which are often specified as the times at which the deformation reaches some characteristic level (for example, 98%; Chopra, 1997). At the same time, completely instantaneous "elastic" responses assumed for equivalent models (e.g., Burgers body; section 1.2.1) are also impossible because of the effects of finite mass in real media.

Figure 3.12 compares several non-linear creep curves having approximately the same relaxation times (3.18) at 98% deformation. As we see, with increasing ν, the initial fast stage of deformation takes longer times, because of increased effective viscosity.

59
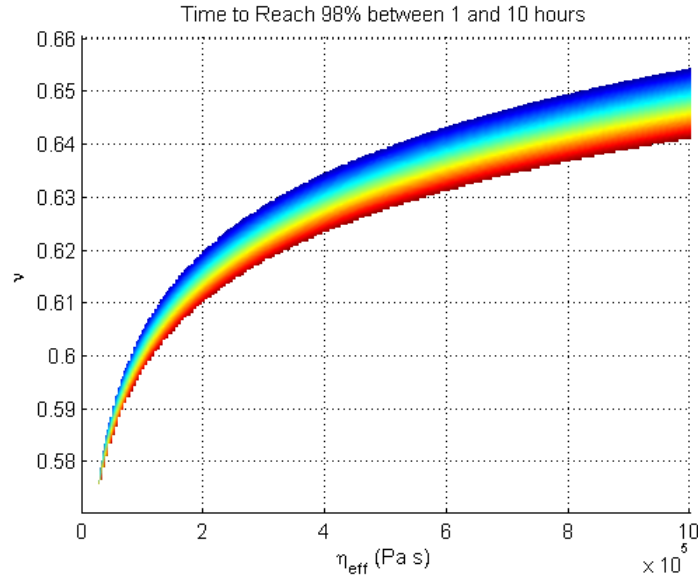
Figure 3.13: Combinations of ν and η_{eff} that yield 98% relaxation rates between 1 (blue) and 10 (red) hours.

In Figure 3.13, the above relation for relaxation time (3.18) is illustrated numerically. For different η and ν, colours in this plots show the times in which the deformation of the cylinder reaches 98% of its asymptotic (stationary) level. The range of values shown (1 to 10 hours) corresponds to typical creep times measured in Earth materials. Note that only a narrow range of ν from 0.58 to 0.66 is shown. Extending this relationship to larger ν shows that in order to achieve characteristic times in the $\sim$1-hour range for near-Newtonian viscosity ($\nu \approx 1$), viscosity values around 9 orders of magnitude higher ($\sim 10^{13}$ Pa·s) would be required (Table 3.2). Such viscosities are usually reported for Burgers' models for rock specimens (Chopra, 1997).

3.3 Combined Viscosity and Thermoelastic Model

The non-linear rheology proposed in section 2.1.2 is unable to produce a phase-lag decreasing with frequency; at best it can produce a phase lag that is constant with frequency. However, phase-lag observations in materials (Tisato et al., 2010; Lakes, 2009; Faul et al., 2004) often show phase lags decreasing with frequency. From section 2.3, the only physical mechanism likely to produce phase lags decreasing with frequency is thermoelasticity.[2] Therefore, I try using a combination of

---

[2]Another possible mechanism that could reduce Q^{-1} with frequency is scattering and variations of geometric spreading (Morozov, 2008, 2010a, 2011f). However, this mechanism is unlikely significant for lab samples and is
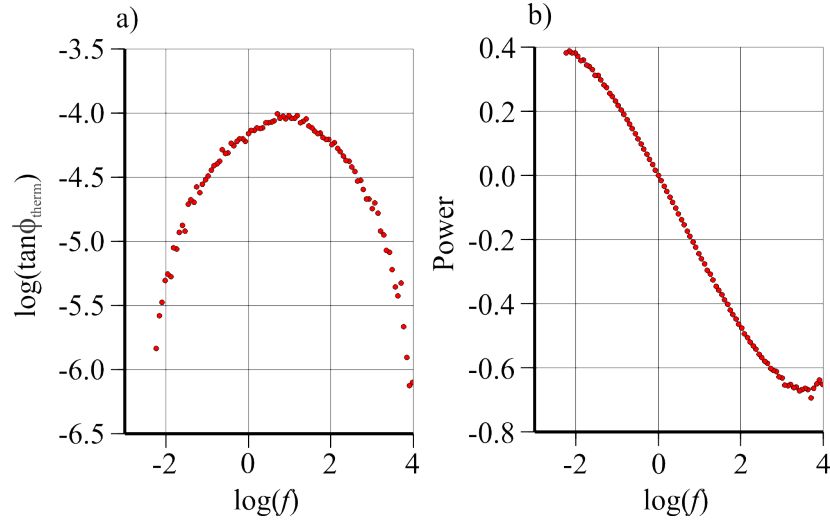
Figure 3.14: Isolation of thermoelastic peak by removing non-linear viscosity ($\nu = 0.5020$, $\eta_{\text{eff}} = 0.18\text{GPa·s}$). a) log-log plot of the isolated thermoelastic peak b) slope of a). The slope corresponds to the power of frequency.

non-linear rheology and thermoelasticity (section 2.3) to produce a model that accounts for these two major sources of energy dissipation.

The final model form is proposed by phenomenologically combining the non-linear viscosity and thermolelastic effects:

$$\tan\phi = \frac{\eta_{\text{eff}}}{M}\omega^{2\nu-1} + \begin{cases} A\omega & \text{for } \omega < \omega_{\text{peak}}, \\ \frac{B}{\sqrt{\omega}} & \text{for } \omega > \omega_{\text{peak}}, \end{cases} \tag{3.20}$$

where A and B are constants related to the thermoelastic effect. Note that for thermoelasticity, we only have the asymptoptic behaviour of dissipation and consequently, there is no rigorous theoretical model for the transition between "high" and "low" ω. It is possible that the frequency range in the data from Tisato et al. (2010) lies entirely in a transition between the two end-members of thermal relaxation: 1) $\tan\phi_{\text{therm}} \propto \omega$ and 2) $\tan\phi_{\text{therm}} \propto \omega^{-0.5}$ (section 2.3).

Assuming that the asymptotic behaviour at low frequencies is linear with ω and at high frequencies is proportional to $\omega^{-0.5}$, we can try describing it in between these limits as $A(p)\omega^p$, where $-0.5 \leq p \leq 1$. If we investigate the data in log-log scales, the points in which the asymptotic regimes begin to dominate can be determined. Taking the logarithm of recorded dissipation power,

---

generally subject to controversy (Morozov, 2009), and consequently not considered here.

61
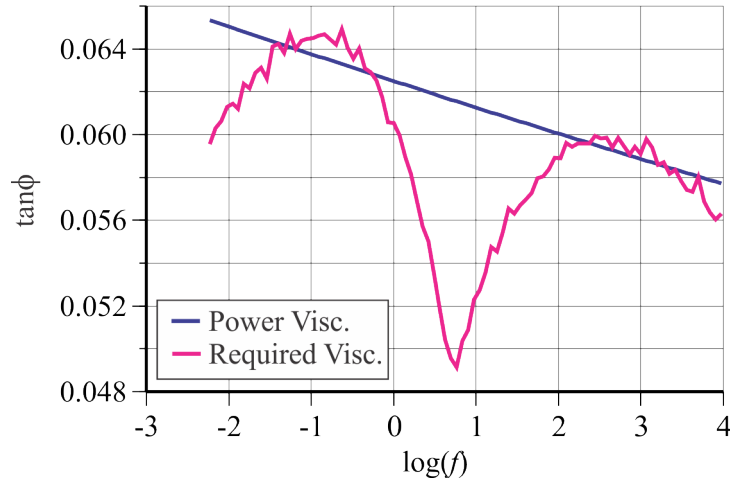
Figure 3.15: Required non-linear dissipation describing the data by Tisato (2011) assuming an idealized thermoelastic peak in (3.20). The blue line shows a power-law rheology with $\nu = 0.49$. Middle frequencies were disregarded in this fitting because the behaviour of thermoelasticity at intermediate frequencies is uncertain.

Figure 3.14b) shows the power of the thermoelastic peak varies from ∼0.4 to ∼-0.65. There seems to be "asymptotic" regions at the low- and high-end of the frequency spectrum where the power flattens out. Of course, this model is only empirical and approximate, and in reality, both the viscous and thermoelastic effects differ from the idealized asymptotics considered above. According to the two thermoelastic end-member regimes (section 2.3), the asymptotic powers should be 1 and -0.5 for low and high frequencies, respectively. This discrepancy may be due to viscosity itself not behaving constantly over the entire frequency range, i.e., the viscosity differing from the simple power law (2.27). This could potentially explain the rise of dissipated power not being strong enough for the low frequencies and the drop being too strong for the higher frequencies.

Thus, I propose that Plexiglas data by Tisato (2010) can be explained by a "background" non-linear rheology with a thermoelastic peak superimposed over it. From the theory of the end-member regimes (section 2.3), a suitable paramter of ν of the background rheology can be estimated. Once this background non-linear rheology is removed, parameters of the remaining thermoelastic peak are constrained by considering its asymptotic regimes.

If we consider the thermoelastic peak to be of the exact form shown in (3.20), we can attribute the whole remaining frequency variation of dissipation to non-linear viscous friction. Figure 3.15 shows the non-linear rheology required for this. Unfortunately, this dependence is only presented as

an empirical variation of $\tan\phi$ with frequency, i.e. exactly as it is commonly done in the viscoelastic approach (section 1.2.4). According to the approach of this Thesis, $\tan\phi(\omega)$ is only an apparent quantity requiring physical explanation in terms of physical properties, such as the non-linearity of dissipation. Nevertheless, an appropriate function $D(\varepsilon, \dot{\varepsilon})$ can apparently be constructed to reproduce this behaviour of $\tan\phi(\omega)$. I do not attempt this here because the shape of the thermoelastic peak (3.20) used above is only a crude approximation. This can especially be seen from the sharp apparent notch in $\tan\phi$ near $\log(\phi) \approx -0.3$ (Figure 3.15).

CHAPTER 4

DISCUSSION AND CONCLUSIONS

In this chapter, I will outline the major findings of this thesis. Determining what properties of internal friction are *intrinsic* to the material and thus qualify as real physical quantities will be discussed based on the frequency dependence of Q and sample dimension dependence of Q. Power-law rheology will be shown to be a physical model that doesn't rely on the existence of hidden variables capable of producing the observed features of anelastic creep or frequency dependent phase-lags.

Finally, I will discuss the findings related to thermoelasticity emphasizing that it can both be an artifact of experimental design and intrinsic to the material, although not purely mechanical in nature.

4.1   Frequency Dependence of Q

In the viscoelastic model, the shapes of the $\tan\phi$ curves shown in Figure 3.2 (on page 54) (Lakes, 2009; Tisato et al., 2010) are explained empirically by a frequency dependence of the material's Q (Jackson and Paterson, 1993; Lakes, 2009). We are interested in determining viscous parameters that are intrinsic to the specimen, that is independent of sample dimensions and frequency of oscillation much the same as the elastic modulus, Poisson ratio and density. While the apparent Q is clearly frequency dependent (Figure 3.2) - it is not an intrinsic property of the specimen. However, the above results (section 3.1.2) indicate that for our "linear" rheology (2.5), phase-lags (3.2) or Q^{-1} (1.37) should increase linearly with frequency within the seismic band. It appears that not the phase lags themselves but rather their derivatives with respect to ω represent the stable and important intrinsic parameters of the specimen. In our interpretation, these parameters are the ratios of solid viscosities to the corresponding elastic moduli.

Figure 3.5 shows the linearity of $\tan\phi(\omega)$ with respect to f for low frequencies. Let us assume that the slopes $m = d\tan\phi/df$ in such plots are measured for the same specimen and try deriving the solid viscosities from them. From eq. (3.2), these slopes equal:

$$m_{\text{tors}} = 2\pi\frac{\eta_\mu}{\mu} \quad \text{and} \quad m_{\text{comp}} = 2\pi\frac{\eta_E}{E}. \tag{4.1}$$

The subscripts "2" were dropped here, as it is understood that the moduli and viscosities above are those of the sample and not the standard. If the bulk viscosity parameter $\eta_K = 0$, the ratio of these slopes $\beta = m_{\text{tors}}/m_{\text{comp}}$ should only depend on the Poisson's ratio of the specimen, σ:

$$\beta_{\eta_K=0} = \frac{3}{2(1+\sigma)}. \tag{4.2}$$

Note that $\beta \geq 1$. In the general case of $\eta_K \neq 0$, because the slopes m_{tors} and m_{comp} linearly depend on η_K and η_μ, the solid viscosity parameters can be inverted from the observed m_{tors} and m_{comp} as:

$$\eta_\mu = \frac{\mu}{2\pi}m_{\text{tors}} \quad \text{and} \quad \eta_K = \frac{E}{2\pi(1-2\sigma)^2}\left[m_{\text{comp}} - \frac{2}{3}(1+\sigma)m_{\text{tors}}\right]. \tag{4.3}$$

Thus, the combination of torsional- and longitudinal testing results yields a way for determining both parameters of solid viscosity experimentally. First, η_μ can be determined directly from the slope of the torsional Q_{phase}^{-1} vs. f plot, and then η_K can be determined through eq. (4.3).

For non-linear power rheology (2.27), phase lags are no longer necessarily linear with frequency and range from ω^0 to $\omega^{1.0}$. The intrinsic property once again is not the quality factor, Q but the viscosity parameters, η_μ and η_K as well as the the power parameter, ν. The power parameter ν gives the most insight into the nature of the viscous process that a specimen possesses while the viscous parameter η would indicate the *amount* of that process. These parameters can be determined in much the same way as linear parameters. However, the frequency-invariant quantities will be derivatives with respect to $\omega^{2\tilde{\nu}-1}$ as opposed to ω in the linear case:

$$\frac{d\tan\phi}{d\omega^{2\tilde{\nu}-1}} = \frac{\eta_{\text{eff}}^\phi}{M}\frac{d\omega^{2\nu-1}}{d\omega^{2\tilde{\nu}-1}}. \tag{4.4}$$

If $\tilde{\nu} = \nu$, then $d\tan\phi/d\omega^{2\tilde{\nu}-1}$ should be constant with frequency and equal to the ratio of effective

viscosity to elastic modulus. The effective viscosity can then be inverted for the intrinsic parameters η_μ and η_K. Note that in the case of torsional experiments, η_{eff}^ϕ depends on sample dimensions (Appendix A).

4.2 Dependence on sample dimensions and experimental geometry

Our results show that dependences on sample dimensions arise in formulations of Q for resonance experiments. This is natural, as the spectral quality factor Q_{spec} depends on the resonant frequency of the specimen. The resonant frequency is highly dependent on the length of the specimen - longer specimens will have lower resonant frequencies and vice versa. The result is that spectral Q is nearly proportional to the length of the specimen. Because of this, Q_{spec} does not represent a direct measure of a property of the material.

Although this appears less practical for actual measurements, it is straightforward to show that slopes $m_{\text{tors}} = dQ_{\text{spec},t}/dH$ and $m_{\text{comp}} = dQ_{\text{spec},c}/dH$ can also be used for inverting for both of the viscosity constants η_K and η_μ:

$$\eta_\mu = \frac{\sqrt{\frac{1}{3}\rho\mu}}{m_{\text{tors}}} \quad \text{and} \quad \eta_K = \frac{\frac{m_{\text{tors}}}{m_{\text{comp}}}\sqrt{2(1+\sigma)\left(1+\frac{3R^2}{2H^2}\sigma^2\right)} - \frac{4}{3}(1+\sigma)^2}{(1-2\sigma)^2}. \tag{4.5}$$

Notice that η_K in eq. (4.5), also depends on sample dimensions - namely, the aspect ratio R/H. This dependence comes from longitudinal experiments only, and enters via the "mass" parameter, I:

$$I = \frac{\rho H^2}{3}\left[1+\frac{3}{2}\left(\frac{R}{H}\sigma\right)^2\right] \approx \frac{\rho H^2}{3}, \quad \text{for long thin cylinders.} \tag{4.6}$$

The quantity R/H is the aspect ratio and is small long thin cylinders (rods). Along with it being multiplied by the Poisson's ratio (σ, a quantity less than 1) and then squared, the effect of sample dimension is relatively weak.

For non-linear rheology, there also exists a dependence of spectral Q on sample dimensions. Linear rheology showed that spectral Q was linearly dependent on sample length, H but this de-
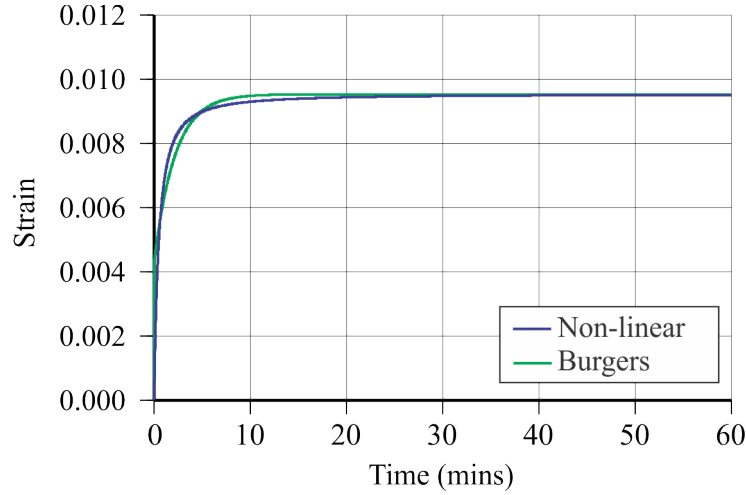
Figure 4.1: Non-linear creep approximating the anelastic part of Burgers'
model for Aheim dunite (Chopra, 1997). Non-linear model parameters are
$\nu = 0.79$, $\eta_\mu = 2.4$ GPa·s, and the Burger's model parameters are: shear
modulus $\mu = 15.75$ GPa and viscosity $\eta = 2040$ GPa·s.

pendence is generalized for non-linear rheology to $Q_{\text{spec}} \propto H^{2\nu-1}$:

$$\frac{dQ_{\text{spec}}}{dH^{2\nu-1}} = \frac{E}{\eta_{\text{eff}}^\phi} E^{\frac{1-2\nu}{2}} \left\{ \frac{\rho}{3} \left[1 + \frac{3}{2} \left(\frac{R}{H} \sigma \right)^2 \right] \right\}^{\frac{2\nu-1}{2}}. \tag{4.7}$$

The derivative will be near constant with sample length and equal to the ratio of elastic modulus
to effective viscosity as well as an additional dependence on elastic modulus and density which
vanish for near "dry" friction ($\nu \approx 0.5$). The effective viscosity can then be inverted for intrinsic
parameters η_μ and η_K. Note that for torsional experiments, η_{eff}^ϕ also has a small dependence on
sample dimensions (Appendix A).

4.3 The Nature of Non-Linear Rheologic Creep

As was shown in Figure 3.7 on page 60, creep curves for linear rheology produce no "instanta-
neous" deformation which is typically observed in experiments. Such instantaneous deformation is
often modelled using massless mechanical models such as Burgers' and SAS (section 1.2.1). While
non-linear rheology, strictly speaking, also produces no instantaneous response, it is nevertheless
capable of showing a very rapid response followed by slow creep towards the equilibrium level
(Figure 3.12).
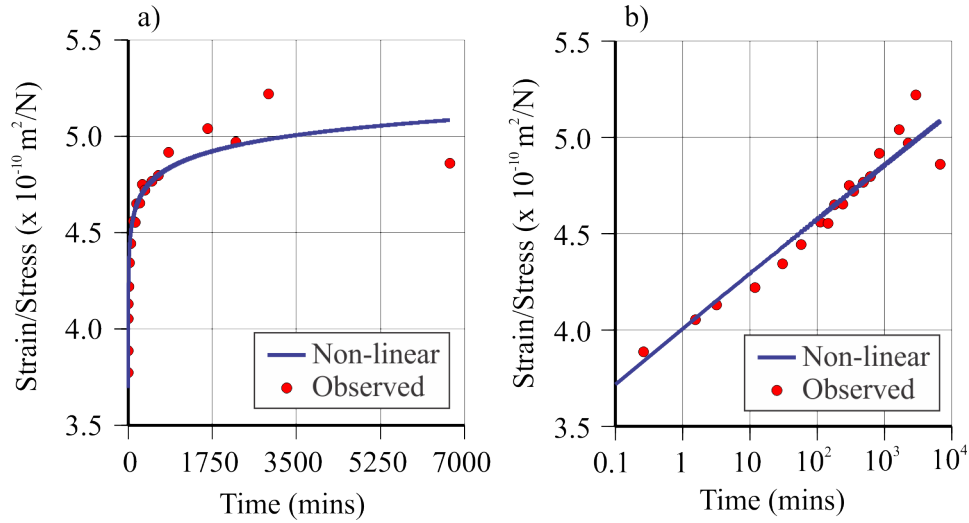
Figure 4.2: Experimental creep data for Plexiglas (red dots; McLoughlin and Tobolsky, 1952) fit by a non-linear rheology model ($\nu = 0.5023$, $\eta_\mu = 101$ GPa·s): a) Using a linear time axis while b) Using logarithmic time axis.

Figure 4.1 shows a comparison of non-linear creep with one of Burger's model for Aheim dunite by Chopra (1997) (Figure 1.14 in section 1.4.1). For this comparison, I removed the steady-state plastic response from Chopra's (1997) solution, thereby reducing the Burgers' body to a SAS body (section 1.2.1). It is clear that non-linear dissipation shows deformations close to the anelastic portion of Burger's models as well as near-instantaneous deformations. In this case, because the anelastic part of sample response is large compared to its "instantaneous" part, and the best-matching value of ν is larger (0.79). Because this value is still significantly below one, the non-linear solid viscosity parameter $\eta_\mu = 2.4$ GPa·s is much lower than the Burger's anelastic element $\eta = 2040$ GPa·s inverted by Chopra (1997).

Finally, I tried explaining the available creep data in Plexiglas (McLoughlin and Tobolsky, 1952; Figure 4.2) by using the non-linear dissipation model (Figure 3.12). In these data, there also appears to be a clear stationary flow at large times, which was removed assuming a constant plastic flow rate. The corrected experimental points (red dots in Figure 4.2) should therefore approximate only of the completely recoverable anelastic portion of deformation. Again, a reasonably good fit to these data can be obtained by using a near-dry internal friction of $\nu = 0.5023$ and solid viscosity of $\eta = 101$ GPa·s. It appears that these data could also be fit with a Burgers' model with relaxation time of about 20-25 min, as in Figure 4.1. Note that plotting in logarithmic time scale

suggests a relative acceleration of deformation after about $\sim$20 minutes (Figure 4.2b). This means that the deformation actually occurs somewhat faster than in our power-law relation (eq. 3.18). Two explanations can be suggested for this discrepancy: 1) the non-linear dissipation function in Plexiglas is not exactly power-law, and 2) unrecoverable changes, such as plastic flow, occur within the material, taking this case out of the scope of the purely anelastic model. Both of these reasons are likely to be the cause for creep measurements in Plexiglas, as well as in other materials.

4.4 Mechanisms of Thermoelasticty

The interpretation of the thermoelastic effect in section 3.3 was principally based on the observation that thermoelasticity is one of the most likely mechanisms explaining absorption peaks in the data. With increasing frequencies, the behaviour of thermoelastic dissipation changes from quickly increasing with frequency (similar to near-Newtonian viscosity) to much slower increase when "temperature waves" develop near grain boundaries (section 2.3). Thus, "grain size", h is the critical parameter controlling the frequency of thermoelastic dissipation peak.

The numerical value for h allows differentiating between the potential causes off thermoelastic losses. If h turns out comparable to the characteristic dimensions of the specimen and measurement device (several centimetres and larger), then it is likely that thermoelastic effects occur, for example, on the contacts of the specimen with the mounting harness and other parts of the apparatus. In contrast, if the frequency of the peak is higher and leads to h much smaller than dimensions of the apparatus, it is likely that thermoelastic effects occur on the internal structure of the material (in this case, more likely of the sample). It is of course also possible that even with small h, thermoelastic dissipation occurs within thin zones where the specimen is in contact with the surrounding environment; however, the magnitude of such thermoelastic dissipation should likely be weak. Thus, it is important to estimate the value of grain size from the observed frequency of the peak.

The grain size can be estimated from the observed frequency of the peak in $\tan\phi$ as follows (Morozov, 2012b). Consider the low-frequency limit $\omega \ll \vartheta/h^2$ first, where ϑ is the thermometric conductivity. At low frequencies, the entire grain volume participates in heat transfer, and the temperature T' within the grain is approximately spatially uniform. For a harmonic deformation in time ($\Delta \propto \cos(\omega t)$) the average heat production rate by deformation per unit volume equals

$\dot{T}'_0 C_V - \omega T'_0 C_V$, where the adiabatic temperature perturbation due to dilatational deformation Δ is (Landau and Lifshitz, 1976a):

$$T'_0 = -\frac{T K_A \alpha}{\rho C_p} \Delta. \tag{4.8}$$

The heat dissipated by conduction equals $\mathrm{div}\mathbf{q} = \kappa \Delta T' \approx \kappa T'/h^2$. By equating these two quantities, Morozov (2012b) showed that the temperature variation is proportional to frequency and strain:

$$T' \approx T'_0 \omega \frac{h^2}{\vartheta}. \tag{4.9}$$

and the energy dissipation rate behaves as Newtonian viscosity:

$$-\dot{E}_{\mathrm{mech}} = \eta_{\mathrm{thermo}} V \Delta^2 \omega^2, \tag{4.10}$$

where V is the volume of the body, and the effective viscosity equals:

$$\eta_{\mathrm{thermo}} = \frac{\kappa}{T}\left(\frac{T'_0 h}{\vartheta \Delta}\right)^2 = \frac{T}{\kappa} K_A^2 \alpha^2 h^2. \tag{4.11}$$

For polycrystalline metals, Landau and Lifshitz (1976a) point out that this quantity is much larger than the viscosity of the grains. Note that this viscosity quickly increases with grain size. The corresponding phase lag is:

$$\tan\phi = \frac{\eta_{\mathrm{thermo}}}{K}\omega. \tag{4.12}$$

For "fine-grained" Plexiglas at room temperature, the effective low-frequency thermoelastic viscosity is low and close to the observed level ($\tan\phi \approx 0.01$ at ~ 1 Hz).

At intermediate frequencies ($\vartheta/h^2 \ll \omega \ll c/h$), mechanical-energy dissipation occurs within layers of thickness $\delta \approx \sqrt{\vartheta/\omega}$ near structural contrasts and boundaries. Taking this value as comparable to the characteristic dimension of the problem, we can estimate (Morozov, 2012b): $\omega_0 \approx \vartheta/h^2$ for dissipation in a medium with spherical heterogeneities of radius h and $\omega_0 \approx \vartheta/R^2$ for thermoelastic dissipation in a uniform cylindrical specimen of radius R. The corresponding phase lags are (*ibid*):

$$\tan\phi \approx \frac{6}{\omega h \delta}\frac{\kappa T \alpha^2 K}{(\rho C_p)^2} \quad \text{for grainy cylinder}, \tag{4.13}$$

$$\tan\phi \approx \frac{2}{\omega R\delta} \frac{\kappa T\alpha^2 K}{(\rho C_p)^2} \quad \text{for uniform cylinder.} \tag{4.14}$$

For a given the frequency of the dissipation peak, ω_0, the corresponding grain size (or cylinder radius) can be estimated by making the above low-frequency and high-frequency expressions meet at ω_0. Although none of these equations are valid in the vicinity of point $\omega = \omega_0$, this extrapolation seems to produce reasonable estimates, and it also creates a continuous $\tan\phi(\omega)$ curve. Equating (4.12) and (4.14) at frequency ω_0, we obtain:

$$h = \frac{1}{\sqrt{\omega_0}} \left[\frac{6\kappa^2}{\sqrt{\vartheta}\,(\rho C_p)^2} \right]^{1/3}. \tag{4.15}$$

For polycrystalline olivine at mantle conditions, Morozov (*ibid*) estimated $h \approx 16$ mm. Note that this is close to the grain size expected within the upper mantle (Karato and Wu, 1993). For a ~ 2.5 Hz spectral peak in Plexiglas at ambient conditions, the same estimate gives $h \approx 0.15$ mm. This grain size appears to be probable in the experiment. Such small value of h suggests that the thermoelastic effect is caused the graininess of the material and not by the effects related to the edges and dimensions of the specimen. At the same time, note that the above estimates are only of order-of-magnitude character, and the actual values of h and the shape of the thermoelastic peak may be somewhat different.

The grain size, h, is also known to be the critical parameter determining the strength and frequency dependence of scattering (Aki and Chouet, 1975). For waves, scattering occurs in distinctly different regimes characterized by the product hk, where $k = \omega/V$ is the wavenumber, and V is the wave speed within the medium. For $hk \ll 0.01$, the wave experiences virtually no scattering, for $hk \ll 0.1$, the medium possesses an apparent Q and (potentially) anisotropy (Rayleigh scattering), and for $hk \sim 0.1$-10, scattering is dominant and highly non-uniform (Mie scattering). For the sub-millimeter grain size inferred above and seismic frequencies of 0.1-10 Hz, and $V \approx 6000$ m/s, $hk \approx 10^{-7}$-10^{-5}, which is very low. Thus, scattering on material grains is hardly significant, but some contribution from it can likely be incorporated in the effective viscosity. By comparison, "scattering" on the boundaries of the whole apparatus (e.g., $h \approx 0.1$ m) suggests $hk \approx 10^{-5}$-10^{-3}, which is also small but closer to the detectable Rayleigh regime. However, such "scattering" on the boundaries of the experimental apparatus is inherently included in my model in the form of

accounting for the shapes and dimensions of the cylinders. For these reasons, as mentioned above, scattering was not considered in this study separately from the viscosity and thermoelastic mechanisms.

4.5 Summary of Key Results

In this Thesis, I attempted applying a conceptually novel model of material anelasticity to describe creep and seismic attenuation measurements in the lab. Instead of the traditional viscoelastic, Q-based model, several key observations were reconsidered from the viewpoint of classical mechanics of continuous media described by Landau and Lifshitz (1976). The most important findings from this thesis are as follows:

1. Classical continuum mechanics with dissipation both qualitatively and quantitatively describes the observed phenomena. It also explains the physical nature of "material memory" and equivalent mechanical models which are often used for describing seismic attenuation measurements in the lab;

2. Power-law solid viscosity (rheology) can produce near-constant "strain-stress" phase lags.

3. Thermoelasticity represents a mechanism capable of producing both phase lags decreasing with frequency and absorption peaks.

4. The combination of thermoelasticity and power-law rheology may be able to explain recent phase-lag measurements in Plexiglas (Tisato et al., 2010). The dissipation peak is explained by thermoelastic effects on the $\sim$0.15-mm granularity.

5. Power-law rheology is capable of producing "near-instantaneous" deformation followed by anelastic creep in creep experiments. Modeling experimental data in Plexiglas by Tisato (2010) suggests a "near-dry" friction within the material, which rheological exponent $\nu \approx$ 0.56. Similar frictional regimes appear to operate within the Earth.

6. Several types of Q values (phase-lag, spectral) were identified in different types of experiments and related to the intrinsic material properties, and also shapes and dimensions of the specimens.

7. The quality factor inferred from phase-lag measurements is intrinsically frequency dependent and therefore is *not a* good candidate for an intrinsic material property.

8. The quality factor inferred from spectral measurements is also fundamentally dependent on the length and other dimensions of the sample and therefore is *not* a good candidate for an intrinsic material property.

9. Within the theoretical model considered here, intrinsic material properties related to viscosity are viscous parameter η and viscous power ν. The goal of experiments measuring the attenuation properties of materials should be the determination of these parameters. This task can be substantially more difficult than attributing a phenomenological frequency-dependent Q to the material. For example, for linear dissipation, η_μ and η_K can be inverted from the slopes of the phase-lag dependences on frequency.

4.6 Conclusions

The general conclusion illustrated by a number of models of this study is that classical continuum mechanics with dissipation allows us to describe the observed creep and phase-lag attenuation effects in solids. Both time-domain and frequency-domain observations are described in terms of four groups of physical processes: 1) solid viscous friction (rheology), 2) thermoelasticity, 3) kinetic transformations, and 4) geometric spreading and scattering. Only the first two of these types of processes were considered in this Thesis and found adequate for describing the available observations. The frequency-dependent Q or time-dependent moduli, compliances, or creep functions which are often used to describe such observations may be empirical characteristics reflection not only the properties of the materials but, for example, dimensions and shapes of the samples.

The theoretical paradigm employed in this study is strongly different from the conventional, Q-based (often called "viscoelastic") model. Instead of a single, but arbitrarily frequency-dependent Q which is specialized for describing relaxation only, a number of more general, physical parameters are attributed to the corresponding energy-dissipation mechanisms (such as viscosity or thermoelasticity). The model is thus based on first physical principles and focuses on inverting for the intrinsic (time- and frequency-independent) properties of the material.

In the approach presented here, the observed frequency-dependent Q's or time-dependent creep ("memory") functions are generally explained by the non-linearity of solid viscosity, which can be described by selecting the Lagrangian dissipation function. This fundamental conclusion was suggested as long ago as by Knopoff (1964) but appeared to be little developed since. I only considered a specific, power-law form of this function, and showed that it is consistent with the strain-rate dependence of effective viscosity used in geodynamics. The selected type of nonlinearity also allows prediction of the key observations in both time- and frequency-domain experiments and to propose methods for inverting for the *in situ* dissipation properties of materials.

4.7   Future Research

This Thesis focused on establishing a first-principle approach to interpreting seismic attenuation observations in the lab, and as such, it probably elucidated more questions than provided definite answers. The experimental environments considered above (Figures 2.1 and 2.2) were quite simplified, whereas the results often suggested that the details of these environments should be significant for understanding the results.

As mentioned in Conclusions, non-linearity of the dissipation function is the key to understanding the time- and frequency dependence of the quantities observed in seismic-attenuation experiments in the lab. This Thesis focused on exploring only a specific form of this dependence, which is the power-law Lagrangian dissipation function (2.18). This form assumed that the dissipation nonlinearly depends on the strain rate, $\dot{\varepsilon}$, but not on the strain itself (ε). This was only the simplest, "minimal" assumption which reflected the principal observation of effective viscosity depending on strain rates (2.20). However, this form of dissipation function also implies that the same power-law dependence applies to the dependence of dissipation on strain levels.

The dependence of viscous dissipation on strain levels is poorly studied experimentally and for simplicity, it was not explored in this Thesis. However, the non-linearity of dissipation with respect to strain levels does not have to be dictated by the non-linearity in strain rate. A natural and interesting extension of the dissipation function (2.18) arises from our approach:

$$D^{\mathrm{nl}} = \int_V \left[\frac{\eta_K}{\tau_K^2} \left(\tau_K^2 \frac{\dot{\Delta}^2}{2} \right)^{\nu_K} \Delta^{2\xi_K} + \frac{2\eta_\mu}{\tau_\mu^2} \left(\tau_\mu^2 \frac{\dot{\tilde{\varepsilon}}_{ij} \dot{\tilde{\varepsilon}}_{ij}}{2} \right)^{\nu_\mu} (\tilde{\varepsilon}_{kl} \tilde{\varepsilon}_{kl})^{\xi_\mu} \right] dV. \tag{4.16}$$

With such a dissipation function, frequency dependences of $\tan\phi$ in forced-oscillation experiments should be the same as described above, but the dependences on strain levels would be proportional to $\varepsilon^{2(\nu+\xi)}$ for each of the two modes of deformation (torsional and longitudinal). In particular, for $\nu+\xi=1$, the dissipation should behave linearly with respect to the strain level. From seismic observations, this behaviour appears to be intuitively preferable, and the condition $\nu+\xi\approx 1$ also appears to be satisfied in a recent model applying this dissipation function to the free oscillations of the Earth (Morozov, 2010c and 2011d).

Thus, one line of further research would consist of extending all of the results of this Thesis to dissipation of the form (4.16). This could be a very significant undertaking, which would require investigating the dependence of behaviour of mechanical systems on additional parameters ξ and also producing reliable experimental data on strain dependence.

Another improvement of the models discussed above should come from more accurate models of the granularity of the material, shape of the specimens, and other details of experimental environments. As suggested in section 3.3, by relaxing the intuitive constraint $\nu\geq 0.5$ and by deviating from the pure power-law dissipation function (2.18), a better fit to the experimental data can be achieved. However, simultaneously, a more accurate model of the thermoelastic peak would be required. Developing such models could require much additional research.

Another major question mentioned but not resolved in this Thesis relates to the relative levels of the bulk and deviatoric viscosity parameters (η_K and η_μ, respectively in eq. 4.1). As mentioned in section 4.1, I mostly used a simple approximation $\eta_K=0$ inspired by an analogy with viscoelasticity. However, as recent studies show (Morozov, 2012b), this analogy may in fact be insufficiently rigorous and lead to rather peculiar theoretic consequences. This problem, however, also applies to the viscoelasticity itself (*ibid*). As Morozov (2012b) suggested, a theoretically more "natural" *ad hoc* approximation in the absence of adequate data could be $\eta_K=2\eta_\mu/3$. This approximation will also need to be explored in the context of experiments modelled in this Thesis.

Finally, the ultimate goal of this study (as well of the experiments with Plexiglas by Tisato et al. (2010) is in applying the resulting techniques to measuring seismic attenuation in rocks. Unfortunately, again, the results if this Thesis show that the models need to be developed specifically for each type of observations. For example, the relative roles of thermoelastic effects and viscosity in a large Plexiglas sample could be quite different from those in small samples of olivine aggregates

on which mantle-rock attenuation is often studied. Also, extremely strong temperature gradients in high-temperature experiments (such as by Jackson and Paterson, 1993) may create strong thermoelastic pre-stressing and even fracturing of the specimens, which could cause major complications in interpreting the results from first principles. Thus, significant work taking into account the specifics of high-pressure, high-temperature experiments with highly heterogeneous, small, and complexly-shaped specimens is still required in order to be able to apply the above results to observations with mantle and deep crustal rock samples. Most importantly, such studies should be based on the physical principles explored in this Thesis.

CHAPTER A

REDUCTION OF THE PROBLEM TO DISCRETE FORM

In this Appendix, I derive the matrix forms of the Lagrangian and dissipation function for the two-cylinder tensional- and torsional-deformation cases as well as the equation of motion for single-cylinder creep and resonance. In both cases, a simple approximation is taken, in which both the specimen and the standard deform uniformly, and therefore the deformation of each of these bodies is described by a single parameter. This approximation was also used in interpreting experimental data (Faul et al., 2004; Tisato et al., 2010; Lakes, 2009; McLoughlin and Tobolsky, 1952). Rigorously, it is only suitable for the low-frequency limit; however, this limit is of the most practical value.

A.1 Longitudinal Deformation

In the case of tension, the force is applied to the top of the sample along the longitudinal axis. Relative extensions in the z-direction are denoted $\alpha_1 = \Delta H_1 / H_1$ for the standard and $\alpha_2 = \Delta H_2 / H_2$ for the sample.

Compression in the z-direction will result in expansion in the r-direction. This expansion is
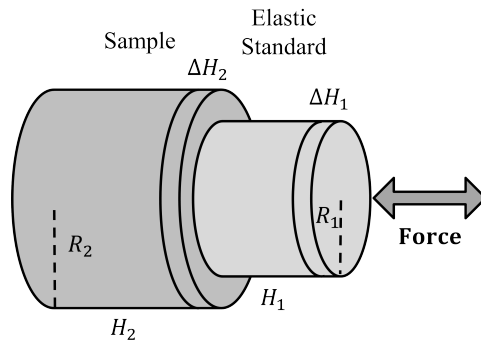
Figure A.1: Schematic for measuring longitudinal phase lags.

governed by the Poisson's ratio (σ) of the material. Displacements of any point in the system can be written as follows:

$$\vec{u}_1 = (\alpha_1 z)\hat{z} - (\alpha_1 \sigma_1 r)\hat{r}, \quad \vec{u}_2 = (\alpha_1 H_1 + \alpha_2 z)\hat{z} - (\alpha_2 \sigma_2 r)\hat{r}, \tag{A.1}$$

where the symbols with hats indicate unit vectors in the corresponding directions.

The strain matrices for each cylinder can be determined from the displacements:

$$\varepsilon_n = \begin{pmatrix} -\sigma_n \alpha_n & 0 & 0 \\ 0 & -\sigma_n \alpha_n & 0 \\ 0 & 0 & \alpha_n \end{pmatrix}, \tag{A.2}$$

where n equals 1 for the standard and 2 for the sample. Notice that there is no shear contribution to strain in the longitudinal case.

The next step is to use the displacements and strains to determine the system's Lagrangian. Kinetic and potential energies as well as linear and non-linear dissipation functions of an anelastic body are:

$$\langle \dot{\alpha}|\mathbf{T}|\dot{\alpha}\rangle = \int_V \frac{\rho}{2}\dot{u}_i\dot{u}_i dV, \tag{A.3}$$

$$\langle \alpha|\mathbf{V}|\alpha\rangle = \int_V \left(\frac{1}{2}K\varepsilon_{kk}^2 + \mu\tilde{\varepsilon}_{ij}\tilde{\varepsilon}_{ij} \right) dV,$$

$$\langle \dot{\alpha}|\mathbf{D}|\dot{\alpha}\rangle = \int_V \left(\frac{1}{2}\eta_K\dot{\varepsilon}_{kk}^2 + \eta_\mu\dot{\tilde{\varepsilon}}_{ij}\dot{\tilde{\varepsilon}}_{ij} \right) dV,$$

$$\dot{\alpha}_i^v D_{ij}^{nl}\dot{\alpha}_j^v = \int_V \left[\frac{\eta_K}{\tau_K^2}\left(\tau_K^2 \frac{\dot{\Delta}^2}{2} \right)^v + \frac{2\eta_\mu}{\tau_\mu^2}\left(\tau_\mu^2 \frac{\dot{\tilde{\varepsilon}}_{ij}\dot{\tilde{\varepsilon}}_{ij}}{2} \right)^v \right] dV.$$

Above, ε_{kk} is the dilatational strain (trace of strain tensor) and $\tilde{\varepsilon}$ is deviatoric strain. By taking the integrals in (A.3), the resulting matrices become:

$$\mathbf{T} = \frac{\pi}{2}\begin{pmatrix} I_1 H_1 R_1^2 + \rho_2 H_1^2 H_2 R_2^2 & \frac{1}{2}\rho_2 H_1 H_2^2 R_2^2 \\ \frac{1}{2}\rho_2 H_1 H_2^2 R_2^2 & I_2 H_2 R_2^2 \end{pmatrix}, \tag{A.4}$$

$$\mathbf{V} = \frac{\pi}{2} \begin{pmatrix} E_1 H_1 R_1^2 & 0 \\ 0 & E_2 H_2 R_2^2 \end{pmatrix},$$

$$\mathbf{D} = \frac{\pi}{2} \begin{pmatrix} \eta_{E1} H_1 R_1^2 & 0 \\ 0 & \eta_{E2} H_2 R_2^2 \end{pmatrix},$$

$$\mathbf{D}^{nl} = \frac{\pi}{2} \begin{pmatrix} \eta_{nl1} H_1 R_1^2 & 0 \\ 0 & \eta_{nl2} H_2 R_2^2 \end{pmatrix}.$$

Simplifying these expressions to the single-cylinder case (for resonance and creep) can be done by just taking the 2nd row 2nd column element of each matrix:

$$T = \frac{\pi}{2} R^2 H I \dot{\alpha}^2, \quad V = \frac{\pi}{2} R^2 H E \alpha^2, \tag{A.5}$$

$$D = \frac{\pi}{2} R^2 H \eta_E \dot{\alpha}^2, \quad D^{nl} = \frac{\pi}{2} R^2 H \eta_{nl} \dot{\alpha}^{2\nu}.$$

Inserting these expressions into the Euler-Lagrange equations (1.13) yields the following equations of motion:

$$\pi R^2 H I \ddot{\alpha} + \pi R^2 H \eta_E \dot{\alpha} + \pi R^2 H E \alpha = F(t). \tag{A.6}$$

Finally:

$$I \ddot{\alpha} + \eta_E \dot{\alpha} + E \alpha = \tilde{F}(t), \quad \tilde{F}(t) = \frac{F(t)}{\pi R^2 H}. \tag{A.7}$$

The same process can be done for the non-linear dissipation function yielding:

$$I \ddot{\alpha} + \eta_{\text{eff}}^c \dot{\alpha}^{2\nu-1} + E \alpha = \tilde{F}(t), \quad \eta_{\text{eff}}^c = \nu \eta_{nl}. \tag{A.8}$$

A.2   Torsional Deformation

In the case of torsional force, the sample is twisted at the top while the base of the standard is fastened. For twisting, I select the dimensionless generalized variables as $\alpha_1 = \theta_1$ for the standard and $\alpha_2 = \theta_2$ for the sample.

Twisting in the θ-direction will not result in any change in the r- or z-directions. Displacements
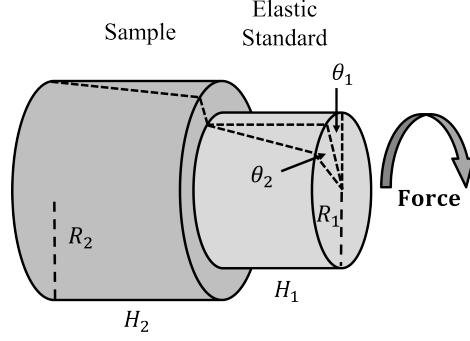
Figure A.2: Schematic for measuring torsional phase lags.

of any point in the system can be written as follows:

$$\vec{u}_1 = \left(\frac{zr}{H_1}\alpha_1\right)\hat{\theta}, \quad \vec{u}_2 = \left(r\alpha_1 + \frac{zr}{H_2}\alpha_2\right)\hat{\theta}. \tag{A.9}$$

The strain matrices for each cylinder can be determined from the displacements:

$$\varepsilon_n = \begin{pmatrix} 0 & 0 & 0 \\ 0 & 0 & \frac{r}{2H_n}\alpha_n \\ 0 & \frac{r}{2H_n}\alpha_n & 0 \end{pmatrix}, \tag{A.10}$$

where n equals 1 for the standard and 2 for the sample. Notice that there is no dilatational contribution to strain, which means that the strain is purely shear in nature. Similar to the longitudinal case, the evaluation of integrals (A.3) leads to the matrices of the kinetic and potential energies ($\mathbf{T}$ and $\mathbf{V}$), as well as linear dissipation ($\mathbf{D}$) and non-linear dissipation ($\mathbf{D}^{\text{nl}}$) and are given by:

$$\mathbf{T} = \frac{\pi}{4}\begin{pmatrix} \frac{I_1 R_1^4}{H_1} + \frac{3I_2 R_2^4}{H_2} & \frac{3I_2 R_2^4}{2H_2} \\ \frac{3I_2 R_2^4}{2H_2} & \frac{I_2 R_2^4}{H_2} \end{pmatrix}, \tag{A.11}$$

$$\mathbf{V} = \frac{\pi}{4}\begin{pmatrix} \frac{\mu_1 R_1^4}{H_1} & 0 \\ 0 & \frac{\mu_2 R_2^4}{H_2} \end{pmatrix},$$

$$\mathbf{D} = \frac{\pi}{4}\begin{pmatrix} \frac{\eta_{\mu 1} R_1^4}{H_1} & 0 \\ 0 & \frac{\eta_{\mu 2} R_2^4}{H_2} \end{pmatrix},$$

80

$$\mathbf{D}^{\mathrm{nl}} = \frac{\pi}{4} \begin{pmatrix} \frac{\eta_{nl1}R_1^4}{H_1} & 0 \\ 0 & \frac{\eta_{nl2}R_2^4}{H_2} \end{pmatrix}.$$

Simplifying these expressions to the single cylinder case can be done by just taking the 2nd row 2nd column element of each matrix:

$$T = \frac{\pi}{4}\frac{R^4}{H}I\dot{\alpha}^2, \quad V = \frac{\pi}{4}\frac{R^4}{H}\mu\alpha^2, \tag{A.12}$$

$$D = \frac{\pi}{4}\frac{R^4}{H}\eta_\mu\dot{\alpha}^2, \quad D^{\mathrm{nl}} = \frac{\pi}{4}\frac{R^4}{H}\eta_{nl}\dot{\alpha}^{2\nu}.$$

Inserting these expressions into the Euler-Lagrange equations (1.13) yields the following equations of motion:

$$\frac{\pi}{2}\frac{R^4}{H}I\ddot{\alpha} + \frac{\pi}{2}\frac{R^4}{H}\eta_\mu\dot{\alpha} + \frac{\pi}{2}\frac{R^4}{H}\mu\alpha = F(t). \tag{A.13}$$

Finally:

$$I\ddot{\alpha} + \eta_\mu\dot{\alpha} + \mu\alpha = \tilde{F}(t), \quad \tilde{F}(t) = \frac{2HF(t)}{\pi R^4}. \tag{A.14}$$

The same process can be done for the non-linear dissipation function yielding:

$$I\ddot{\alpha} + \eta_{\mathrm{eff}}^c\dot{\alpha}^{2\nu-1} + \mu\alpha = \tilde{F}(t), \quad \eta_{\mathrm{eff}}^c = \nu\eta_{nl}. \tag{A.15}$$

CHAPTER B

PARAMETER SUMMARIES FOR NON-LINEAR RHEOL-OGY

In this section, I summarize the variables used in phase lag, resonance and creep experiments for both longitudinal and torsional deformations. I also summarize various thermal properties of several Earth materials and Plexiglas.

Table B.1: Parameter summary for time domain (creep) problem.

	Longitudinal	Torsional
Equation of motion	$I\ddot{\alpha} + \eta_{\text{eff}}^c \dot{\alpha}^{2\nu-1} + M\alpha = \tilde{F}$	
I	$\dfrac{\rho H^2}{3}\left[1 + \dfrac{3}{2}\left(\dfrac{R}{H}\sigma\right)^2\right]$	$\dfrac{\rho H^2}{3}$
η_{eff}^c	$\dfrac{\nu}{2^{\nu-1}}\left[\eta_K\left(1-2\sigma\right)^{2\nu} + \dfrac{2^{\nu+1}}{3^\nu}\eta_\mu\left(1+\sigma\right)^{2\nu}\right]$	$\dfrac{\nu\eta_\mu}{2^{2\nu-2}\left(\nu+1\right)}\left(\dfrac{R}{H}\right)^{2(\nu-1)}$
M	E	μ
$\tilde{F}$	$\dfrac{F(t)}{\pi R^2 H}$	$\dfrac{2HF(t)}{\pi R^4}$

Table B.2: Parameter summary for frequency domain (two-cylinder phase lag) problem.

	Longitudinal	Torsional
Equation of motion	$\vec{\alpha} = \left(-\omega^2 \mathbf{T} + i\omega^{2\nu-1}\tilde{\mathbf{D}} + \mathbf{V}\right)^{-1}\vec{F}$	
$\mathbf{T}$	$\dfrac{\pi}{2}\begin{pmatrix} I_1 H_1 R_1^2 + \rho_2 H_1^2 H_2 R_2^2 & \frac{1}{2}\rho_2 H_1 H_2^2 R_2^2 \\ \frac{1}{2}\rho_2 H_1 H_2^2 R_2^2 & I_2 H_2 R_2^2 \end{pmatrix}$	$\dfrac{\pi}{4}\begin{pmatrix} \frac{I_1 R_1^4}{H_1} + \frac{3 I_2 R_2^4}{H_2} & \frac{3 I_2 R_2^4}{2 H_2} \\ \frac{3 I_2 R_2^4}{2 H_2} & \frac{I_2 R_2^4}{H_2} \end{pmatrix}$
$\tilde{\mathbf{D}}$	$\dfrac{\pi}{2}\begin{pmatrix} \eta^{\phi}_{eff1} H_1 R_1^2 & 0 \\ 0 & \eta^{\phi}_{eff2} H_2 R_2^2 \end{pmatrix}$	$\dfrac{\pi}{4}\begin{pmatrix} \frac{\eta_{\mu1} R_1^4}{H_1} & 0 \\ 0 & \frac{\eta_{\mu2} R_2^4}{H_2} \end{pmatrix}$
$\mathbf{V}$	$\dfrac{\pi}{2}\begin{pmatrix} E_1 H_1 R_1^2 & 0 \\ 0 & E_2 H_2 R_2^2 \end{pmatrix}$	$\dfrac{\pi}{4}\begin{pmatrix} \frac{\mu_1 R_1^4}{H_1} & 0 \\ 0 & \frac{\mu_2 R_2^4}{H_2} \end{pmatrix}$
η^{ϕ}_{eff}	$2\nu\alpha^{2\nu-2}\langle\cos^{2\nu}y\rangle\eta_{nl}$	
η_{nl}	$\dfrac{1}{2^{\nu-1}}\left[\eta_K\left(1-2\sigma\right)^{2\nu} + \dfrac{2^{\nu+1}}{3^{\nu}}\eta_{\mu}\left(1+\sigma\right)^{2\nu}\right]$	$\dfrac{\eta_{\mu}}{2^{2\nu-2}\left(\nu+1\right)}\left(\dfrac{R}{H}\right)^{2(\nu-1)}$

Table B.3: Parameter summary for frequency domain (single-cylinder resonance) problem.

	Longitudinal	Torsional
Equation of motion	$\alpha = \left(-\omega^2 T + i\omega\tilde{D} + V\right)^{-1} F$	
T	$\dfrac{\pi}{2} R^2 H I$	$\dfrac{\pi}{4} \dfrac{R^4 I}{H}$
$\tilde{D}$	$\dfrac{\pi}{2} R^2 H \eta_{\text{eff}}^{res}$	$\dfrac{\pi}{4} \dfrac{R^4 \eta_{\text{eff}}^{res}}{H}$
V	$\dfrac{\pi}{2} R^2 H E$	$\dfrac{\pi}{4} \dfrac{R^4 \mu}{H}$
η_{eff}^{res}	$2\nu \left(\alpha\omega\right)^{2\nu-2} \langle \cos^{2\nu} y \rangle \eta_{nl}$	
η_{nl}	$\dfrac{1}{2^{\nu-1}} \left[\eta_K \left(1 - 2\sigma\right)^{2\nu} + \dfrac{2^{\nu+1}}{3^\nu} \eta_\mu \left(1 + \sigma\right)^{2\nu} \right]$	$\dfrac{\eta_\mu}{2^{2\nu-2}\left(\nu + 1\right)} \left(\dfrac{R}{H}\right)^{2(\nu-1)}$

Table B.4: Thermal properties of several Earth materials and Plexiglas

Material	κ, W/m/K	α, K (at room temperature)	ρ kg/m^3	C_p J/K/kg	K, GPa **	μ, GPa	Δ_K (bulk modulus defect)*
Sandstone	1.7	30×10^6	200-2600				
Quartz	3		600-2800				
Granite at 500 K	2.0 [3]	2.4×10^{-5}	700	90	57 (V_p = 6.2 km/s, V_s = 3.6 km/s)	5 (V_s = 3.6 km/s)	0.0076 (Q = 200)
Basalt, gabbro, diabase	1.7-2.0	15×10^{-6}	800-3000	40	79 (V_p = 7 km/s)		0.002 at T = 800 K (Q = 780)
Polycrystalline olivine at 1200 K	2.0 [2]	3.8×10^{-5}[1]	251 [1]	236 [1]	107.8 [1]	5.8 [1]	0.0465 (Q = 34)
Plexiglas	0.19	$3 \times (3.9 - 7.2) \times 10^{-5}$ (linear expansion coeff. cited)= $(1.2 - 2.2) \times 10^{-4}$	190	470	2960		0.007-0.02 at T = 300 K (Q = $80 - 220$)

* $\Delta_K \equiv \frac{K_A - K_I}{K_I} = \frac{K_A T \alpha^2}{\rho C_p}$, where K_A and K_I are the adiabatic and isothermal elastic moduli. The corresponding thermoelastic Q: $Q \approx \pi/2\Delta_K$.

** Where K is not available, we estimate it from seismic V_p: $K = \rho \left(V_p^2 - \frac{4}{3}V_s^2 \right) \approx \frac{5}{9}\rho V_p^2$.

BIBLIOGRAPHY

Aki, K. and Chouet, B. Origin of coda waves: source, attenuation, and scattering effects. *Journal of Geophysical Research*, 80(23):3322–3342, 1975.

Aki, K. and Richards, P.G. *Quantitative seismology*. Univ Science Books, 2002.

ALTUGLAS, International. Average physical properties plexiglas g, (2002). `http://www.atoglas.com/literature/pdf/88.pdf`, 1987. Accessed on July 2, 2011.

Anderson, D.L. and Archambeau, CB. The anelasticity of the earth. *Journal of Geophysical Research*, 69(10):2071–2084, 1964.

Anderson, D.L. and Minster, J.B. The frequency dependence of q in the earth and implications for mantle rheology and chandler wobble. *Geophysical Journal of the Royal Astronomical Society*, 58(2):431–440, 1979.

Anderson, D.L.; Archambeau, C.B., and Ben-Menahem, A. Attenuation of seismic energy in the upper mantle. *J. Geophys. Res.*, 70(6):1441–1448, 1965.

Anderson, D.L.; Kanamori, H.; Hart, R.S., and Liu, H.P. The earth as a seismic absorption band. *Science*, 196(4294):1104, 1977.

Andrade, E.N. da C. On the viscous flow in metals, and allied phenomena. *Proceedings of the Royal Society of London. Series A*, 84(567):1–12, 1910.

Biot, M.A. Theory of propagation of elastic waves in a fluid-saturated porous solid. i. low-frequency range. *J. Acoust. Soc. Am*, 28(2):168–178, 1956.

Bourbié, T.; Coussy, O., and Zinszner, B. *Acoustics of porous media*. Editions Technip, 1987.

Butcher, J.C. and Wiley, J. *Numerical methods for ordinary differential equations*, volume 2. Wiley Online Library, 2003.

Carcione, J.M. *Wave fields in real media: Wave propagation in anisotropic, anelastic, porous and electromagnetic media*, volume 38. Elsevier Science, 2007.

Chopra, P.N. High-temperature transient creep in olivine rocks. *Tectonophysics*, 279(1-4):93–111, 1997.

Claytor, K.E.; Koby, J.R., and TenCate, J.A. Limitations of preisach theory: Elastic aftereffect, congruence, and end point memory. *Geophys. Res. Lett*, 36:L06304, 2009.

Cooper, R.F. Seismic wave attenuation: energy dissipation in viscoelastic crystalline solids. *Reviews in mineralogy and geochemistry*, 51(1):253–290, 2002.

Faul, U.H.; Gerald, J.D.F., and Jackson, I. Shear wave attenuation and dispersion in melt-bearing olivine polycrystals: 2. microstructural interpretation and seismological implications. *J. Geophys. Res*, 109:B06202, 2004.

Green, D.H.; Cooper, R.F., and Zhang, S. Attenuation spectra of olivine/basalt partial melts: Transformation of newtonian creep response. *Geophysical Research Letters*, 17(12):2097–2100, 1990.

Gribb, T.T. and Cooper, R.F. Low-frequency shear attenuation in polycrystalline olivine: Grain boundary diffusion and the physical significance of the andrade model for viscoelastic rheology. *J. Geophys. Res.*, 103(B11):27267–27279, 1998.

Guyer, R.A.; McCall, K.R., and Boitnott, G.N. Hysteresis, discrete memory, and nonlinear wave propagation in rock: A new paradigm. *Physical review letters*, 74(17):3491–3494, 1995.

Hayden, H.W.; Moffatt, W.G., and Wulff, J. The structure and properties of materials. v. 3. mechanical behavior. *John Wiley and Sons, NY*, 1965.

Ito, E. and Sato, H. Aseismicity in the lower mantle by superplasticity of the descending slab. 1991.

Jackson, I. and Paterson, MS. A high-pressure, high-temperature apparatus for studies of seismic wave dispersion and attenuation. *Pure and Applied Geophysics*, 141(2):445–466, 1993.

Jackson, I.; Faul, U.H.; Gerald, J.D.F., and Tan, B.H. Shear wave attenuation and dispersion in melt-bearing olivine polycrystals: 1. specimen fabrication and mechanical testing. *J. Geophys. Res*, 109(10.1029), 2004.

Johnson, P.A.; Zinszner, B., and Rasolofosaon, P.N.J. Resonance and elastic nonlinear phenomena in rock. *J. Geophys. Res*, 101:11553–11554, 1996.

Johnson, P.A.; Zinszner, B.; Rasolofosaon, P.; Cohen-Tenoudji, F., and Van Den Abeele, K. Dynamic measurements of the nonlinear elastic parameter in rock under varying conditions. *J. Geophys. Res*, 109:10129–10139, 2004.

Karato, S. *Deformation of earth materials: an introduction to the rheology of solid earth*. Cambridge Univ Pr, 2008.

Karato, S. and Wu, P. Rheology of the upper mantle: a synthesis. *Science*, 260(5109):771–778, 1993.

Karato, S.I. and Spetzler, HA. Defect microdynamics in minerals and solid-state mechanisms of seismic wave attenuation and velocity dispersion in the mantle. *Reviews of Geophysics*, 28(4): 399–421, 1990.

Knopoff, L. Solid-earth geophysics. *Q. Rev. Geophys.*, 2:625–660, 1964.

Knopoff, L. and MacDonald, G.J.F. Attenuation of small amplitude stress waves in solids. *Reviews of Modern Physics*, 30(4):1178, 1958.

Lakes, R.S. *Viscoelastic materials*. Cambridge University Press, Cambridge, UK, 2009.

Landau, L.D. and Lifshitz, E.M. *Theory of Elasticity: Volume 7*. Pergamon Press, 1976a.

Landau, L.D. and Lifshitz, E.M. *Mechanics: Volume 1*. Pergamon Press, 1976b.

Liu, H.P.; Anderson, D.L., and Kanamori, H. Velocity dispersion due to anelasticity; implications for seismology and mantle composition. *Geophysical Journal of the Royal Astronomical Society*, 47(1):41–58, 1976.

Lomnitz, C. Linear dissipation in solids. *Journal of Applied Physics*, 28(2):201–205, 1957.

Mavko, G. and Nur, A. Melt squirt in the asthenosphere. *J. Geophys. Res.*, 80(11):1444–1448, 1975.

McLoughlin, J.R. and Tobolsky, A.V. The viscoelastic behavior of polymethyl methacrylate. *Journal of Colloid Science*, 7(6):555–568, 1952.

Morozov, I.B. Geometrical attenuation, frequency dependence of Q, and the absorption band problem. *Geophys. J. Int.*, 175:239–252, 2008.

Morozov, I.B. Thirty years of confusion around "scattering Q"? *Seism. Res. Lett.*, 80:5–7, 2009.

Morozov, I.B. On the causes of frequency-dependent apparent seismological Q. *Pure Appl. Geophys.*, 167:1131–1146, 2010a.

Morozov, I.B. Attenuation coefficients of rayleigh and lg waves. *J. Seismol.*, DOI 10.1007/s10950-010-9196-5, 2010b.

Morozov, I.B. Viscosity model for the earth from free oscillations. `http://seisweb.usask.ca/ibm/papers/Q/Morozov_bulk_and_shear_dissipation.preprint.pdf`, 2010c.

Morozov, I.B. Anelastic acoustic impedance and the correspondence principle. *Geophys. Prosp.*, DOI 10.1111/j.1365-2478.2010.00890.x., 2011a.

Morozov, I.B. Temporal variations of coda Q: An attenuation-coefficient view. *Phys. Earth Planet. Inter.*, 187:47–55, 2011b.

Morozov, I.B. Mechanisms of geometrical seismic attenuation. *Annals Geophys.*, 54:235–248, 2011c.

Morozov, I.B. Unified solid-viscous mantle rheology. *2011 AGU Fall Meeting*, MR11B-2171, 2011d.

Morozov, I.B. Physical character of seismic viscoelasticity. `http://seisweb.usask.ca/ibm/papers/Q/Morozov_Q_AG.2011.preprint.pdf`, 2011e. submitted to Annals Geophys.

Morozov, I.B. Mechanics of tidal and seismic energy dissipation in planets. i: Fundamentals. `http://seisweb.usask.ca/ibm/papers/Q/Morozov_Mechanics_2011.part1.preprint.pdf`, 2011f.

Morozov, I.B. Frequency dependence of long-period t. *J. Seismol.*, DOI 10.1007/s10950-012-9315-6, 2012a.

Morozov, I.B. Thermoelastic relaxation in cylindrical material specimens. `http://seisweb.usask.ca/ibm/papers/Q/thermal_relaxation_in_cylindrical_samples.pdf`, 2012b.

Morozov, I.B. Bulk and shear dissipation. `http://seisweb.usask.ca/ibm/papers/Q/Morozov_bulk_and_shear_dissipation.preprint.pdf`, 2012c.

Nowick, A.S. and Berry, B.S. *Anelastic relaxation in crystalline solids*, volume 1. Academic Press, 1972.

Petersson, N.A. and Sjögreen, B. Stable and efficient modeling of anelastic attenuation in seismic wave propagation. *Center for Applied Scientific Computing*, 50:422, 2010.

Phillips, P. The slow stretch in indiarubber, glass, and metal wires when subjected to a constant pull. *The London, Edinburgh, and Dublin Philosophical Magazine and Journal of Science*, 9 (52):513–531, 1905.

TenCate, J.A. Slow dynamics of earth materials: An experimental overview. *Pure and Applied Geophysics*, pages 1–9, 2011.

Tisato, N.; Madonna, C.; Boutareaud, S., and Burg, J. A new instrumentation to measure seismic waves attenuation. In *AGU Fall Meeting Abstracts*, volume 1, page 1464, 2010.

Tropea, C.; Yarin, A.L., and Foss, J.F. *Springer handbook of experimental fluid mechanics*, volume 1. Springer Verlag, 2007.